DETERMINING THE EFFICACY OF DUNE ENHANCEMENT AND BEACH NOURISHMENT PRACTICES TO MITIGATE STORM WASHOVER ON A LOW-LYING BARRIER ISLAND

A Thesis

by

CLAIRE RYDMAN POLLARD

BS, Texas State University, 2009

Submitted in Partial Fulfillment of the Requirements for the Degree of

MASTER of SCIENCE

in

Environmental Science

Texas A&M University-Corpus Christi
Corpus Christi, Texas

December 2017

DETERMINING THE EFFICACY OF DUNE ENHANCEMENT AND BEACH NOURISHMENT PRACTICES TO MITIGATE STORM WASHOVER ON A LOW-LYING BARRIER ISLAND

A Thesis

by

CLAIRE RYDMAN POLLARD

This thesis meets the standards for scope and quality of
Texas A&M University-Corpus Christi and is hereby approved.

James C. Gibeaut, PhD
Chair

Michael J. Starek, PhD
Committee Member

Philippe Tissot, PhD
Committee Member

December 2017

ABSTRACT

Tropical cyclones that enter or form in the Gulf of Mexico generate storm surge and large waves that impact low-lying coastlines. Along much of the Gulf Coast, barrier islands are the primary line of defense against these powerful forces. Galveston Island, located 70 km south-southeast of Houston at the mouth of Galveston Bay, TX, is a major tourist and commercial center that has endured numerous hurricanes. Hurricane Ike is the most recent hurricane to make landfall on Galveston Island in September of 2008, causing dramatic changes to the coastal landscape. Discontinuous and densely vegetated foredunes less than 3-m tall and 30-m wide were the primary protection for 30 km of developed coastline on Galveston Island. The purpose of this study is to investigate the protective function of a foredune and determine if a larger dune system would have mitigated coastal erosion and flooding during Hurricane Ike.

A coupled hydrodynamic and morphodynamic numerical model, called XBeach, is used to simulate erosion and deposition induced by Hurricane Ike on a 2.6-km long portion of West Beach on Galveston Island. Six different simulated topographic scenarios were incorporated into the XBeach model to test the efficacy of dune enhancement and beach nourishment strategies. Results show that XBeach is a useful tool in simulating the effect of Hurricane Ike from the nearshore to the back barrier flats. Model results are assessed by comparing the post-storm computed surface to lidar data collected over the island three months after Hurricane Ike made landfall. XBeach displayed an excellent Brier skill score of 0.67 up to 0.92 within the foredune zone alone, and described erosion and deposition patterns well. Dune enhancement testing results indicate an unrealistically high foredune (6.5-m tall and 37-m wide) is required to prevent overwash by the 3.14-m high surge. Enhancing the dune system without nourishing the beach leaves the dune line exposed to direct wave attack, and consequently, the lower dunes are eroded

and overwashed. However, by increasing the width of the beach and adding sand to the nearshore, wave and surge energy was further dissipated resulting in less erosion of the beach and foredune zones. A lower foredune (4.5-m tall by 37-m wide) in conjunction with a 25-m wide beach nourishment provided the greatest degree of protection for the study area and was the best use of sand. This research effort is intended to inform coastal managers of the best use of sand resources to protect the island from a future Ike.

DEDICATION

To my grandfather, Pancho, who encouraged me to never stop learning, to never stop asking questions. The universe we live in hosts an infinite amount knowledge we should all be seeking. For the life we are given is a gift and one of the greatest gift we can give in return is to get to know what we are given, from the center of our planet to the outer space, and everything in between.

ACKNOWLEDGEMENTS

I would like to thank, firstly, my undergraduate professor, Dr. Julie Westerlund. Thank you for giving me the confidence that I could be accepted into graduate school after being away for six years. Thank you for recommending Texas A&M University-Corpus Christi, and most importantly, for recommending that I reach out to Dr. James Gibeaut.

I am especially grateful to my committee chair and mentor, Dr. Gibeaut, for accepting me into the Coastal and Marine Geospatial Lab. Thank you for believing in my aptitudes to become the Coastal Geoscientist I am today. I could not have found a more perfect place for me to pursue my research dreams. Thank you for the invaluable education you have given me through the coastal geomorphology research you have accomplished and for sharing your teachings with me. It has been an honor to study and work under your guidance. I would also like to thank my committee members Dr. Michael Starek and Dr. Philippe Tissot. Thank you for taking a sincere interest in my thesis. I appreciate your technical and professional advice, as well as your genuine nature. I also owe a huge debt of gratitude to Dr. Anthony Reisinger. Thank you for teaching me all the great Matlab tricks, and for helping me get through some of the most challenging parts of this project. Thank you to everyone in CMGL, past and present. A special thank you to Luz Lumb for taking me under your wing when I first started here.

I am the first to work with XBeach at this university, so it was with the help of outside professionals that I was able to gain a better understanding of the model. Thank you Dr. Onur Kurum and Dr. Joseph Long for your technical advice, time, and approachability. Thank you to Dr. Andrew Kennedy for providing Hurricane Ike wave data.

Finally, I would like to thank my friends and family for their love and for cheering me on throughout this journey. A huge thank you to my husband, Sean Pollard, for standing by my side

through every step. Thank you for reminding me to stay confident and focused when I felt the floor moving under my feet.

This publication was made possible by the National Oceanic and Atmospheric Administration, Office of Education Educational Partnership Program award (NA11SEC4810001). Its contents are solely the responsibility of the award recipient and do not necessarily represent the official views of the U.S. Department of Commerce, National Oceanic and Atmospheric Administration.

TABLE OF CONTENTS

CONTENTS PAGE

LIST OF FIGURES

LIST OF TABLES

CHAPTER I: INTRODUCTION

Coastal erosion is a serious environmental problem in coastal zones worldwide and is expected to become more crucial in the future as global sea levels are projected to rise. Low-lying barrier islands are highly susceptible to erosion, especially during storm events due to large waves, runup processes and storm surge. The damages to development on barrier islands caused by extreme storms is of great concern, while the occurrence of these storms is important to the natural morphodynamics of the barrier island system and its future existence (Donnelly *et al.*, 2006; Houser *et al.*, 2008; Leatherman, 1979; McBride *et al.*, 1995; Stone *et al.*, 2004). Barrier islands are a valuable and dominant coastal feature along the U.S. Atlantic and Gulf coasts, serving as the primary line of defense against storms, and contributing to a substantial portion of the U.S. economy through tourism and coastal urbanization. Understanding a barrier island's morphodynamic response to storms is increasingly critical to coastal communities as sea levels rise and extreme storms continue to ravage the coast. If barrier islands are not sustainably managed, the communities and habitats thriving there become increasingly threatened by the encroaching seas and impending storms (Bilskie *et al.*, 2016; Neumann *et al.*, 2015). Management strategies to increase coastal resilience on barrier islands range from traditional beach nourishment and dune restoration projects to building a "coastal spine", to even building an artificial barrier system (Frey *et al.*, 2016; Jonkman *et al.*, 2015; Rebuild by Design). Successful designs of these projects, as well as their implications, require a full understanding of the processes controlling barrier island evolution. Numerical models have been increasingly used in the recent decades to help not only explain the morphologic and hydrodynamic processes that occur during a storm, but more importantly to predict a coastline's future vulnerability (Frey *et* *al.*, 2016; Irish *et al.*, 2010; Kriebel and Dean, 1985; Kurum and Overton, 2013; Larson and Kraus, 1989; Roelvink *et al.*, 2009; Vousdoukas *et al.*, 2012).

This study focuses on the morphodynamic response of a barrier island under the destructive processes of an extreme storm, Hurricane Ike, which struck Galveston Island, Texas, in 2008. Galveston Island is a developed progradational barrier island, inhabiting over 49,000 residents and millions of tourists annually. Coastal development which infringes upon beaches and dunes can obstruct the barrier island's natural inland migration in response to sea level rise (SLR), can interfere with the natural post-storm recovery of the foredune system, and can be destroyed from the impact of the storm (Morton, 1976; Morton and Paine, 1985; Morton *et al.*, 1994). Galveston Island is experiencing an increase in sea level of approximately 6.47 mm/year, which corresponds to an average shoreline retreat of -0.88 m/year (Paine *et al.*, 2012). The beach and dune system of a barrier island serve as a buffer, dissipating energy from waves and defending against storm surge. Densely vegetated discontinuous foredunes less than 3-m-tall and 30-m-wide were the primary protection on Galveston Island (Paine *et al.*, 2013). Maximum water levels recorded during Hurricane Ike on Galveston Island, measured from Pleasure Pier's tidal gauge, reached 3.14 meters and caused severe erosion to the beach and foredune system. Coastal protection practices such as dune restoration and beach nourishment are encouraged by the city to increase resilience to coastal erosion (Galveston, TX Code of Ordinances).

Purpose and Objectives

The purpose of this research is to gain an understanding of the morphodynamic response of a developed barrier island during an extreme storm using a two-dimensional dune-erosion model, XBeach. Using the calibrated model, this study was further designed to test the efficacy of hypothetical coastal protection projects in mitigating coastal flooding and erosion caused by an extreme storm event. This study meets the following objectives:

1. Visually explain the morphologic evolution of a subsection of Galveston Island, TX during Hurricane Ike.
2. Digitize a two-dimensional dune restoration and beach nourishment project using geospatial techniques.
3. Determine the approximate dimensions of an artificial foredune needed to protect against the waves and surge during Hurricane Ike.
4. Determine the efficacy of a designed project to mitigate coastal erosion on Galveston Island.

Coastal Dynamics and the Barrier Island Framework

Fundamental to applied coastal geomorphology is the study of coastal processes - waves, currents and tides, and how they drive coastal landform development over time. The resulting morphological changes over time affect the waves and currents in return. The entire process is therefore a dynamic cycle, which is commonly referred to as morphodynamics. This study is focused on a barrier island's morphodynamic response to an extreme storm. To begin the study, a description of a barrier island's geomorphology and its response to the driving forces is discussed.

A barrier island is defined as an elongate, usually shore parallel, island composed dominantly of unconsolidated sediment. Barrier islands protect the adjacent land mass from which they are separated by some combination of open water and wetland environments (Davis, 1994). A barrier island can be divided into geomorphic zones based on their depositional environment and the processes which shape them. Figure 1A shows a diagram of a cross-shore profile of a typical progradational barrier island in the Gulf of Mexico. The subaerial zones of a barrier island typically consist of an intertidal, seaward sloping foreshore leading to a beach berm with a flat or gently sloping backshore extending to the toe of the foredune. The foredune is marked by a rapid rise in elevation, cresting at the highest elevation on the island, typically, before decreasing in elevation and merging with barrier flats, or a ridge and swale topography. Back-island dunes may or may not be present before merging with a marsh and tidal flat. This study is focused on the interaction of marine processes on the Gulf-facing side of the barrier island, therefore, the subaqueous offshore profile is further explained in the following sub-sections (figure 1B), followed by a description of the beach and foredune system.

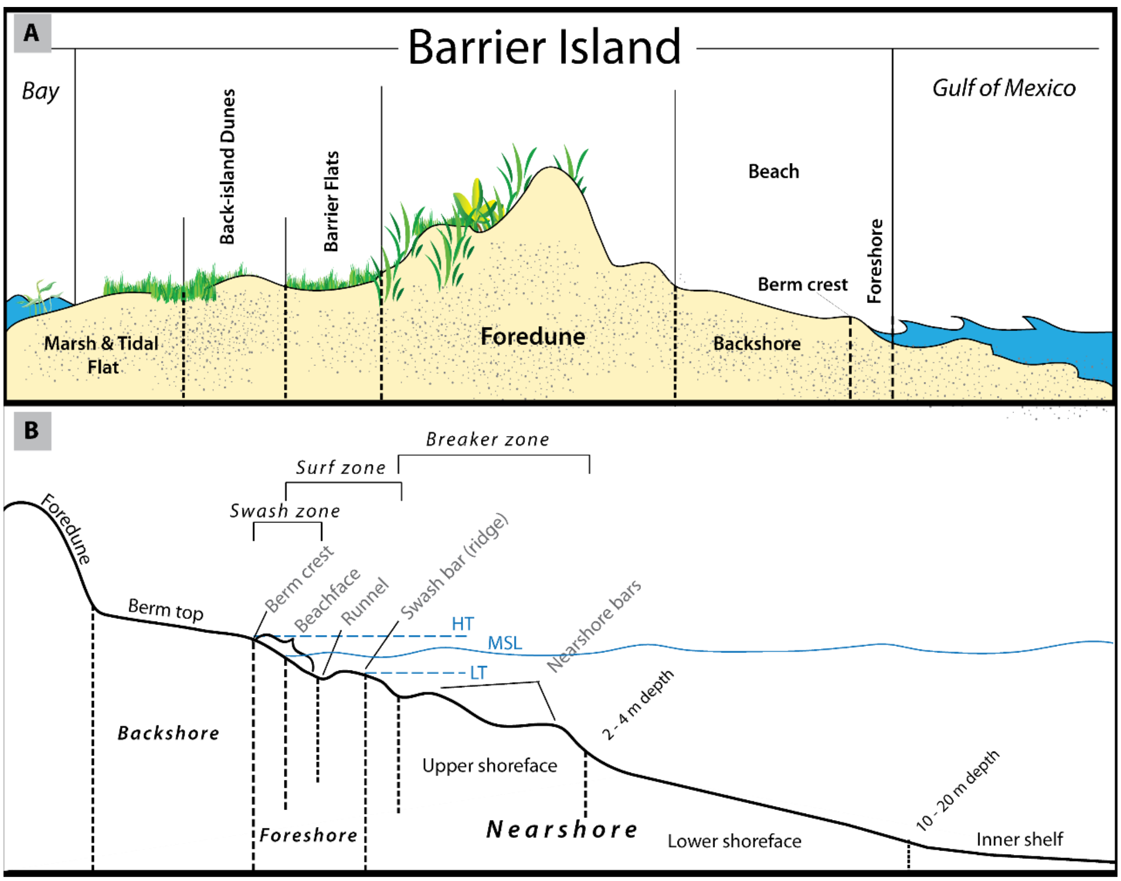

Figure 1. (A) A typical progradational barrier island cross-shore profile. (B) The subaqueous profile of a barrier island.

Nearshore

Shoreface. The nearshore is comprised of the shoreface, the breaker zone and part of the surf zone until reaching the low tide line. Niedoroda *et al.* (1984) discuss the shoreface morphodynamics on wave-dominated coasts. The shoreface extends from the edge of the inner continental shelf to immediately seaward of the surf zone or the breaker zone. The shoreface has a concave upward shape with the steepest slope near its top. The depths of the upper and lower boundaries of the shoreface are variable depending on the local sediment supply and the wave and current climate. The shoreface profile strives toward an equilibrium shape in response to an unconsolidated coast to the typical wave and current regime of a region (Bruun, 1962; Niedoroda and Swift, 1981). Strong onshore winds during storm events generate high waves and bottom currents moving offshore due to downwelling over the shoreface. Strong offshore winds following the storm rapidly reduce wave heights and cause onshore bottom currents due to upwelling over the shoreface. The net bedload transport is offshore as more energy is generated during downwelling flow (Niedoroda *et al.*, 1984). The upper shoreface forms a reservoir for sand removed from the surf zone during storm events. The sand generally returns to the surf zone and beach during non-storm conditions (Houser *et al.*, 2008; Houser *et al.*, 2015; Leatherman, 1976; Morton *et al.*, 1994). Shorefaces can be erosional or depositional features depending on the local supply of coastal sediments from longshore processes and slow changes in relative sea level (RSL) (Niedoroda *et al.*, 1984).

Breaker zone. The breaker zone is where waves start to break, which happens when the water depth reaches about 1.3 times the breaker height (Munk, 1949). The location of this zone also varies at different beaches. Within this environment are multiple longshore sandbars (also called breaker bars) and intervening troughs, typically parallel to the shoreline, and are formed by the breaking waves. Troughs serve as channelways for longshore currents. Waves generally break only over the innermost bar except under high wave conditions. Sand is also stored in the nearshore bars during a storm and is redeposited onto the foreshore by wave runup and landward bar migration (Morton *et al.*, 1994).

Foreshore

Surf zone. The foreshore is the most dynamic subenvironment of the barrier island profile because it is continually subject to wave action. The foreshore extends from the low tide line to the berm crest and includes the surf and swash zones. The surf zone extends from mean sea level into the nearshore until it comes in contact with the breaker zone. Waves are generally small or diffuse in the surf zone, but longshore currents are strong (McGowen *et al.*, 1977). Wright and Short (1984) discuss the variability of surf zones and beaches. The different states of the beach (reflective, dissipative, or intermediate) are distinguished on the basis of the surf-scaling parameter, ϵ. The surf zone widens and turbulent dissipation of incident wave energy increases with increasing ϵ:

$$\epsilon = \frac{a_b \omega^2}{g\ tan^2 \beta}$$

where a_b is the breaker amplitude, ω is incident wave radian frequency ($2\pi/T$; T = period), g is acceleration due to gravity and β is beach/surf zone gradient (Guza and Bowen, 1977; Guza and Inman, 1975). The slope of the beach (β) is controlled by the size of the sand and the intensity of wave action (Bascom, 1951). Fine grained beaches have a relatively flat profile compared to beaches with larger grain sizes. The surf-scaling parameter is used to describe the ways in which energy was reflected or dissipated from a beach under different breaker types. When $\epsilon \leq 2.5$, breakers are of the surging type, and a large proportion of the incident wave-energy is reflected from the beach back into incoming waves. When $\epsilon > 2.5$ waves begin to plunge, dissipating energy and when $\epsilon > 33$ they showed that spilling breakers formed and most wave-energy is dissipated within a wide surf zone. A dimensionless parameter, Ω, is used to identify threshold values which separate the reflective and dissipative extremes:

$$\Omega = \frac{H_b}{\varpi_s T}$$

Where H_b is the breaker height, ϖ_s is the sediment fall velocity, and T is the wave period. The surf zone width expands with increasing Ω and contracts with decreasing Ω (Wright and Short, 1984).

Swash zone. The swash bars, also called ridges, develop from an antecedent dissipative profile in an accretionary sequence (Wright and Short, 1984). The runnel is a shallow trough that separates the ridge from the beach. The ridge and runnel system are heavily influenced by waves and tides. The landward migration of these intertidal swash bars also aid in the post-storm recovery of the beach (Morton *et al.*, 1994). The landward sediment transport is caused by breaking wave-generated currents, and depending on the tidal range, it takes about two weeks to more than a month for the ridge to migrate onto the upper intertidal beach (Hine, 1979). Once the ridge welds onto the beach, it becomes subject to the back and forth movement of the swash zone. The swash zone is the area on the beach face and bermtop where the uprush and return of water following the final wave break occurs. Clifton *et al.* (1971) describe the wave orbital velocities, sediment transport and water movement between the swash zone and the surf zone. Within the seaward half of the surf zone, the landward surge remains stronger than the seaward surge. In and immediately seaward of the swash zone, the seaward water movement is more significant in the transport of sediment along the seafloor. On gently sloping beaches, the dominance of seaward surge continues a longer distance seaward of the swash zone in comparison to steep sloping beaches.

Wave runup. The elevation of wave runup is essential in designing coastal engineering projects and can be used in making storm impact predictions, as wave runup delivers much of the energy responsible for dune and beach erosion (Ruggiero *et al.*, 2001; Sallenger, 2000). Wave runup is the time-varying elevation of water level at the shoreline, measured in reference to the still water level (SWL). The complex process has been studied and described through theory, laboratory flume experiments, and evaluation of field data (Bowen *et al.*, 1968; Hunt, 1959; Holman and Sallenger, 1985; Holman, 1986; Longuet-Higgins and Stewart, 1964; Stockdon *et al.*, 2006). Wave runup occurs when a wave breaks and is propelled onto the beach, and it consists of two parts: wave setup and swash (figure 2). Wave setup is the mean water surface elevation over time, and swash is the time-varying location of the intersection between the ocean and the beach. The elevation of wave runup, *R(t)*, is calculated from a common set of environmental parameters: the slope of the forebeach, β_f, the deep-water wave height, H_0, and the deep-water wave length, L_0. Stockdon *et al.* (2006) developed an empirical parameterization for estimating extreme runup, defined by the 2% exceedance value, on natural beaches over a wide range of conditions. The following expression may be used to calculate the runup over the full range of beach conditions (dissipative, intermediate, and reflective beaches):

$$R_2 = 1.1\left(0.35\beta_f(H_0L_0)^{\frac{1}{2}} + \frac{\left[H_0L_0\left(0.563\beta_f^2 + 0.004\right)\right]^{\frac{1}{2}}}{2}\right)$$

For highly dissipative beaches, the slope of the foreshore can be excluded from the calculation. Runup is then calculated with the following equation:

$$R_2 = 0.043(H_0L_0)^{\frac{1}{2}}$$

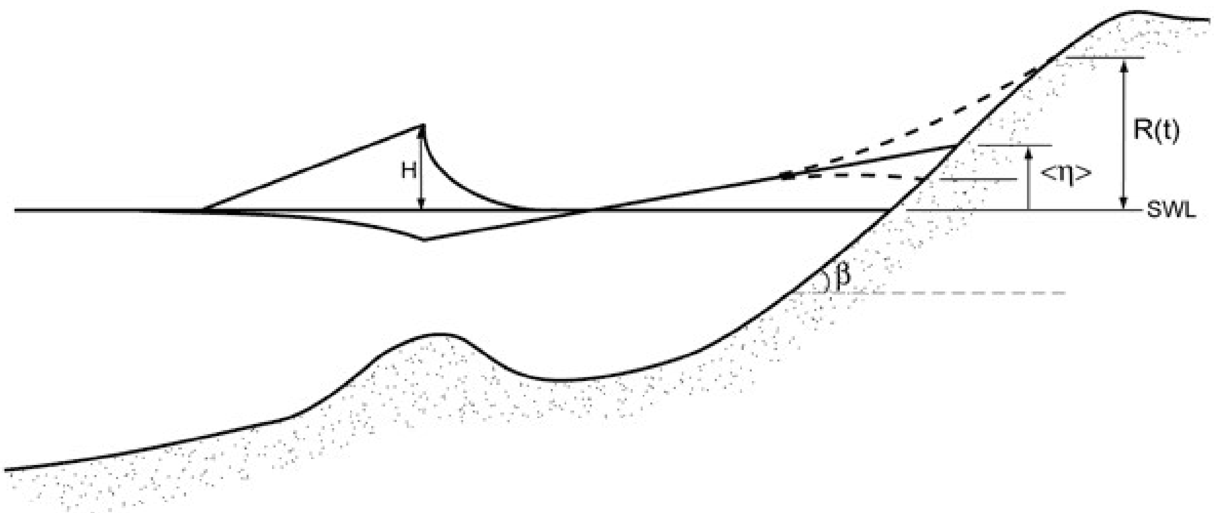

Figure 2. The schematic shows the breaker height (H), the still water level (SWL), the slope of the foreshore (β), wave runup (R), and its components, time-averaged wave setup (η) and time-varying swash (dashed line). From USGS Coastal and Marine Science Center (https://coastal.er.usgs.gov).

Backshore and Foredunes

Beach/dune interaction. The backshore berm extends from the berm crest to the dune toe. Its width is dependent upon the availability of sediment in the littoral system, as well as the geomorphology of the adjacent land. The backshore berm provides the basal surface for foredune development (McLean and Shen, 2006). During non-storm conditions, sand is transferred from the backshore to the dune. Hesp (2002) discussed the morphological development of established foredunes. Foredunes can be classified into two main types, incipient and established. Incipient foredunes are new, or developing foredunes forming within pioneer plant communities. Morphological development primarily depends on plant density, distribution, height and cover, wind velocity, and rates of sediment transport. Secondary factors involved in foredune development are the rate and occurrence of swash inundation, storm wave erosion, overwash incidence, wind direction, beach width, and seasonal climate variation. Psuty (1988) discusses the inter-related nature of beaches and dunes. He proposes dune development is fostered and enhanced under conditions of a net negative sediment budget whereby the dune is positive and the beach is negative. Finally, foredunes play at least three important roles during storm conditions: they function as sand reservoirs, energy dissipaters, and barriers to storm waves and swash (Leatherman, 1979). Seaward transport of sand caused by erosion of the foredune and beach leads to development of an offshore storm bar which further aids in dissipation of wave-energy during storm events (Leatherman, 1976). Dunes are also important sources of sediment to the subaerial beach during storms. Leatherman (1979) states barrier dunes are effective buffers to high-energy surf if the shoreline is relatively stable or accreting. If the immediate shoreline is rapidly eroding, dunes cannot be relied upon over the long term without beach nourishments.

Post-storm recovery. The resiliency of a barrier island is dependent upon the rate of post-storm dune recovery. The long-term mobility of these coastlines are partially controlled by intense storms that transport large volumes of sand moderate distances in brief periods (Morton *et al.*, 1995). A study performed by Morton *et al.* (1994) tracked beach and dune recovery following Hurricane Alicia (1983) along Galveston Island, TX. The study describes the stages of post-storm recovery of fine-grain sand beaches along a microtidal coast. The results of their study found four stages of recovery, lasting 4 to 5 years. Stage 1 is rapid forebeach accretion, which occurs immediately after the storm-wave energy wanes. The sand that was stored in the nearshore bars and on the upper shoreface is redeposited by wave runup onto the foreshore and by the landward bar migration. Stage 2 is backbeach aggradation. The predominant processes occurring here are minor flooding of the backshore and aeolian transport of sand just seaward of the erosional escarpment. High winter waves narrow and steepen the beach by eroding the foreshore and depositing the sand on the backshore, creating a high berm crest. The raised backshore elevations reduce frequency of flooding and encourage the formation of incipient dunes. This occurs after the second post-storm summer and does not progress to the next stage of recovery until the beach reaches a width of 50 m and a height of 1.5 m. Stage 3 is foredune formation. This stage emphasizes the accumulation of wind-blown sand and the re-establishment of backshore vegetation. This stage could take years depending on the extent of ground cover before the storm and the depth of scour. Stage 4 is foredune expansion and vegetation recolonization, occurring as the dunes have grown taller and the extent of ground cover has increased. The narrow beach width on developed beaches limited dune recovery, and only undeveloped beaches went through all stages of post-storm recovery. The post-storm dune height was unable to reach pre-storm height due to the lack of new sediment. Morton and Paine (1985) documented the impacts of Hurricane Alicia on Galveston Island and placed those changes in the context of storm history and shoreline stability. Following the post-storm recovery period after Hurricane Carla in 1961, research indicates the average annual rate of erosion accelerated due to removal of sand from the littoral system. Morton *et al.* (1995) extended upon this study to include a decadal analysis of shoreline movement and transfer of sand during and after a storm between two barrier islands separated by a tidal inlet. Results from their study reveal beach erosion vulnerability partly depends on the antecedent beach state, which in turn depends on the frequency of storms and the recovery period.

Coastal Modeling for Forecasting Coastal Change

Storm-induced coastal change results from a combination of the physical processes associated with the storm as well as the geomorphology of the impacted coastline. To mitigate the damage caused by such storm processes and to forecast coastal response to storms, coastal morphology models are essential. Various empirical, analytical, and process-based models have been developed to simulate and predict coastal erosion and dune overwash. Examples include conceptual models (Plant and Stockdon, 2012; Sallenger, 2000), to numerical models (Kriebel and Dean, 1985; SBeach : Larson and Kraus, 1989). These models, however, assume uniformity in the longshore dimension and therefore do not account for longshore variations in the dune profile, sediment transport, and hydraulic forcing. Studies have shown that coastal erosion and dune overwash is highly influenced by spatial variations in the topography and forcing (Donnelly *et al.*, 2006; Houser *et al.*, 2008; Stockdon *et al.*, 2007; Thornton *et al.*, 2007). XBeach, which stands for eXtreme Beach behavior model, is the first two-dimensional, depth-averaged (2DH) numerical model to assess the natural coastal response during time-varying storm and hurricane conditions (Roelvink *et al.*, 2009).

XBeach is designed to model processes in different regimes described by Sallenger (2000). Sallenger (2000) proposed a qualitative storm-impact scale that compares hydrodynamics (storm surge, tides, and wave-induced water levels (R_{high} and R_{low}) and pre-storm elevation of the dune crest (D_{high}) and dune toe (D_{low}) to forecast the expected type of coastal response. With the implementation of such parameters, the erosive impacts of a storm can be classified into four regimes: swash, collision, overwash, and inundation (figure 3). Under the swash regime, wave runup is confined to the forebeach ($R_{high} < D_{low}$). The forebeach erodes and sand is transported and deposited offshore then returns to the beach within weeks to months. The collision regime occurs under more severe conditions. Waves will reach the dune toe causing dune erosion by scarping ($D_{low} < R_{high} < D_{high}$). The eroded sand is transported seaward and leads to a longer recovery. Under the overwash regime, a further increase in wave height, or a decrease in dune height, will allow waves to overtop the dune and cause dune erosion as well as landward sediment transport ($R_{high} > D_{high}$). Impacts may be more long-lasting, or even permanent. And last, the inundation regime occurs under the most severe conditions. The combination of storm surge, tides, and wave setup exceeds the dune crest elevation ($R_{low} > D_{high}$). The beach system is completely submerged, allowing wind and wave-driven currents to alter erosion and deposition patterns over the entire island. Sallenger's classification method is routinely applied to forecast coastal erosion hazards. However, it does not provide a quantitative measure of the storm-induced erosion of the protective dunes, and again it assumes uniformity in the longshore dimension with regard to hydrodynamic forcing and sediment transport.

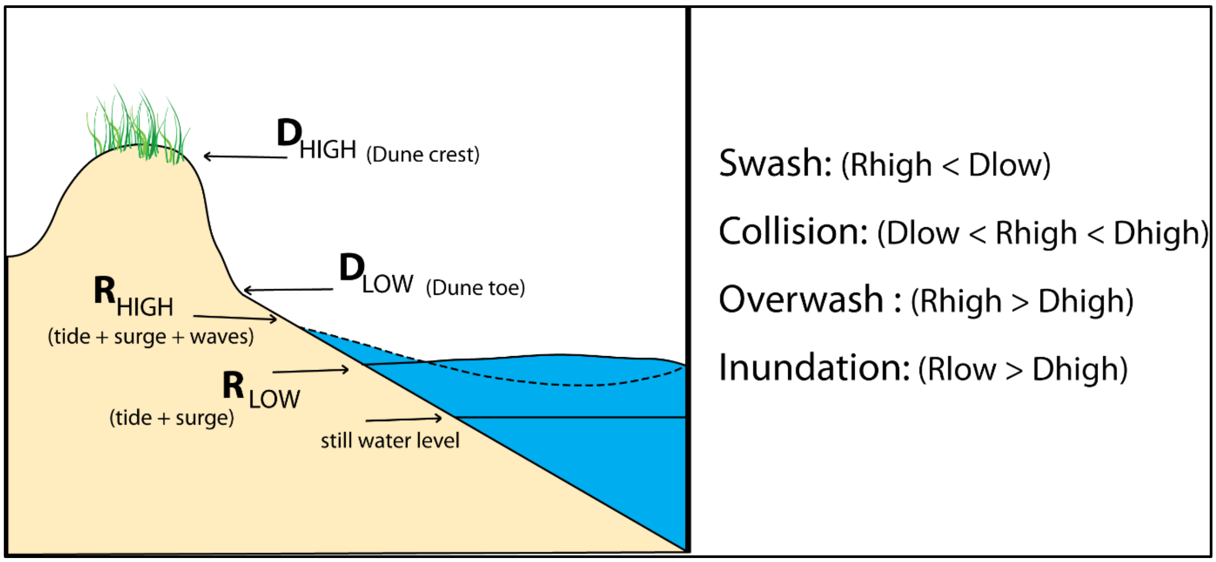

Figure 3. Schematic describing Sallenger's (2000) storm-impact model and the four regimes (modified from Sallenger, 2000).

XBeach is open-source, first developed in 2007, and has since been tested and validated through laboratory flume experiments and field cases both in 1D and 2D mode (de Vet *et al.*, 2015; Lindemer *et al.*, 2010; McCall *et al.*, 2010; Mehvar *et al.*, 2015; Roelvink *et al.*, 2009; Van Theil de Vires, 2009). The XBeach model solves coupled 2D horizontal equations for wave propagation, flow, sediment transport, and bottom changes for varying wave and flow boundary conditions. In order to resolve the swash dynamics, the model takes into account the variation in wave height over time. To model the collision regime, slumping and avalanching mechanisms are triggered by the combination of infragravity swash runup on the previously dry dune face and the defined critical wet slope. The overwash morphodynamics are taken into account with the wave-group forcing of infragravity waves in combination with a momentum-conserving drying/flooding formulation and simultaneous sediment transport and bed level changes. With these innovations, XBeach is better able to model the morphological development throughout the regimes. Further description of the XBeach model can be found in section 3 of this paper.

Hurricane Ike

Hurricane Ike has been a subject of significant interest for researchers due to its large size, its varied response physics, and the availability of measured wave and water level data. The storm system traveled a great distance, impacting several regions throughout its journey across the Atlantic and into the Gulf of Mexico. On September 1, 2008, a tropical wave 1,250 km west of Cape Verde was identified as a tropical depression (Berg, 2009). That same day, Tropical Storm Ike became the ninth named storm of the 2008 hurricane season. By September 4, Ike was in the western Atlantic and had intensified to a category 4 storm. Hurricane Ike continued on a west, southwesterly path and crossed the Gulf of Mexico making landfall on Galveston Island, TX at 2 a.m. on September 13, 2008 as a strong category 2 storm. Hurricane Ike was a unique storm attributed to the largest freely-propagating shelf wave ever reported (Kennedy *et al.*, 2011). A large, unpredicted storm surge appeared along a substantial section of the western Louisiana and northern Texas coasts 12-24 hours before Ike made landfall. The forerunner surge is proposed to be generated by Ekman setup, which is most significant on wide, shallow shelves subject to large wind fields. The forerunner surge generated a freely propagating continental shelf wave that travelled coherently along the coast to Southern Texas, and was 300 km in advance of the storm track at landfall. Hurricane Ike generated a very high storm surge for a category 2 storm, with the maximum surge height recorded at 5.3 meters in Chambers County, TX, located to the northeast of Galveston Island (FEMA, 2008). Ike is one of the top five most damaging hurricanes on record in the United States with damage estimates totaling $29 billion (Berg, 2009).

Various studies have quantified the amount of coastal erosion caused from Hurricane Ike (Doran *et al.*, 2009; Harter and Figlus, 2017; HDR, 2014). Doran *et al.* (2009) and HDR (2014) relied on pre- and post-storm lidar to derive shoreline change statistics and to calculate volume change of the beach and dune system. This method only provides a before and after snapshot of the event. The XBeach model is able to describe and quantify the morphodynamic response with hourly outputs during the entire passage of the storm. Harter and Figlus (2017) used XBeach to model the real-time morphodynamic response of the beaches and dune system on Follets Island, TX during Hurricane Ike. No study exists which utilizes the XBeach model as a tool for quantifying Galveston Island’s real-time response to Hurricane Ike.

CHAPTER II: STUDY AREA

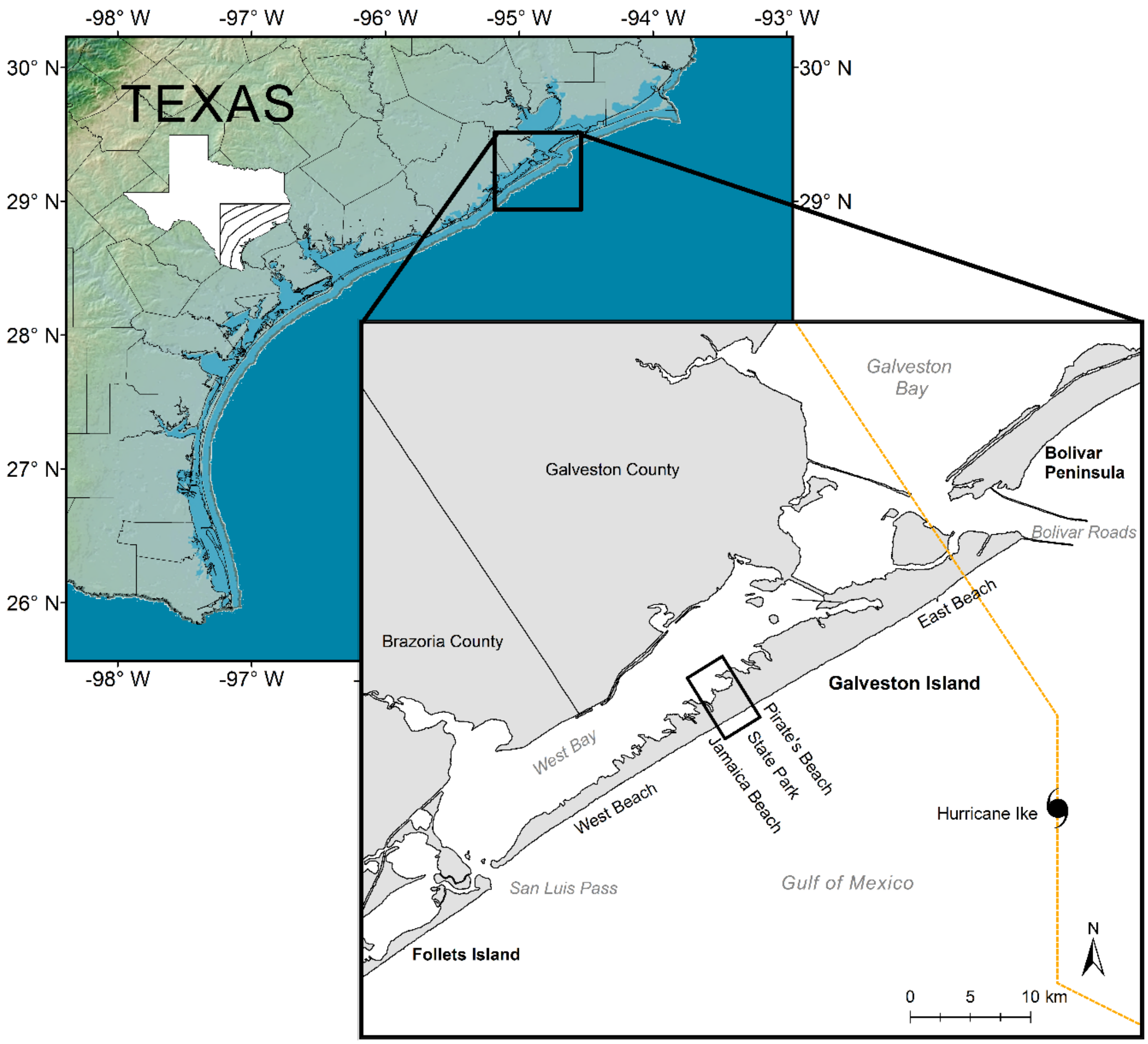

Figure 4. Map showing study area and Hurricane Ike track. Small black rectangle on Galveston Island shows location of XBeach domain.

This study is focused on Galveston Island which is located on the Upper Texas Coast (UTC). Galveston is a 46-km-long, 1-to-5 km wide barrier island. The island becomes progressively narrower to the southwest and is oriented at an angle of approximately 235°. The area of interest within the domain for the XBeach model is about 2.6 km alongshore, located at Galveston Island State Park (GISP) and extends into the town of Jamaica Beach, located towards the central section of the island (figure 4). This location was chosen due to the absence of human structures adjacent to the shoreline, which is beneficial for initial calibration of the XBeach model. Directly northeast of GISP is Pirate's Beach which is heavily developed and contained geotextile tubes buried under the foredunes, intended to help prevent erosion. The eastern end of the island is also heavily developed and protected by a 16-km-long seawall and groin field.

Processes setting

Galveston Island's morphology is characteristic of a wave-dominated, microtidal coast (Hayes, 1979). Shallow water waves generally approach the coast from the southeast with mean significant wave heights (Hs) of 1.2 m and mean peak wave period (Tp) of 5.8 s (Herbertz and Brooks, 1989). Tides are predominantly diurnal with a range of 0.62 m as measured from the Gulf-facing Pleasure Pier tide gauge. The predominant direction of sediment transport is to the southwest. Due to its shoreline orientation and seasonal wind patterns, the direction of littoral drift reverses periodically.

Galveston Island is experiencing an increase in relative sea level that averages 6.47 mm/yr, measured from over 100 years of sea level data at Galveston Pier 21, located in the Galveston Channel on the east end of the island (figure 5). This rate is greater than the global eustatic sea level rise rate over the 20^{th} century of 1.0-2.0 mm/yr (Church and White, 2011). This sea level trend, accompanied with other processes such as sediment influx and storm frequency results in shoreline change rates that vary from -3.6 to 5.6 m/yr (Paine *et al.*, 2012) (figure 6). This rate is calculated as a net shoreline change from 1950 to 2012.

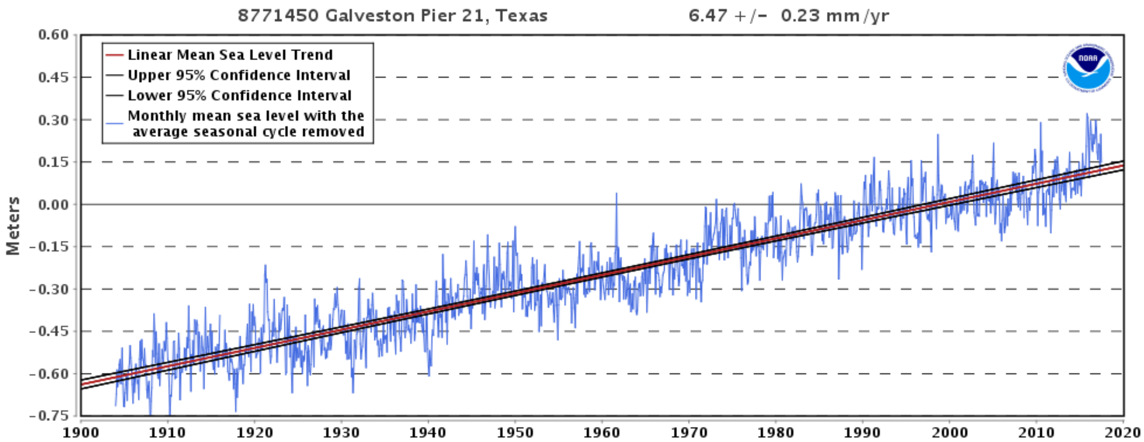

Figure 5. Plot showing monthly sea level trends for Galveston Pier 21. From NOAA (https://tidesandcurrents.noaa.gov)

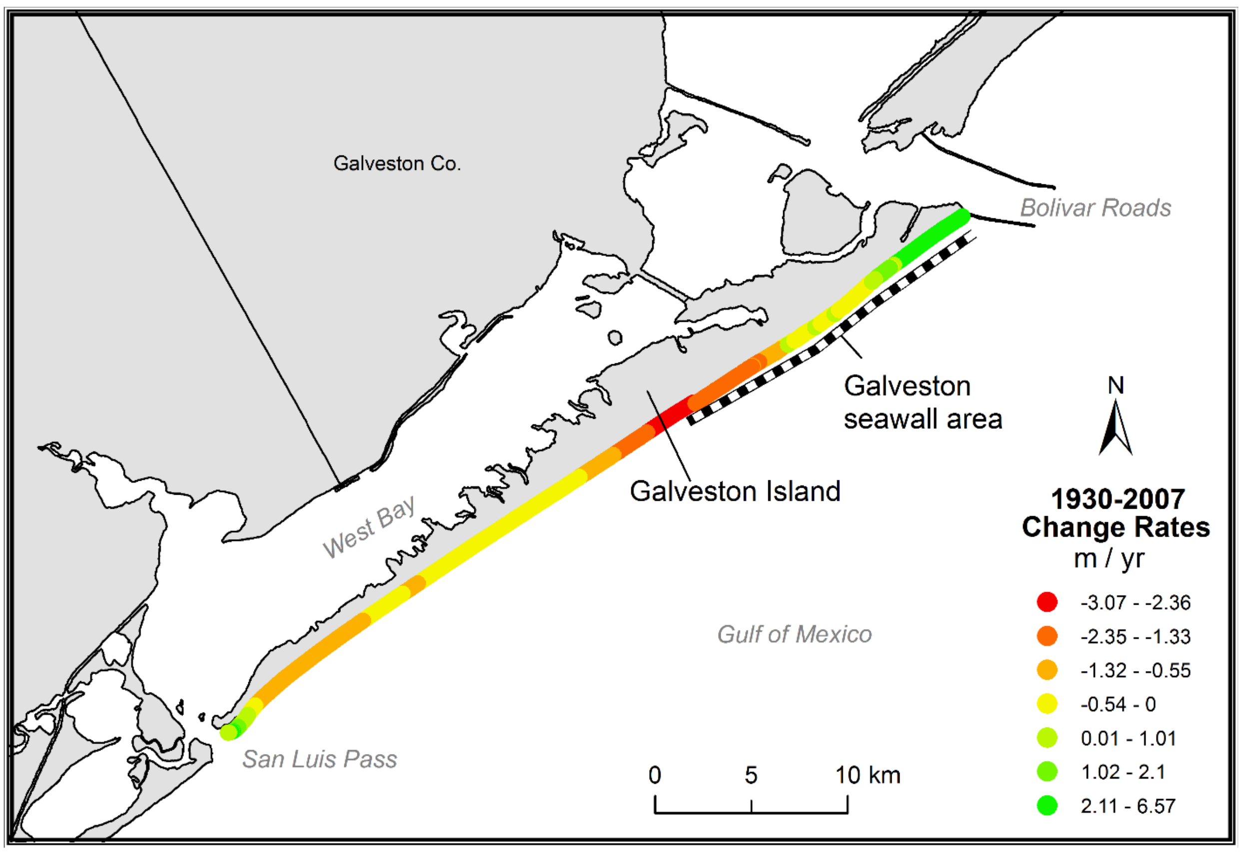

Figure 6. Map showing net shoreline change rates from 1930 to 2007. Data courtesy of The University of Texas Bureau of Economic Geology

The impact of storms is an important process affecting the erosional state of the island. Along any 50 mile stretch of the Texas coast, the frequency of hurricanes is about one every six years, while the annual average for a tropical cyclone or hurricane is 3 per every 4 years (Roth, 2013). Galveston Island has been directly hit by several hurricanes over the century, causing severe erosion to the topography and destroying development on the island (FEMA, 2008; Gibeaut *et al.*, 2002; Morton *et al.*, 1995; HDR, 2014; Roth, 2013; USACE, 2015). The most critical parameters that influence erosion potential are surge height and surge duration. The longer the surge remains elevated above normal heights, the greater the potential for redistribution of sediment eroded from the beach and dunes. This becomes an even greater issue for beaches that are shorter in width and have low lying foredunes, as is the case on undernourished beaches on Galveston Island. Hurricane Alicia struck the western end of Galveston Island in 1983 as a Category 3 storm with a maximum open coast surge of 3.8 m that lasted about 3 hours. The large amount of destruction from the storm was directly related to the beach and dune erosion resulting in a vegetation line retreat of as much as 40 m (Morton and Paine, 1985). Hurricane Ike, a Category 2 storm, caused shoreline erosion averaging 67 m (HRI, 2009). Both of these storms obliterated the dunes and required reconstruction of the pre-existing dunes in order to complete post-storm beach recovery (Morton *et al.*, 1994; HRI, 2012). Tropical storms and hurricanes that occur in the Gulf of Mexico but do not directly strike the island can also cause coastal erosion, especially if storms occur before the beach has enough time to recover. Tropical Storm Josephine in 1996 made landfall on the Florida Panhandle, yet still caused a vegetation-line retreat of 5 to 15 m along western Galveston Island (Gibeaut *et al.*, 2002). Two years later, Tropical Storm Frances made landfall north of Corpus Christi, about 250 miles southwest of Galveston. Frances completely eroded foredunes that rose only 2.5 m above berm tops and caused vegetation line retreats of 15 to 25 m (Gibeaut *et al.*, 2002).

Geomorphic setting

Galveston Island is classified as a progradational barrier island based on the prominent display of ridge and swale topography and an overlapping facies architecture (Bernard *et al.*, 1970; Morton, 1994). Overwash channels, which formed when the island was still narrow, are abundant on the landward side of the island. Seaward progradation of the island ended about 2,000 years ago, and since that time the island has been eroding. Due to the erosional rate of both the shoreline and the bayline and a high rate of relative sea level rise, the island is essentially drowning in place (Gibeaut *et al.*, 2003; Paine *et al.*, 2012).

The beaches on Galveston Island are about 50 to 60 m wide at low tide, and slope gently toward the Gulf (Morton *et al.*, 1995). This gentle slope is attributed to the unimodal distribution of fine grained sands averaging around 0.13 mm (Boscom, 1951; Lisle and Comer, 2011). West of the seawall, Galveston Island is protected by densely vegetated discontinuous foredunes averaging less than 3-m-tall and 30-m-wide. These dunes provide protection from a 20-year storm or less (Paine *et al.*, 2013). A 20-year storm has a maximum surge of 1.91 m, a maximum wave height of 5.85 m, and a peak wave period of 12.3 s (Paine *et al.*, 2013). The threshold for episodic beach erosion on Galveston Island are open-coast water levels that exceed 0.9 m above MSL and coincident wave heights that exceed 3 m for at least 12 hours (Gibeaut *et al.*, 2002). These conditions will be lower if beaches and dunes have not fully recovered from a previous storm.

Based upon the morphology and process signatures observed offshore Galveston Island, the beach and surf zone is regularly in a dissipative state (Wright and Short, 1984). On a normal day, Galveston Island's surf zone has a relatively low gradient of $tan\ \beta = 0.01$ and a wide multi-barred surf and breaker zone (~100-200 m) (Rogers and Ravens, 2008). The first bar is located at the toe of the forebeach, and the third bar is located in water depths of about 3 m (Morton, 1988). Waves break by spilling and dissipating progressively as they cross the surf zone to become very small at the beachface. The beach state changes to intermediate during and immediately after a storm, when the beach slope steepens, waves begin to plunge and runup is high (Morton *et al.*, 1994). The increased energy creates rip currents and infragravity waves dominate the spectrum (Guza and Thornton, 1982; Holman *et al*., 1978; Wright and Short, 1984).

Galveston Island's geomorphology is influenced by two prominent tidal deltas: Bolivar Roads to the northeast and San Luis Pass to the southwest. Bolivar Roads is highly influenced by anthropogenic activities such as dredging and the construction of jetties, while San Luis Pass is almost entirely natural. San Luis Pass is a smaller delta with both a prominent flood- and ebb-tidal delta (Israel *et al.*, 1987). A net advance of shoreline is occurring on the east and west end of the island as a result of sediment influx related to these inlets (Paine *et al.*, 2012) (figure 6). Research suggests San Luis Pass is a sediment sink of at least 76,000 m^3/yr. The ebb shoal may contain 3.1 million cubic meters of sand, however growth or loss rates are unavailable (Morang, 2006). Morang (2006) suggests the sand flux for the Bolivar Roads tidal inlet system equals ~389,000 m^3/yr, of which ~189,400 m^3/yr can be attributed to longshore transport to the east and west.

Shoreface sands extend on average about 3 to 5 km offshore to depths of 10 m and rarely deeper than 12 m (Wallace *et al.*, 2010; Morton *et al.*, 1995). The change in sand volume for any length of beach is proportional to shoreline change and the sum of the berm height and the depth of closure (Ravens and Sitanggang, 2007). The depth at which sediment transport becomes negligible (the depth of closure) is debated in literature for this study area. A long-term time-sequence of cross-shore profiles is not available along Galveston Island. Knowledge of the value for the depth of closure is necessary in calculating the sediment budget for an area, which in turn is necessary for improving management of sand resources and beach nourishment projects. Morang (2006) and Ravens and Sitanggang (2007) both use a value of 4 m for the depth of closure, based on negligible changes in before and after bathymetric profiles. Morang (2006) relied on bathymetric profiles, sediment grab samples, dredging records, aerial photographs and elevation data to develop a sediment budget for the UTC. Ravens and Sitanggang (2007) used GENESIS modeling to determine the amount of sand needed to maintain the 2001 shoreline on Galveston Island. Other studies have looked at seismic, core, and bathymetric data, which indicate a value of at least 8 m for the depth of closure (Anderson *et al.*, 2004; Rodriguez *et al.*, 2001). The difference in calculated sediment flux for the UTC between these two values is quite significant. Wallace *et al.* (2010) calculated the sediment flux between 4 and 8 m depths for the UTC using previously collected offshore profile core data to determine radiocarbon ages of the sediment. In contrast to Morang (2006) and Ravens and Sitanggang (2007), their study also included the sand contributions from storm impacts and represents sediment transport over the last 2660 years. Ravens and Sitanggang (2007) determined nourishing the seawall and West Beach along Galveston Island would likely require ~400,000 m^3/yr. The study by Wallace *et al.* (2010) determined the shoreface environment between 4 and 8 m sequesters ~160,000 ± 39,000 m^3/yr sand from the east end of Bolivar Peninsula to the west end of Follets Island. This equals 17% of the entire previously estimated sediment flux, and 37% of the previously calculated total longshore flux. The extension of the closure depth increases the volume needed to successfully nourish beaches on Galveston island by at least ~115,000 ± 28,000 m^3/yr (Wallace *et al.*, 2010).

CHAPTER III: METHODS

XBeach model physics

XBeach was developed by UNESCO-IHE, Delft University of Technology, Deltares and University of Miami with funding from the USACE MORPHOS-3D project. XBeach is written in Fortran 90/95. The model uses a staggered grid in which conservative quantities such as bed level and water depth are calculated in the cell centers, while fluxes such as sediment transport and velocities are calculated in the cell interfaces. The different functionalities of XBeach are divided amongst four main modules made up of two hydrodynamic modules and two morphodynamic modules (figure 7). In a single numerical step, each module is called in a specific sequence. XBeach starts with the short wave module where radiation stress gradients are calculated. The flow module uses the given output of radiation stress gradients from the short wave module to calculate surface elevations and velocities. Wave and current output from the short wave and flow modules are used in the sediment transport module, and eventually the flow and sediment transport modules update the bed level in the morphology module. In the new time-step, the short waves module uses the output from the morphology and flow modules.

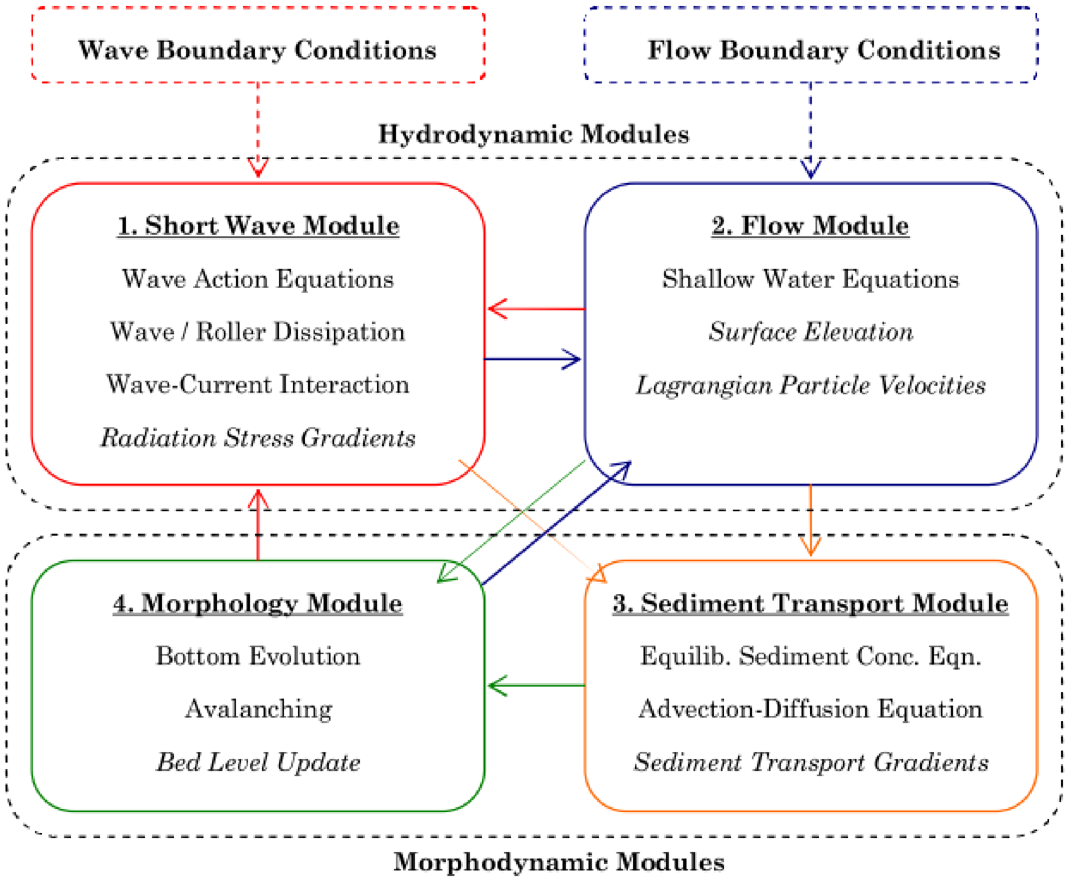

Figure 7. Schematic showing component modules in XBeach. Arrows indicate connectivity.

(from Daly, 2009)

Hydrodynamics. The model uses a time-dependent version of the wave action balance equation defined here as:

$$\frac{\partial A}{\partial t} + \frac{\partial c_x A}{\partial x} + \frac{\partial c_y A}{\partial y} + \frac{\partial c_\theta A}{\partial \theta} = -\frac{D_{waves}}{\sigma}$$

where the wave action, A, is defined by:

$$A(x, y, t, \theta) = \frac{E_{w(x,y,t,\theta)}}{\sigma(x, y, t)}$$

and where E_w represents the wave energy density in each directional bin, θ represents the angle of incidence with respect to the x-axis, σ represents the intrinsic wave frequency, D_{waves}

represents the wave energy dissipation, and c_x, c_y, c_θ represent the wave action propagation speeds in x-, y-, and θ- space respectively.

The roller energy balance is coupled with the wave action balance where calculation of the roller energy balance is derived from the short wave energy dissipation, defined as:

$$\frac{\partial E_{roller}}{\partial t} + \frac{\partial c_x E_{roller}}{\partial x} + \frac{\partial c_y E_{roller}}{\partial y} + \frac{\partial c_\theta E_{roller}}{\partial \theta} = -D_{roller} + D_{waves}$$

where $E_{roller}(x,y,t,\theta)$ represents the roller energy in each directional bin, and D_{roller} represents the total roller energy. According to the linear wave theory, the gradients in radiation stress can be calculated by adding together the roller energy balance and the wave action balance. The radiation stress tensor is then used in the shallow water equations. The shallow water equations are built into a depth-averaged Generalized Lagrangian Mean (GLM) formulation. The Eulerian velocities plus the Stokes drift (in x and y-directions) are replaced with a Lagrangian equivalent. The resulting equations are given by:

$$\frac{\partial u^L}{\partial t} + u^L \frac{\partial u^L}{\partial x} + v^L \frac{\partial u^L}{\partial y} - f v^L - v_h \left(\frac{\partial^2 u^L}{\partial x^2} + \frac{\partial^2 u^L}{\partial y^2} \right) = \frac{\tau_{sx}}{\rho h} - \frac{\tau_{bx}^E}{\rho h} - g \frac{\partial \eta}{\partial x} + \frac{F_x}{\rho h}$$

$$\frac{\partial u^L}{\partial t} + u^L \frac{\partial u^L}{\partial x} + v^L \frac{\partial v^L}{\partial y} - f u^L - v_h \left(\frac{\partial^2 v^L}{\partial x^2} + \frac{\partial^2 v^L}{\partial y^2} \right) = \frac{\tau_{sy}}{\rho h} - \frac{\tau_{by}^E}{\rho h} - g \frac{\partial \eta}{\partial y} + \frac{F_x}{\rho h}$$

$$\frac{\partial \eta}{\partial t} + \frac{\partial h u^L}{\partial x} + \frac{\partial h v^L}{\partial y} = 0$$

where u^L and v^L are Lagrangian velocities, f is the Coriolis coefficient, v_h is the horizontal eddy viscosity, h is the local water depth, τ^E_{bx} and τ^E_{by} are the Eulerian bed shear stresses, η is the water level, and F_x and F_y are the radiation stress tensors from the wave action and roller energy balance.

Morphodynamics. XBeach models sediment transport with the use of a depth-averaged advection-diffusion scheme with a source-sink term based on equilibrium sediment concentrations:

$$\frac{\partial hC}{\partial t} + \frac{\partial hCu^E}{\partial x} + \frac{\partial hCv^E}{\partial y} + \frac{\partial}{\partial x}\left[D_h h \frac{\partial C}{\partial x}\right] + \frac{\partial}{\partial y}\left[D_h h \frac{\partial C}{\partial y}\right] = \frac{hC_{eq} - hC}{T_s}$$

where C represents the depth-averaged sediment concentration, u^E and v^E are Eulerian mean velocities, D_h is the sediment diffusion coefficient, and T_s is an adaptation time scale based on sediment fall velocity and local water depth. The default transport formulation for the equilibrium sediment concentration are calculated according to the Van Thiel-Van Rijn transport equations:

$$C_{eq,b} = \frac{A_{sb}}{h}\left(\sqrt{v_{mg}^2 + 0.64u_{rms,2}^2)} - U_{cr}\right)^{1.5}$$

$$C_{eq,s} = \frac{A_{ss}}{h}\left(\sqrt{v_{mg}^2 + 0.64u_{rms,2}^2)} - U_{cr}\right)^{2.4}$$

where A_{sb} and A_{ss} stand for the bed load and suspended bed load coefficient, U_{cr} is the critical velocity for currents, and u_{rms} is the RMS orbital velocity from wave action. Here A_{sb} and A_{ss} are functions of the median grain size (D_{50}), the ratio of densities of sediment grains to water, and the water depth. Furthermore, U_{cr} is a function of $D_{50,}$ $D_{90,}$ and local water depth.

The bed level is updated based on gradients in sediment transport rates according to:

$$\frac{\partial z_b}{\partial t} + \frac{f_{mor}}{1-p}\left(\frac{\partial q_x}{\partial x} + \frac{\partial q_y}{\partial y}\right) = 0$$

where z_b is the bed level, f_{mor} is a morphological acceleration factor, p is the sediment porosity, and q_x and q_y represent the sediment transport rates in x- and y-directions respectively.

Finally, in order to simulate the slumping of sandy material from the dune face to the foreshore during storms, dune erosion avalanching is introduced to update the bed evolution.

Since inundated areas are much more prone to slumping, two separate critical slopes for dry and wet points are used (default values are 1.0 and 0.3 respectively). When the critical slope is exceeded, material is exchanged between adjacent cells to the amount needed to bring the slope back to the critical slope. Bed level change is then calculated by:

$$\Delta z_b = \min\left(\left(\left|\frac{\partial z_b}{\partial x}\right| - m_{cr}\right)\Delta x, v_{av,max}\Delta t\right), \frac{\partial z_b}{\partial x} > 0$$

$$\Delta z_b = \max\left(\left(\left|\frac{\partial z_b}{\partial x}\right| - m_{cr}\right)\Delta x, - v_{av,max}\Delta t\right), \frac{\partial z_b}{\partial x} < 0$$

where m_{cr} is the critical slope and $v_{av,max}$ is a maximum speed to prevent the generation of large shockwaves due to sudden changes of the bottom level. A more in-depth description with all equations used in the model can be found in the most recent manual (Roelvink et el., 2015).

Model relief development

The fundamental elements in modeling storms with XBeach is the availability of pre- and post- storm topographic data, measured hydrodynamic storm conditions, and bathymetric data of the bay and nearshore. The availability of these data from Hurricane Ike makes Galveston Island a robust testbed for the purposes of this study. The model domain relief was developed by merging bathymetric and topographic data from two sources and interpolating the x-, y- and z-coordinates onto a defined 2-m-resolution regular grid. To accurately model the barrier island's morphologic response to the storm, high-resolution topographic data of the pre-storm surface is essential. The most recent pre-storm high-resolution topographic data over the study area was acquired by a lidar survey during the fall of 2006. In order to validate the XBeach model, computed model results are compared to measured post-storm lidar data. The post-storm lidar data were collected in December of 2008, three months after the storm. The coverage of the pre-and post-storm lidar data extends from the swash zone to approximately 300 m landward into the back barrier flats. The pre-storm bathymetric data is obtained from a digital elevation model (DEM) developed for Galveston, TX in 2007, which covers Galveston Bay and extends offshore to a depth of -25 m. After combining the two pre-storm surfaces, the grid was re-interpolated onto a rectilinear grid with a varying grid size to efficiently model the storm's propagation across the island. The following section describes the data sources used in this project, pre-processing steps, and a description of the model setup.

Data sources

Pre-Ike 2006 lidar. The 2006 lidar survey was performed by Sanborn Mapping Company, Inc. for the Texas Water Development Board (TWBD) and the Federal Emergency Management Agency (FEMA). The data were acquired in LAS format with an average point spacing of 1.5 meters, Universal Transverse Mercator (UTM) zone 15 projection, North American Datum of 1983 (NAD83) horizontal coordinate system, and North American Vertical Datum of 1988 (NAVD88) vertical coordinate system with units in meters relative to Geoid03. The LAS files were interpolated onto a 1-m-resolution raster using inverse distance weighted interpolation, with a fixed search distance of 2 m and a power of 1. Only the last return points were used in the interpolation of the surface. First, heights above 15 m were filtered from the point cloud to eliminate extraneous noise from power lines or birds. Next, the scan angle was filtered from -38 to 44 to -20 to 20. This helped smooth out extraneous undulations that were visible in the first output surface. Last of all, the final interpolated surface was converted from Geoid03 to Geoid99 using NOAA's VDatum application. This was done to match the geoid used in the post-storm lidar data's vertical units. The final output is a pre-Ike DEM.

Post-Ike 2008 lidar. The 2008 post-storm lidar data were acquired by The University of Texas Bureau of Economic Geology (UT-BEG). Data were provided as an ER Mapper compressed image. The second return band was exported from the file to create a new 1-m-resolution DEM with only second return signals. This filtered the data to exclude noise such as birds or power lines. The DEM is projected in the UTM Zone 15 with elevations in meters relative to NAVD88 and Geoid99. Horizontal and vertical positional accuracy were reported for the lidar data. Lidar elevations were compared with ground survey points. Ground points were estimated to have a vertical accuracy 0.01-0.05m. The lidar data was determined to have an average elevation bias ranging between -0.17m and 0.11m with a root mean square error (RMSE) of 0.058m for the second return. Mean elevation differences between the lidar and ground elevations were used to estimate and remove bias from the lidar.

Bias correction. The systematic error between the 2006 and 2008 lidar surveys was assessed through a comparison of elevation values between the pre- and post-storm DEMs. A shape file containing points placed along roads was used to extract elevation values from each raster. The elevation differences between the rasters was calculated using the 2008 surface as the reference elevation. The elevation differences varied greatly across the study area from -0.63m to 0.60m with a mean error of -0.16m and a standard deviation of 0.11m. Because the surface bias varied significantly alongshore, a diffusion kernel raster was created using the points with the calculated difference as the input dataset. The shape file with the points along the roads was copied laterally across the study area, each approximately 40 m apart from the next in order to fill the surface for interpolation. The diffusion kernel uses a Gaussian kernel function which is based upon the heat equation and produces predictions on automatically selected grids. The result is a raster with the same resolution as the pre- and post-storm rasters, with values in each cell corresponding to the interpolated bias. The diffusion raster was then subtracted from the 2006 raster to correct the bias. The resulting error between these two data sources was largely reduced to a mean error of 0.004m and a standard deviation of 0.07.

Galveston DEM. The 2007 Galveston DEM was developed for the Pacific Marine Environmental Laboratory (PMEL) NOAA Center for Tsunami Research by the National Geophysical Data Center (NGDC), an office of the National Oceanic and Atmospheric Administration (NOAA). Several datasets were used to compile the topographic and bathymetric DEM. The bathymetric datasets in the DEM are derived from hydrographic surveys by the USACE, Galveston District, spanning from 1996 to 2006, as well as by the National Oceanic Service (NOS) spanning 1897 to 2002. The resolution of the DEM is 1/3 arc second, approximately 10 m. Data were provided in geographic coordinates with elevations relative to Mean High Water (MHW). The DEM was re-projected to the working coordinate system (UTM) and elevations were converted to NAVD88 using NOAA’s VDatum application.

Grid generation

XBeach uses a coordinate system where the computational x-axis is always oriented towards the coast, perpendicular to the coastline, the y-axis is oriented alongshore with the grid origin at the lower left corner at the offshore boundary (figure 8). This orientation allows the variable x-resolution to efficiently resolve cross-shore features like the foredune.

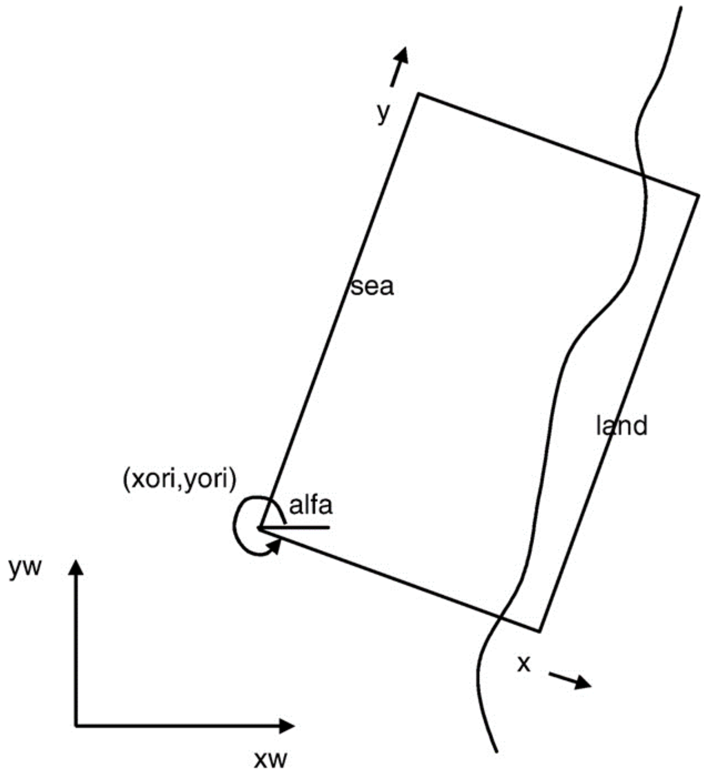

Figure 8. Diagram showing XBeach coordinate system. (From Roelvink et al., 2009)

The XBeach Matlab toolbox, available through OpenEarth tools subversion network, was used to re-interpolate the 2-m-resolution regular grid onto a variable resolution rectilinear grid. The model domain was generated with a function in the toolbox by specifying the x-, y-, and z-matrices, a minimum cross-shore resolution, minimum and maximum alongshore resolution, a rotation component of 123°, and a Boolean indicating to use world coordinates in contrast to a local coordinate system. The variable resolution is automatically calculated using a specified Courant condition of 0.7 with the maximum offshore boundary resolution calculated based on a minimum mean period and the user defined minimum cross-shore resolution. The final cross-shore resolution varied from 25 m at the offshore boundary to 2 m at the shoreline. The longshore resolution varied from 20 m at the lateral boundaries to 5 m at the center of the study area. The model of Hurricane Ike needs to have large shadow zones since waves do not travel perpendicular towards the shore. The waves during Ike approached the shore predominantly from the east and southeast. The model domain is extended both to the northeast and southwest to account for the shadow zone. The final model grid extends 7 km alongshore and 4 km offshore to a depth of 11 m (figure 9).

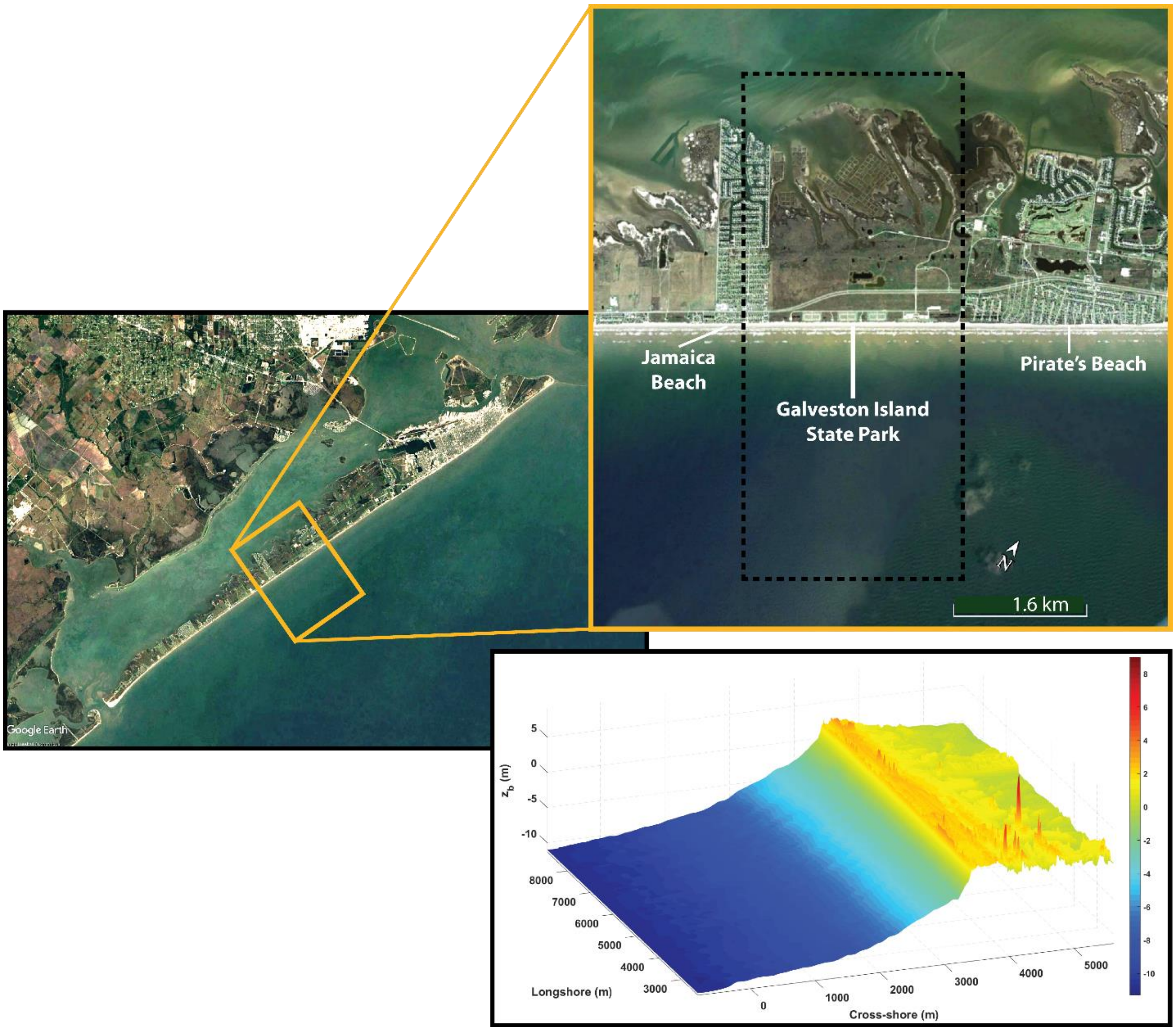

Figure 9. Map showing location of XBeach domain. Model domain is extended east and west of GISP to account for shadow zone. Dashed rectangle represents area of interest where results will be analyzed. Graph shows 3D surface of domain. Images courtesy of Google Earth.

Model setup

Boundary conditions

The XBeach model is forced with wave and water level boundary conditions on all boundaries of the domain. The hydrodynamic conditions used in XBeach are derived from real-time water surface elevations, significant wave height, peak wave period, and mean wave direction measured during the passage of Hurricane Ike. The following subsection briefly describes each data source and its application in the model.

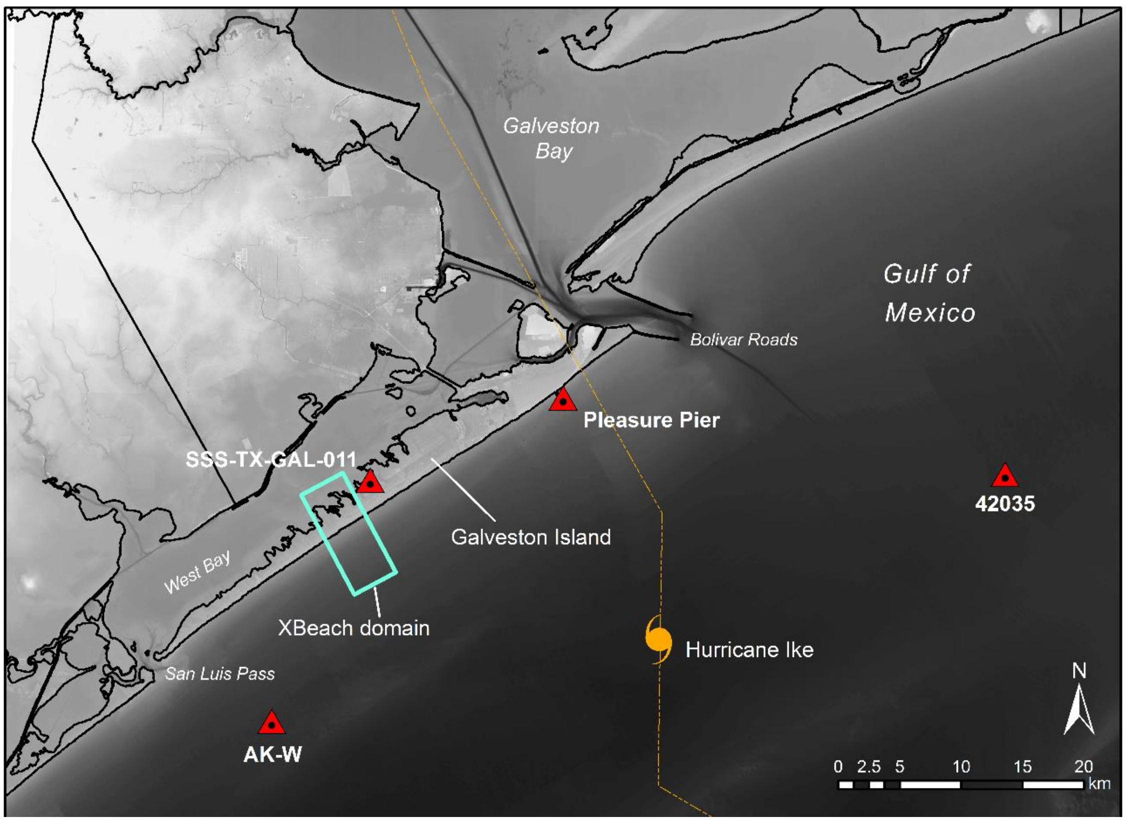

Figure 10. Map showing locations of hydrodynamic data used in XBeach model. The location of the XBeach domain is outlined in light blue. Map also shows Hurricane Ike track with orange dashed line.

Tide and surge. Pleasure Pier is a Gulf-facing pier located at the northeastern end of Galveston Island 0.3 km southeast of Seawall Boulevard (figure 10). The tide gage is located at the southeast corner of the pier. Data were acquired from the NOAA tides and currents website.

Hourly water levels were extracted from 00:00 September 11 to 00:00 September 15 for input into the XBeach model (figure 11).

Bayside water levels were retrieved from a storm surge sensor, SSS-TX-GAL-011, deployed by the U.S. Geological Survey (USGS) (figure 10). The USGS deployed a temporary monitoring network of 117 pressure transducers (sensors) at 65 sites to record the timing, aerial extent, and magnitude of inland hurricane storm surge and coastal flooding generated by Ike (East *et al.*, 2008). The pressure gauge recorded water levels only during the most intense part of the storm from 06:00 September 12 to 08:00 September 14. Data were delivered with water levels recorded in minute intervals from 13:00 September 10 to 17:41 September 19 with units in feet above NAVD88. Values were converted to meters and hourly water levels were extracted from 00:00 September 11 to 00:00 September 15 for input into the XBeach model (figure 11).

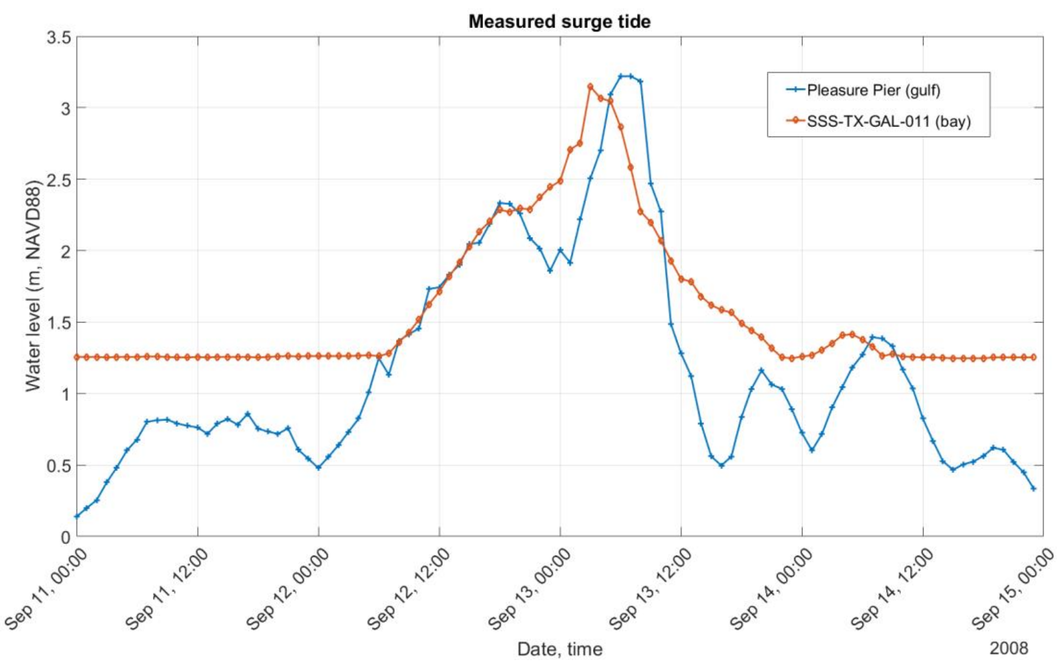

Figure 11. Graph showing water level data used in XBeach model.

Hourly time histories of the Gulf and bayside tide and surge levels are placed in a single separate file where the length of each tidal signal is specified. The tidal signal is interpolated to the time step of the XBeach simulation which is 96 hours. The water surface boundary conditions are also spatially interpolated along the boundary edges.

Waves. The XBeach model uses a spectral wave boundary condition, which describes a spectrum shape, to generate a random wave time series. A JONSWAP wave spectrum input is parametrically defined in a file that is referenced in the model simulation. The length and resolution of the generated time series is determined, along with the significant wave height, peak period, and mean wave direction in a time-varying JONSWAP definition file. The time steps of wave parameters are linearly interpolated onto the model time step.

Real time recordings of significant wave height and peak period are defined from data acquired through personal correspondence with Andrew Kennedy from the University of Notre Dame. Kennedy *et al.* (2011) deployed temporary wave gauges in nine locations off the Texas coast in 9-15 m water depth to record wave data during the passage of Ike. Gauge W is positioned off the southwestern end of Galveston Island respectively, approximately 9.5 km offshore in water depths of 14 m (figure 10). Data were delivered with recordings of peak frequency and significant wave heights from September 10 to September 22 in half-hour intervals. Peak frequency was converted to peak period and hourly mean values were calculated for each variable from 00:00 September 11 to 00:00 September 15 for input into the XBeach model (figure 12).

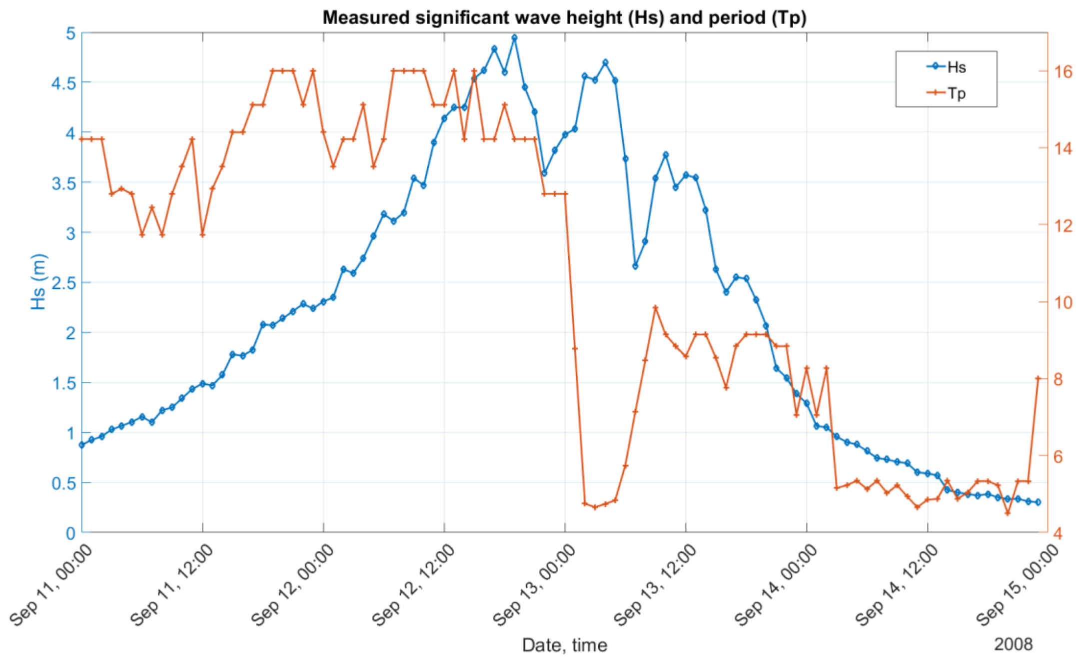

Figure 12. Graph of significant wave height and peak wave period used in XBeach model.

Mean wave direction was acquired from NOAA's National Data Buoy Center (NDBC) station 42035 which is located 40 km offshore southeast of the northeastern end of Galveston Island respectively (figure 10). Data were provided in nautical degrees in hourly intervals for the entire year of 2008. Hourly mean wave direction was extracted from 00:00 September 11 to 00:00 September 15 for input into the XBeach model (figure 13). Modest gaps in the data (>7 hours) were filled with a simple linear interpolation.

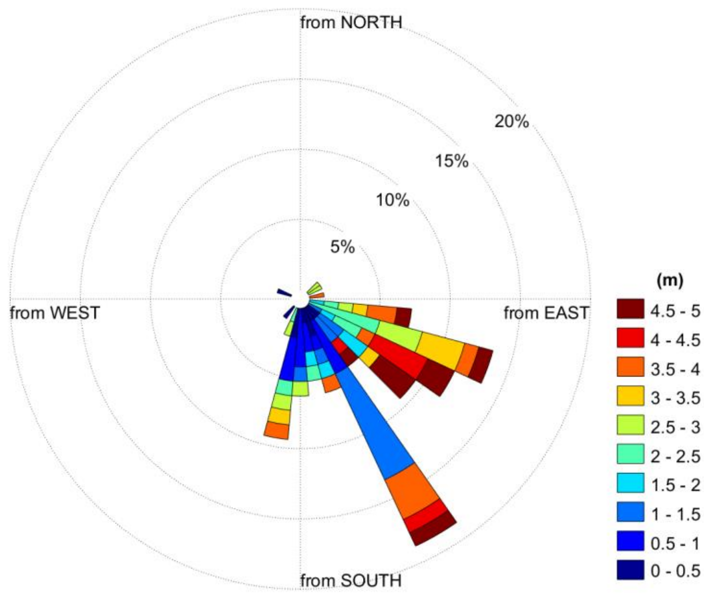

Figure 13. Wave rose showing the directional distribution of significant wave height from September 11-14, forced into the XBeach model.

Model parameters

The XBeach model is capable of running with all parameters set to their default values. The user must only define the initial bed level and the storm's hydrodynamics. However, the XBeach model has a number of free parameters which can be used to calibrate the model. Nederhoff (2014) recommends applying a two-step morphological calibration approach. The first step is to increase the parameterized wave asymmetry sediment transport component (facua). A higher value will result in less net offshore sediment transport making it suitable for calibrating dune erosion. The default value is 0.1, while Nederhoff (2014) found that a facua of 0.25 lead to good agreement in morphological development during Hurricane Sandy for New Jersey. The area of interest on Galveston Island experienced overwash and inundation and therefore no measurements exist to calibrate this regime. An increase in the facua parameter was examined, and the computed post-storm surface was compared to the measured post-storm lidar. Increasing the facua parameter did not improve morphological development over Galveston Island, and therefore the default value is used.

The second step is to increase the roughness of the barrier island. A higher roughness will result in less sediment transport over the barrier and therefore is applied to calibrate the overwash regime. The default value in XBeach is a constant Chezy coefficient of 55 $m^{0.5}.s^{-1}$. In theory, values as low as 10 $m^{0.5}.s^{-1}$ can be applied, however, the XBeach model allows a minimum of 20 $m^{0.5}.s^{-1}$ (Roelvink *et al.*, 2015). A spatially varying bed friction file can be applied to increase the roughness over the island. A lower Chezy value can be seen as friction generated by the combined effort of both vegetation and structures and can be used as a sum of all kinds of different contributions that can have an impact on flow (Nederhoff, 2014). This project investigates the effects of applying a spatially varying bed friction across the domain.

By default, XBeach treats every cell in the model domain as sand and therefore is subject to erosion. An area that represents a hard structure, such as a building or a seawall, will erode unless the user defines it as non-erodible. To manage this, the location of structures can be specified in an external file referenced by a keyword in the model's main parameter file. The non-erodible file has the same format as the bathymetry file where values in the file define the thickness of the erodible layer on top of the non-erodible layer. For example, a non-erodible file with only zeros defines a fully non-erodible bathymetry. A file with only tens means an erodible layer of 10 m. In order to investigate how the model simulates erosion and deposition patterns near buildings, a non-erodible layer is included in the model setup. Cells in the model domain which represented structures were assigned a value of zero, meaning they were infinitely deep and non-erodible. All other cells were defined a value of 100, meaning they could erode down to 100 m.

The XBeach model is a computationally intensive model. In order to reduce the run time, a morphological acceleration scheme (morfac) was built into the code. This enables the user to decouple the morphological and hydrodynamical time. For example, running a simulation with a morfac value of 10 means the hydrodynamics are run for 6 minutes each hour, and the bottom changes at each time step are multiplied by a factor of 10. Lindemer *et al.* (2010) and McCall *et al.* (2010) performed sensitivity analyses of the morfac parameter. They each concluded that for values between 1 and 20, there was little to no difference, 2% at most, in the resulting coastal response. A morfac value of 10 is used in the XBeach base simulations of the above-mentioned literature and thus a value of 10 is used in this project.

The default grain size for the XBeach model is 200 µm for both D_{50} and D_{90}. Sediment samples on Galveston Island were collected in 2010 by the USGS. Sample statistics and grainsize distributions indicate a median grain size (D_{50}) of 132.3 µm and a 90th percentile (D_{90}) of 186.9 µm for the well sorted fine sand on Galveston Island (Lisle and Comer, 2011). These values are used for the bed composition parameters instead of the default.

A table of the input parameters is included in the Appendix. All other free parameters contained in XBeach, which govern short wave dynamics, flow, critical avalanching slope, etc., are left at their default value.

Evaluation methods

In order to evaluate if the model can be used as a predictive tool, an objective evaluation method is needed. According to Sutherland *et al.* (2004), the performance of numerical models of coastal morphology can best be assessed by calculating the skill and bias.

A useful skill score in coastal engineering is the Brier Skill Score (BSS), which compares the mean square difference between the computed bed level change and the measured bed level change with the mean square difference between the baseline prediction and the measured bed level change. In morphodynamic modeling, the initial bathymetry is used as the baseline prediction. Perfect agreement gives a BSS of 1, whereas modeling the baseline prediction gives a score of 0. If the BSS is less than 0, the model is worse than predicting zero bed level change. The skill is defined in this thesis as:

$$Skill = 1 - \frac{\sum_{i=1}^{N} \left(dz_{b_{lidar,i}} - dz_{b_{XBeach,i}}\right)^2}{\sum_{i=1}^{N} \left(dz_{b_{lidar,i}}\right)^2}$$

where N is the number of data points covered by both pre- and post-storm lidar measurements, $dz_{b_{lidar,i}}$ is the measured bed level change in point i and $dz_{b_{XBeach,i}}$ is the modeled bed level change in point i.

The mean error describes the potential bias. A positive bias means the bed level is higher in the computed results than in the measured results. The bias is calculated as:

$$Bias = \frac{1}{N}\sum_{i=1}^{N}\left(z_{b_{post-storm,XBeach,i}} - z_{b_{post-storm,lidar,i}}\right)$$

Scenario testing

Hypothetical barrier island protection practices were tested under Hurricane Ike hydrodynamic conditions by manipulating the pre-storm topography. To investigate possible practices that could have mitigated the damage caused by Ike, six protection methods were tested: three dune restoration designs, one beach nourishment, and two dune restorations with added beach nourishment. A construction design for each method is developed using past nourishment designs for Galveston Island as a reference, as well as recommendations stated in the Coastal Engineering Manual (USACE, 2008). The designs were then digitized in 2D space using geospatial techniques, manipulating the pre-Ike DEM.

Dune restoration design

The various dune designs were built under the guidelines of the Galveston, Texas Code of Ordinances. Based on research regarding dune locations, the city adopted a definition for restored (man-made) dunes which states that a restored dune should have a 3:1 slope, an average height of 75% of the island's base flood elevation as measured from mean sea level (MSL), a naturally established connection to the dune contour, and shall not extend further seaward than 4.5 feet above NAVD88, which is defined as the potential vegetation line (PVL) (Galveston, Texas – Code of Ordinances). The Coastal Engineering Manual recommends a typical dune design to have dimensions on the order of a 5-meter high dune crest above MSL, 10-meter dune crest width, and one on five side slopes (USACE, 2008). Three dune designs based upon these recommendations are built onto the pre-Ike topography (see figure 14 and table 1 for dune design dimensions and illustrations).

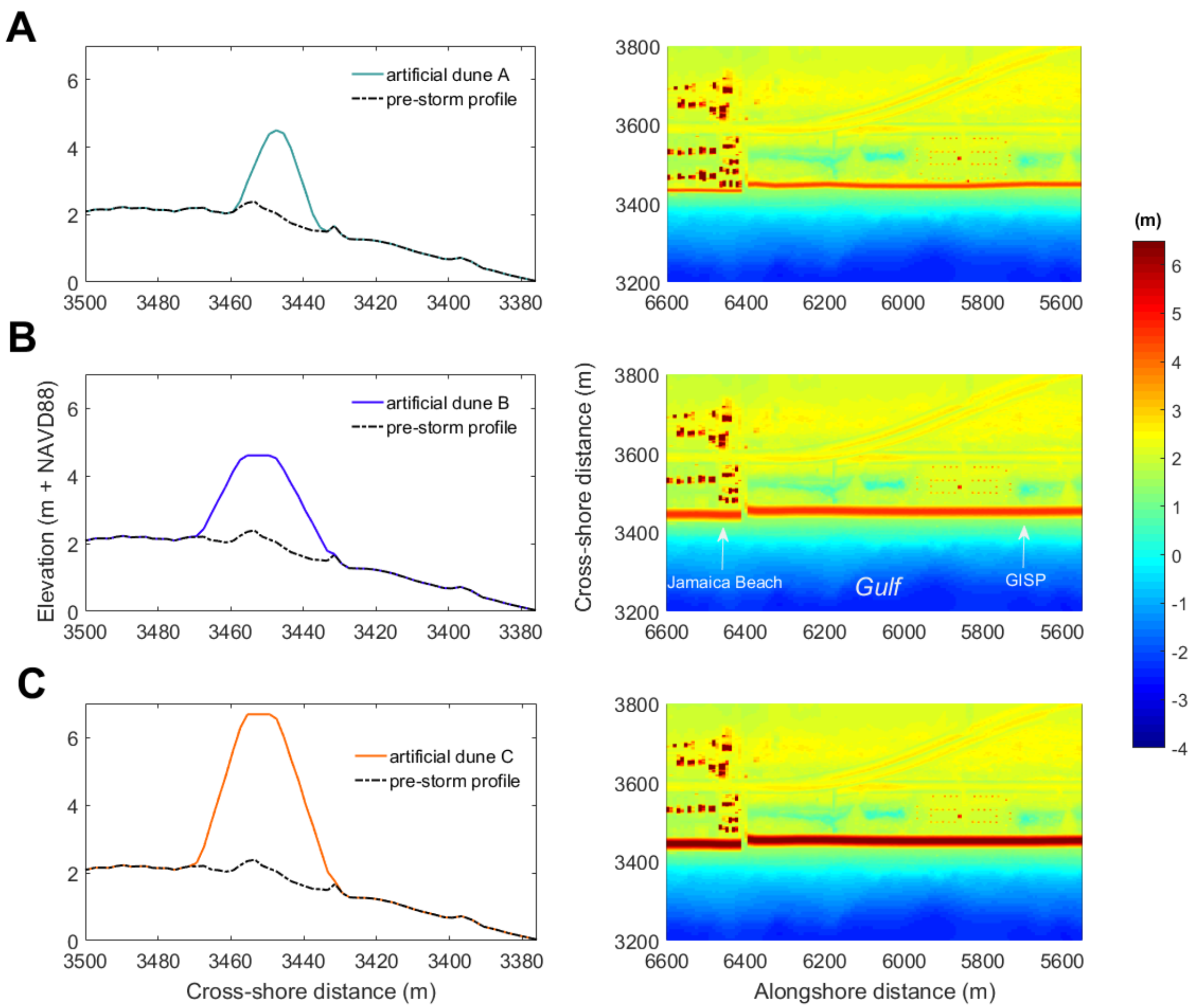

Figure 14. 1D and 2D views of each artificial dune design. Image shows only a section of domain from Jamaica Beach to western end of GISP. 1D plots are of the same cross-shore profile.

Table 1. Artificial dune design dimensions

	Width (m)	Height (m + NAVD88)	Crest width (m)	Seaward slope	Volume added (m^3)
Dune A	21	4.5	4	3:1	6,537
Dune B	37	4.5	10	5:1	10,729
Dune C	37	6.5	10	3:1	20,306

For each design, the restored dune starts at the naturally established dune toe and extends landward to a specified distance. For the first design, the dune width is defined at 21 meters. This is the greatest width allowed due to development beginning just landward of the restored dune.

In order to investigate the effects of a wider dune, the first row of houses are removed from the pre-Ike topography. This allows room for the additional two dune designs to have a width of 37 meters.

Beach nourishment design

An additional scenario tested the influence of beach nourishment practices in mitigating storm damage. A nourishment project usually involves widening the berm which creates a sand buffer for dissipating storm wave energy. Nourishment projects are designed to include a volume of sand that the waves and currents will transport offshore to fill the rest of the beach profile out to the depth of closure, resulting in an equilibrium profile over time. On West Galveston Island, the berm top typically extends from the PVL (1.27 m NAVD88) to the shoreline (0.67 m NAVD88). The depth of closure used in this study is -6 m (NAVD88) determined from King (2007). The design profile was determined by translating an equilibrium profile from the shoreline to the depth of closure 25 meters seaward, and then connecting the translated profile to the PVL with an interpolated linear slope. The equilibrium profile before translation was determined using the following equation from Bruun, 1954:

$$h(y) = Ay^{\frac{2}{3}}$$

where *h* is the water depth at a seaward distance, *y*, and *A* is a scale parameter which depends primarily on sediment characteristics. This project is assuming a beach fill with the same sediment characteristics as the native sediment (D_{50} = 0.13 mm). The resulting beach fill volume is added to all profiles along the study area. This resulted in an added volume of 32,704 m^3 of sand placed along the foreshore and nearshore zones of the entire domain, a distance of 6.6 km alongshore. This nourishment only scenario was tested along with applying nourishment to the first two dune repair alternatives, creating three additional comprehensive practices to increase resilience to erosion (figure 15).

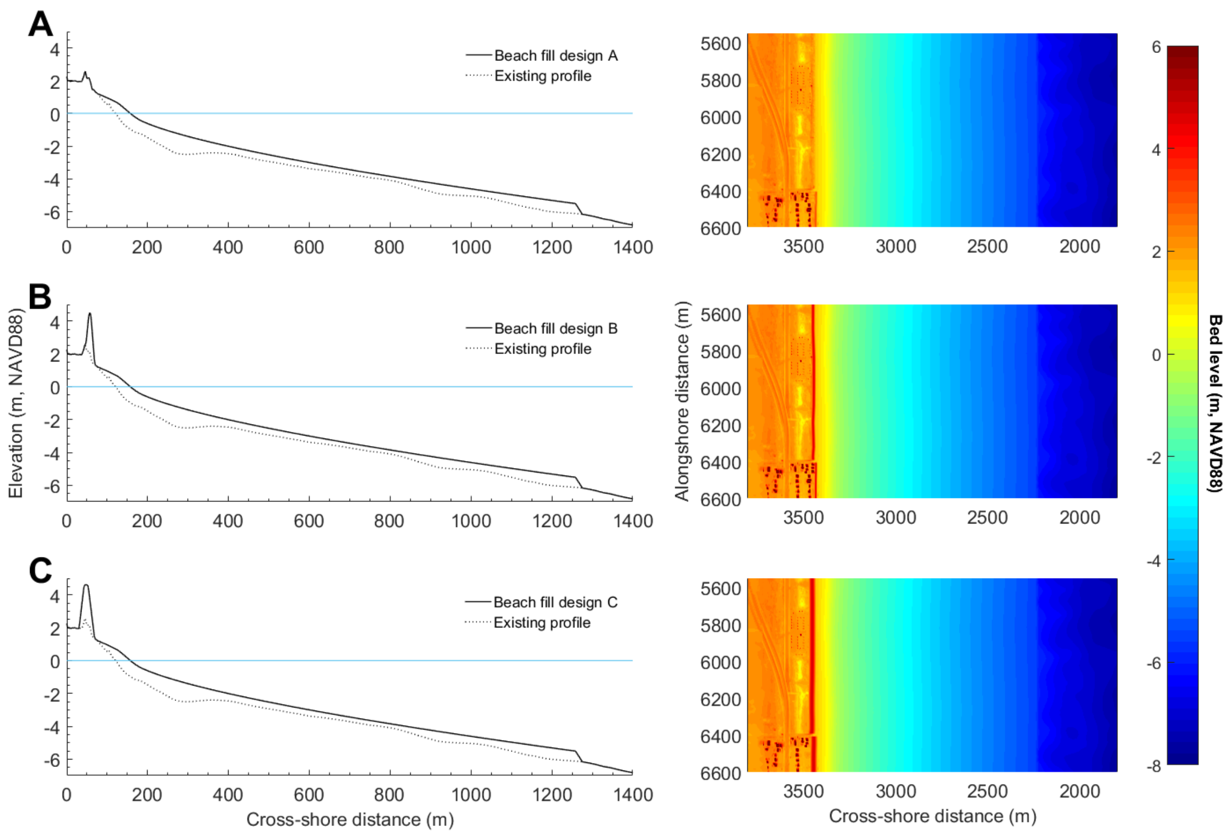

Figure 15. 1D and 2D views of beach fill designs. Design A is beach nourishment only. Design B is beach nourishment with Dune A. Design C is beach nourishment with Dune B. 2D images show a 1000 m alongshore section of the study area.

CHAPTER IV: MODEL ANALYSIS AND RESULTS

XBeach model simulations were run on a high performance computer (HPC) using 40 core processors. This allowed the simulation to run in under twelve hours for the 96 hour storm event. The following sub-sections describe the morphological evolution of the island in response to Hurricane Ike, the model calibration and validation results, and the effect of hypothetical soft engineering scenarios.

Morphological evolution

The XBeach model simulation shows Galveston Island's morphodynamic response to Hurricane Ike clearly captures the processes involved in the storm regimes outlined by Sallenger (2000). In addition to these regimes, storm surge ebb also plays a significant role in transporting sediment seaward. The morphological evolution of the island during each regime is discussed in the following sub-sections.

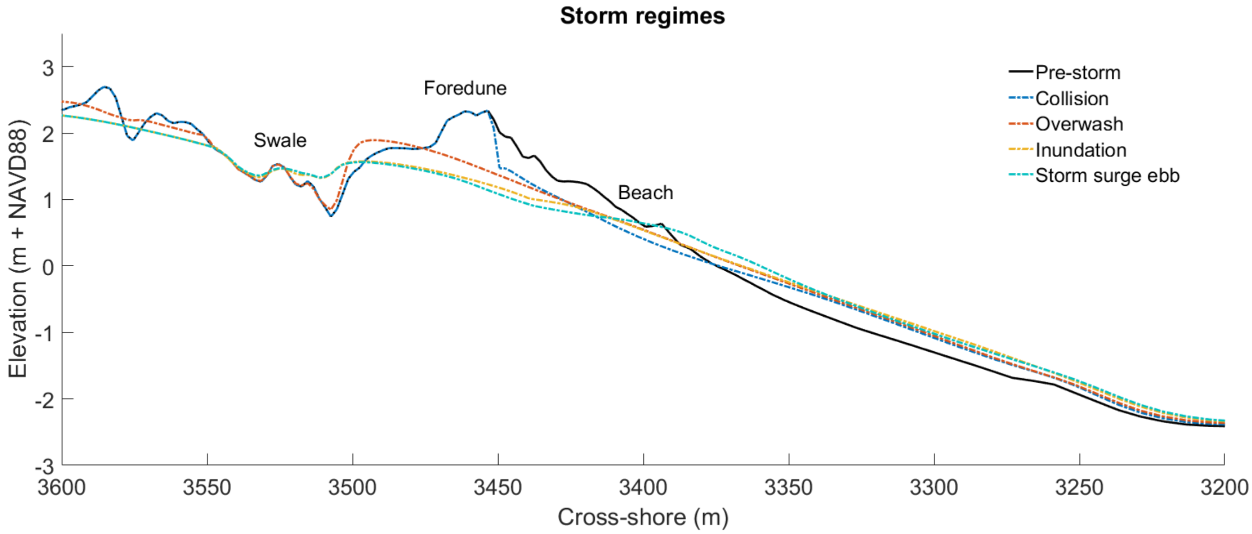

Figure 16. A cross-shore profile showing a snapshot of the bed level during each storm regime and during the storm surge ebb.

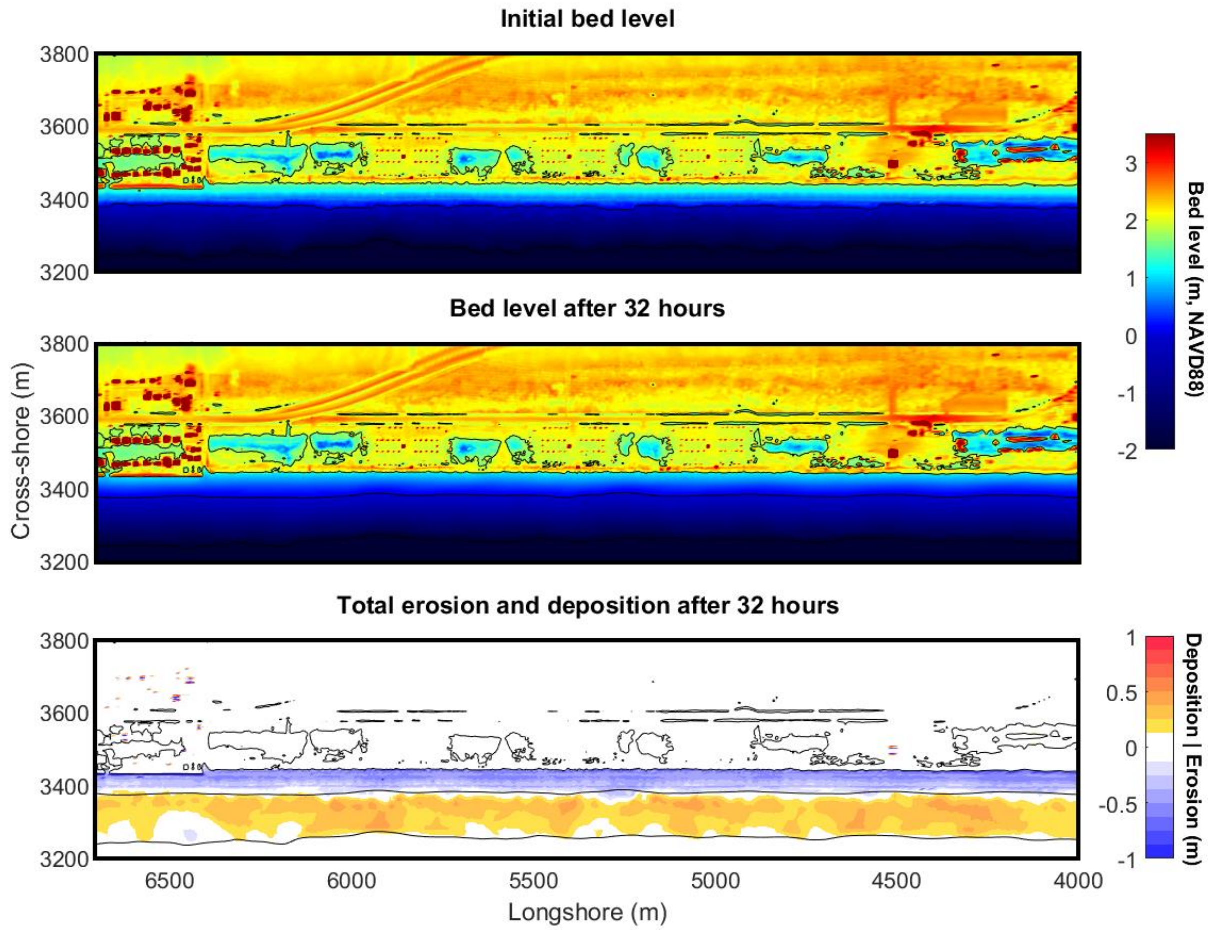

Figure 17. Initial bed level, and bed level and erosion/deposition patterns simulated after 32 hours. Post-storm regime contour lines drawn at -2 m, 0 m, and 1.8 m.

For the first 31 hours of the simulation, (September 11, 00:00 to September 12 07:00), the barrier island is essentially in the swash regime as water levels have not yet reached the natural dune toe. Sediment is eroding from the beach and is depositing in the surf zone, creating a gentler foreshore slope (figure 16). A feature to take note of is the man-made dune that was built in front of the houses of Jamaica Beach, near x = 6500 in figure 17. It is eroding to a greater extent than the foredunes along GISP due to its proximity to the shoreline.

Collision regime (32 to 36 hour)

During the 32nd hour of the simulation, the island has transformed into the collision regime. The combination of the tide, surge and waves (R_{high}) have increased the water level to reach the dune toe (~1.8 m NAVD88). The island remains in the collision regime for 4 hours (figure 18). This period is characterized by a scarping of the seaward slopes of the foredunes along with a landward migration of the mean water line. The eroded foredune sediment is deposited on the backshore (figure 19), and two overwash throats have started to form at x = 6175 and x = 5640. The total amount of erosion and deposition during this period can be seen in figure 19.

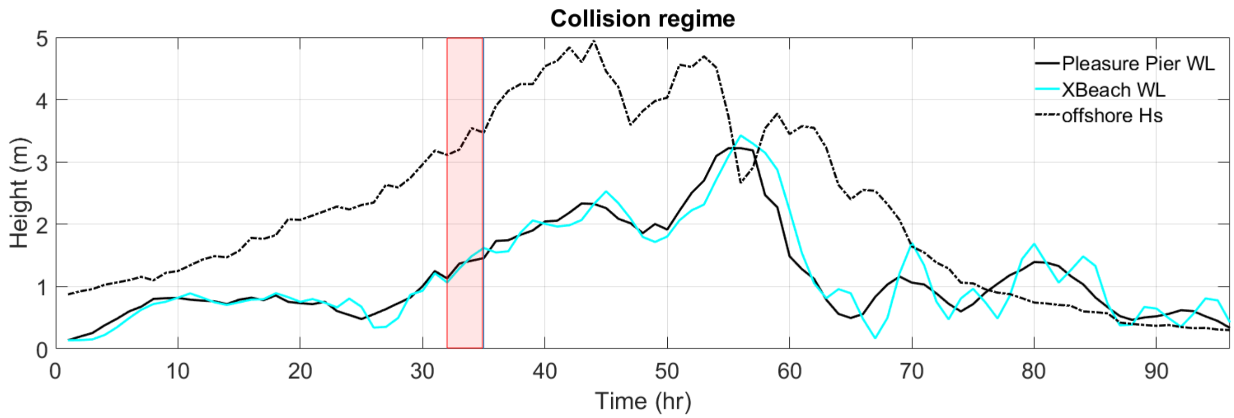

Figure 18. Graph of wave heights and water levels measured from September 11 00:00 to September 14 23:59. Blue line is the computed water level. Red box highlights the height of the water levels and measured wave heights during the collision regime.

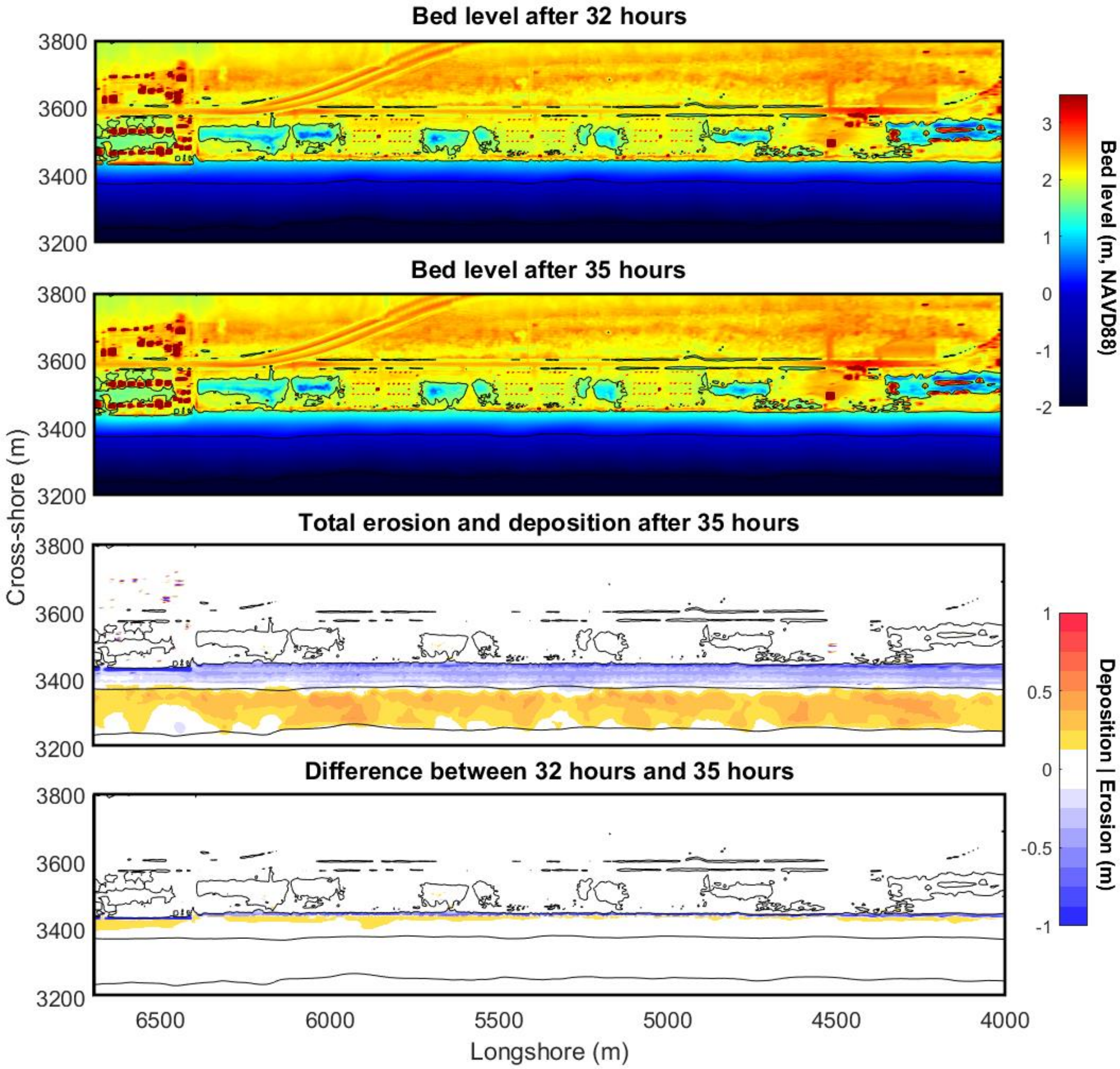

Figure 19. Bed level and erosion/deposition during the collision regime. Post-storm regime contour lines drawn at -2 m, 0 m, and 1.8 m.

Overwash regime (36 to 53 hour)

At the start of the 36th hour of the simulation, the barrier island system changes to a strong overwash regime, and remains in this period for 17 hours. This period is marked by the first peak in offshore wave heights, reaching 4.8 meters, and the first peak in water level, reaching 2.33 meters (figure 20). A large majority of the dunes in this region are only around 2 meters high, and were already subject to erosion during the collision regime. Two main morphological changes occur during this period. The first is the development of several overwash throats, as can be seen in figure 21. The second large change is the lowering and distruction of the foredunes, and the deposition of foredune sediment both landward of the dune system and seaward on the beach. Beach erosion during this regime was minimal, and there is no difference in sediment deposition in the surfzone.

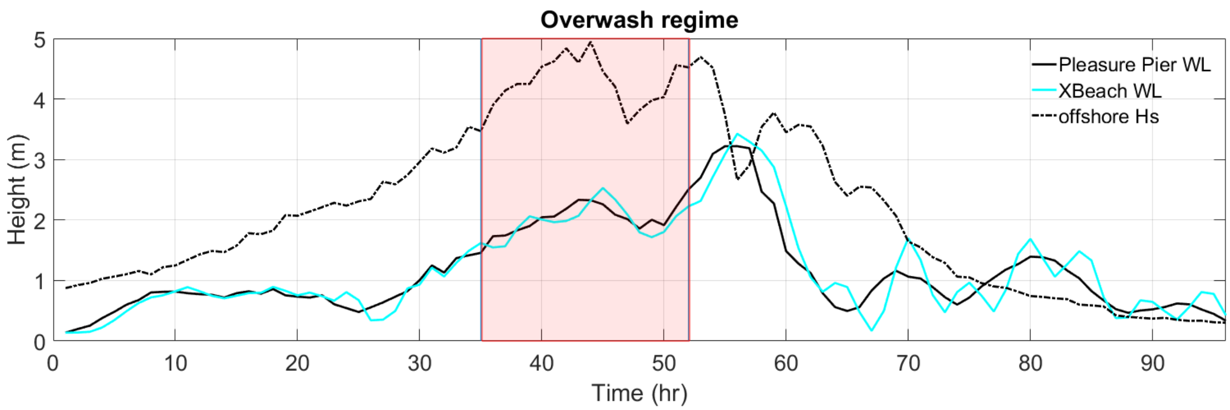

Figure 20. Graph of wave heights and water levels measured from September 11 00:00 to September 14 23:59. Blue line is the computed water level. Red box highlights the height of the water levels and measured wave heights during the overwash regime.

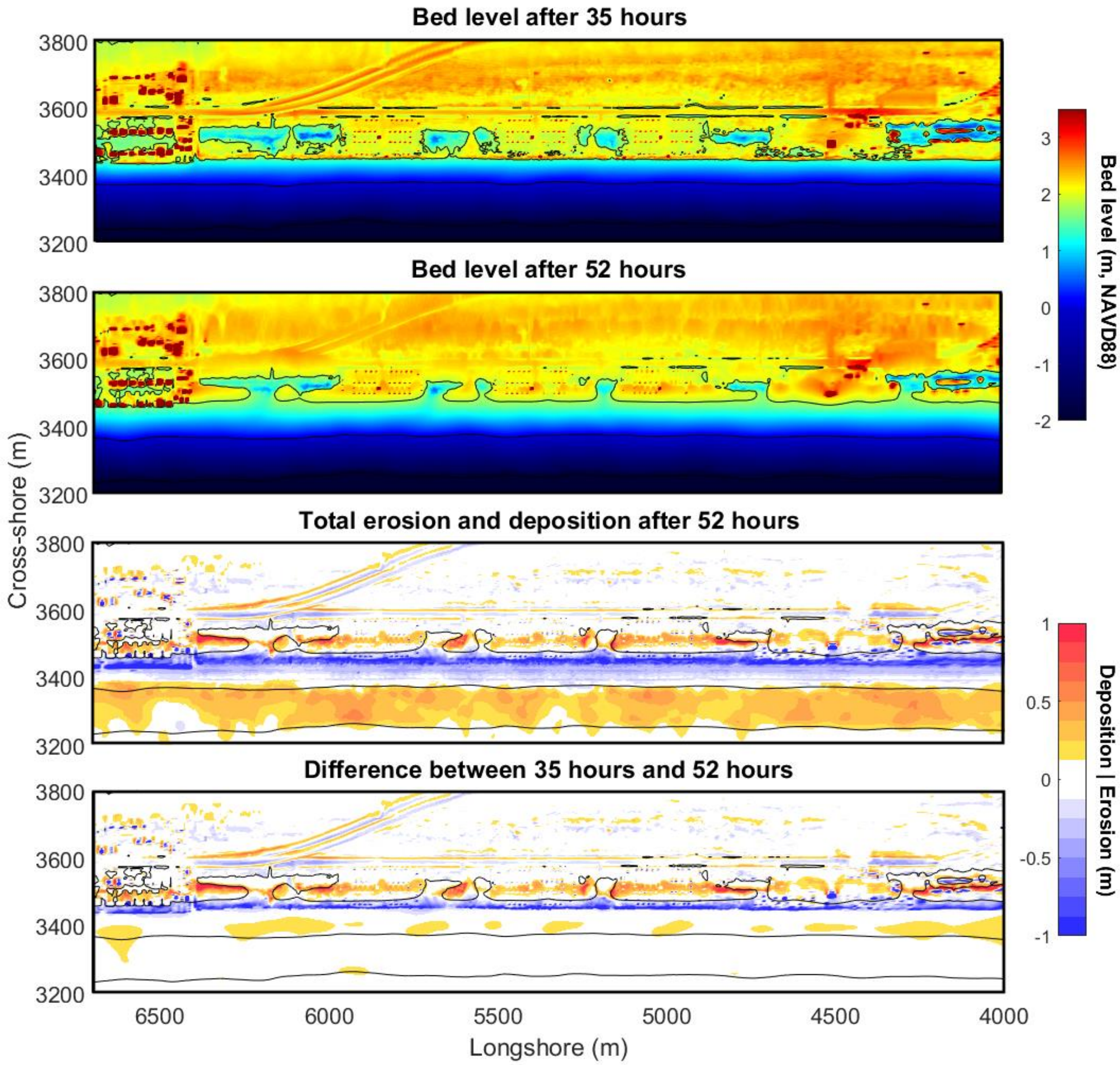

Figure 21. Bed level and erosion/deposition during the overwash regime. Post-storm regime contour lines drawn at -2 m, 0 m, and 1.8 m.

Inundation regime (52 to 62 hour)

As Hurricane Ike made landfall at 02:00 on September 13, Galveston Island was entering the inundation regime. The offshore wave heights were climbing to their second peak reaching 4.7 meters 3 hours after landfall (figure 22). The highest measured water level on the island reached 3.22 meters during the 57th hour of the simulation, which was 7 hours after landfall. During this period, Galveston Island experienced massive erosion of the foredune, which had already been lowered during the overwash regime. The foredunes were uniformly inundated during this period. The existing overwash throats were widened and another breach formed at x = 6100, shown in figure 23. At the peak of the surge, wave action over the island was minimal coincidently as offshore wave heights dropped rapidly, by over 2 meters between hours 54 and 56. Minimal changes occurred in the erosion and deposition patterns over the island during this period (figure 23). As water levels began to recede, offshore wave heights reached their last peak at 3.77 meters and slowly dropped over the following 10 hours. The combination of water levels and waves continued to inundate the island until the 62nd hour of the simulation, which was 12 hours post-landfall.

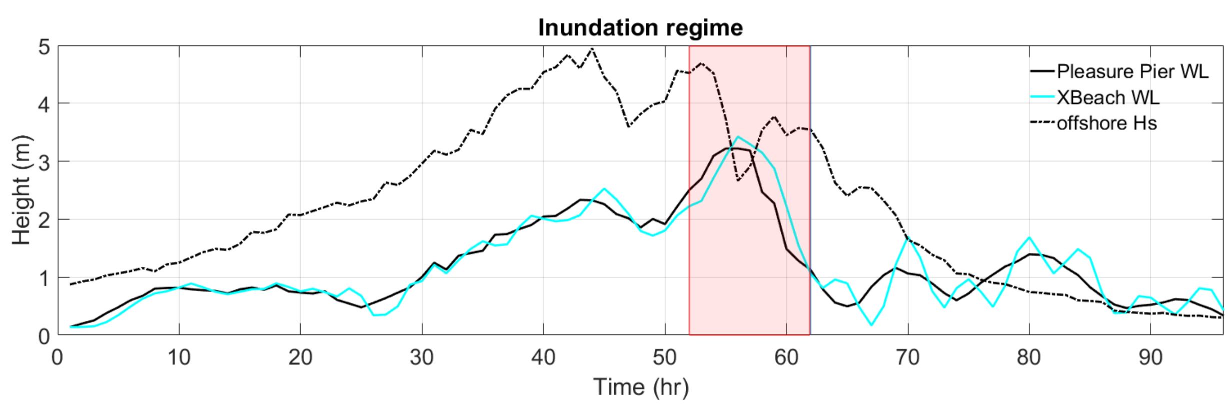

Figure 22. Graph of wave heights and water levels measured from September 11 00:00 to September 14 23:59. Blue line is the computed water level. Red box highlights the height of the water levels and measured wave heights during the inundation regime.

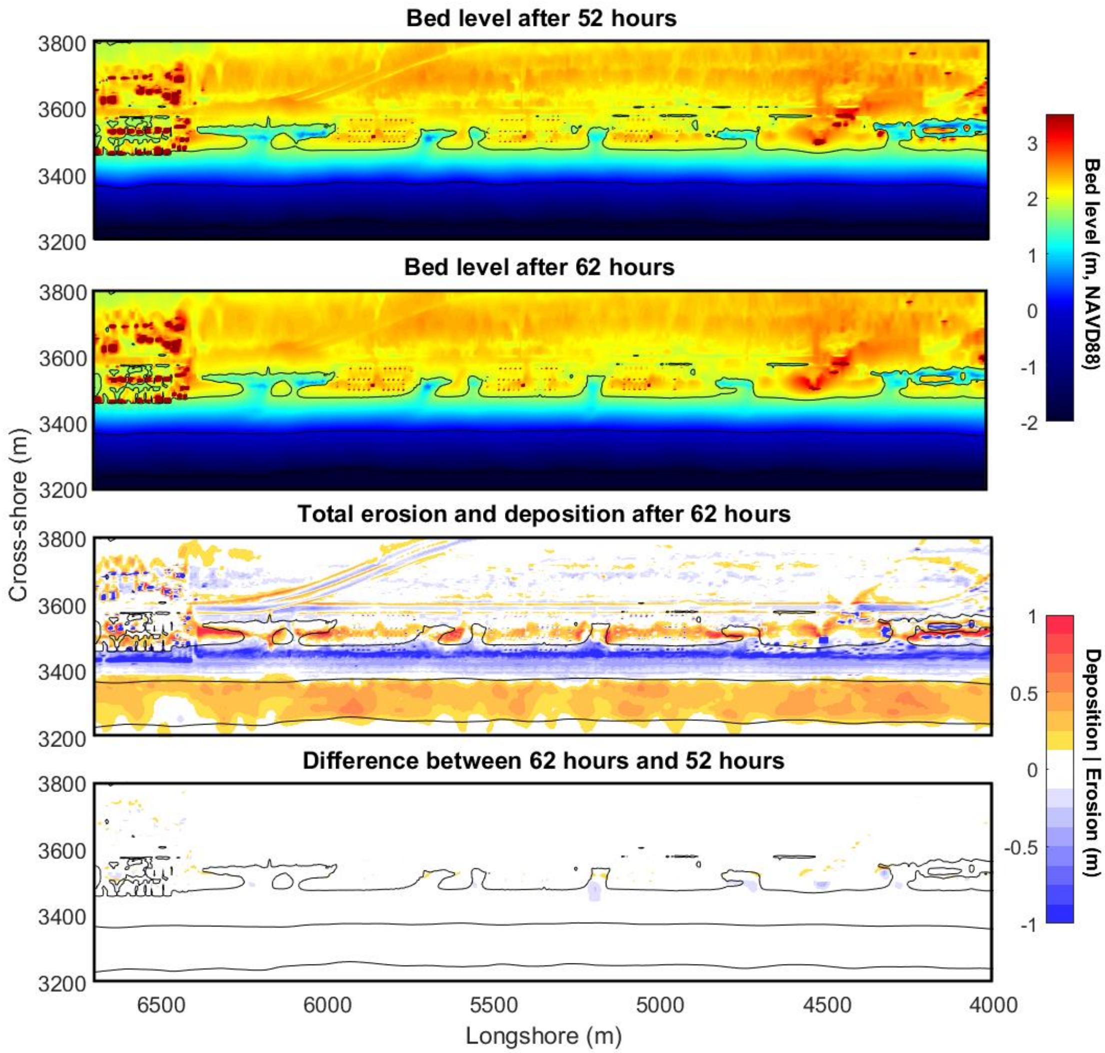

Figure 23. Bed level and erosion/deposition during the inundation regime. Post-storm regime contour lines drawn at -2 m, 0 m, and 1.8 m.

Storm surge ebb (58 to 68 hour)

During hour 58 to 68, the ebbing storm surge pulled volumes of sediment seaward through the overwash throats and deposited along the beachface (figure 25). After the storm surge ebb, the island experienced a resurgence wave, where water levels peaked again at 1.4 meters. This, however, was not high enough to overwash the island a second time.

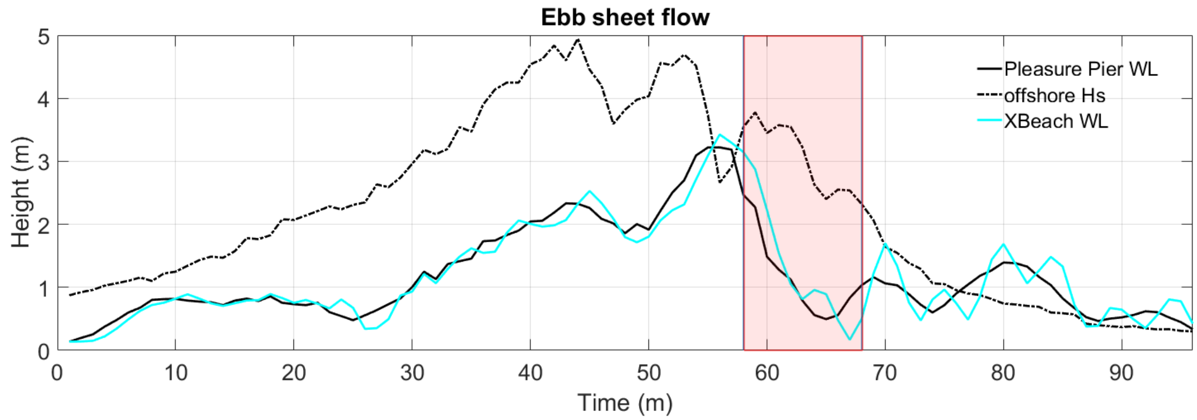

Figure 24. Graph of wave heights and water levels measured from September 11 00:00 to September 14 23:59. Blue line is the computed water level. Red box highlights the height of the water levels and measured wave heights during the storm surge ebb.

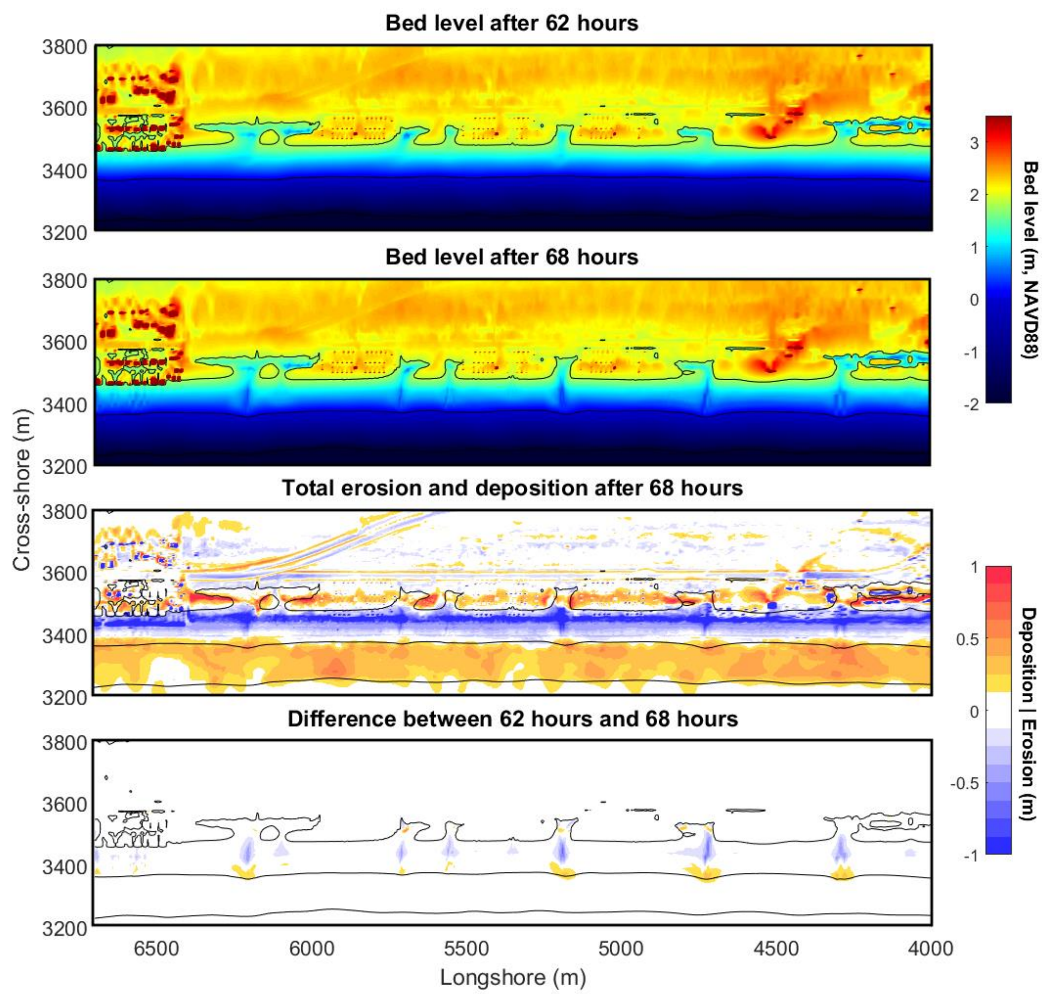

Figure 25. Bed level and erosion/deposition during the ebb sheet flow. Post-storm regime contour lines drawn at -2 m, 0 m, and 1.8 m.

Model validation results

In order to prove this model is a valid model for forecasting and explaining the island's morphodynamic response to a storm, the post-storm computed bed level is compared to the post-storm measured lidar data. Unfortunately, the post-storm lidar data only covers about 300 meters cross-shore from the low tide line to the back barrier, so the nearshore deposition patterns cannot be validated. The final, 96 hour, XBeach and lidar bed elevation are shown in figure 26.

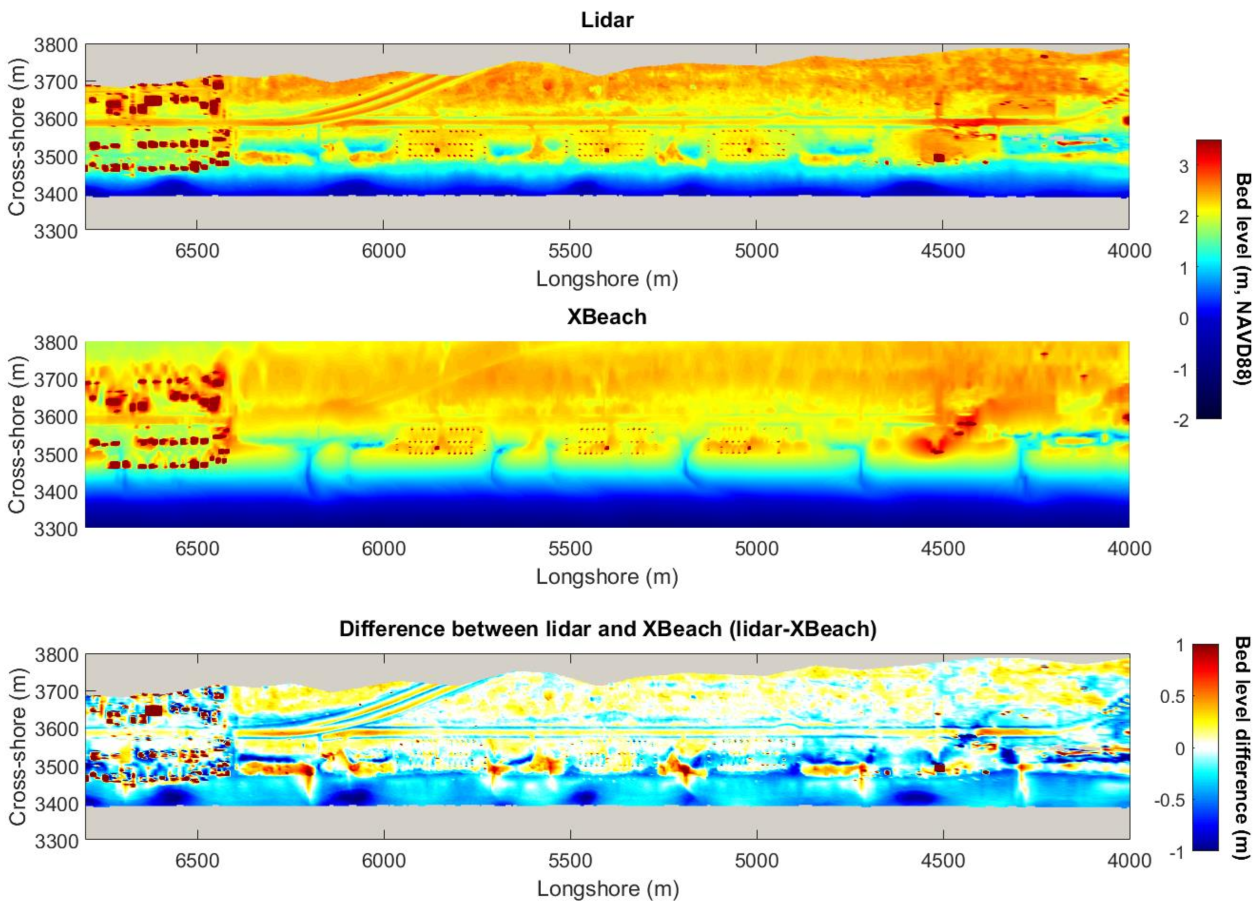

Figure 26. Final post-storm bed level comparison between the measured lidar and computed XBeach. Grey background signifies no data due to the restricted extent of lidar coverage. Third image shows the difference between two post-storm surfaces. Reds signify higher post-storm measured bed levels, blue signifies lower post-storm measured bed levels, and whites are areas of no difference.

Final bed level

There are a few noticeable differences in figure 26. First is the foredune breaches that are well defined in the XBeach surface. Second is the lidar data shows a greater variation in elevation than the XBeach results, specifically near y = 3500. The XBeach model shows a gradual slope from less than 1 meter elevation to greater than 2 meter elevation, while the lidar shows a steeper slope. This could be influenced by the dense vegetation in the region that the XBeach model is unable to accurately resolve. The last noticeable difference between these two surfaces is the rhythmic topography that is present on the backshore of the lidar surface. XBeach did not simulate this morphologic response.

Erosion and deposition patterns

A clear look at the distribution of sediment can be examined by comparing the storm-integrated erosion and deposition patterns, shown in figure 27. Close examinations of the patterns of sediment distribution reveals a remarkable resemblance between the measured lidar and the simulated model. In both images, the concentration of sediment is deposited just landward of the foredune zone, near y = 3500. Both show similar densities of sediment deposition on top of the paved parking lots, and each show greater densities of sediment deposition between the parking lots around the edges of the swales. Both also show at least a meter of erosion along the foredune zone. One obvious difference is the greater amount of erosion along the beach that is measured with the lidar. This difference will be further discussed in the final section of this paper. Overall, the simulated erosion and deposition patterns clearly resemble what was measured with the lidar data.

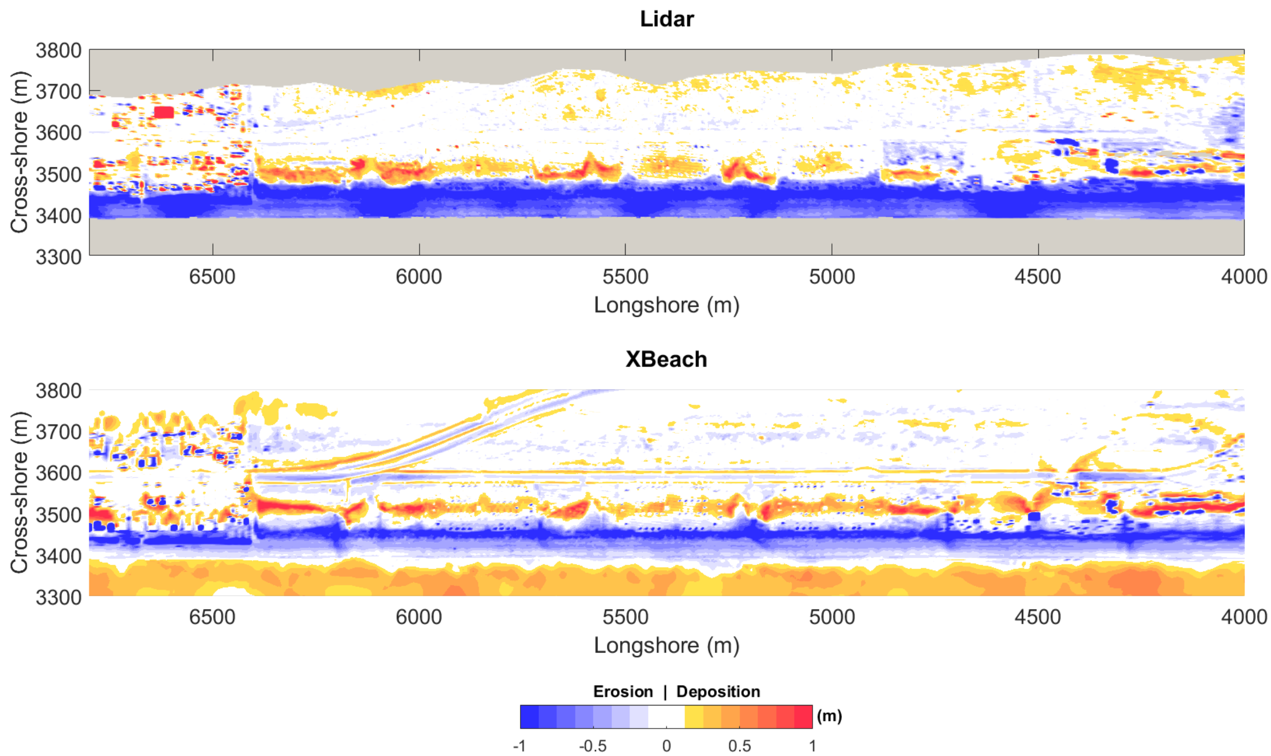

Figure 27. Total erosion and deposition comparison between measured and computed results.

Brier Skill Score and bias

A quantitative validation method is carried out by calculating the Brier Skill Score (BSS). XBeach is capable of reproducing the morphological response of the barrier island during Hurricane Ike in an accurate way with a BSS of 0.67 and a bias of + 0.06 m. The BSS has a large spatial variation and can be observed by calculating the skill score with a 6x6 m moving window across all grid cells. This gives a clear insight of the different skill scores per region instead of focusing on a mean score. Figure 28 shows how well the model performs within the foredune and backshore regions. Areas on the back barrier are either not well represented or the change in bed level is very minimal. A mean score of just the foredune zone equals 0.92 with a bias of + 0.28. This calculation can be concluded as "excellent" according to the classification of Van Rijn *et al.*, 2003. A plot of the change in dune crest (D_{max}) alongshore is shown in figure 29. Although the elevation of D_{max} in the XBeach output is not exact at each cross-shore profile when compared to the post-storm lidar data, the difference between the pre-storm D_{max} and post-XBeach D_{max} is remarkably accurate. Both the lidar and XBeach show an average decrease in the crest of around 0.5 m. Each are also in agreement with the destruction of the man-made dune in front of Jamaica beach, which experienced about a 1.5 m lowering of D_{max}. Figure 30 compares the post-storm computed surface vs. the lidar along three different cross-shore profiles

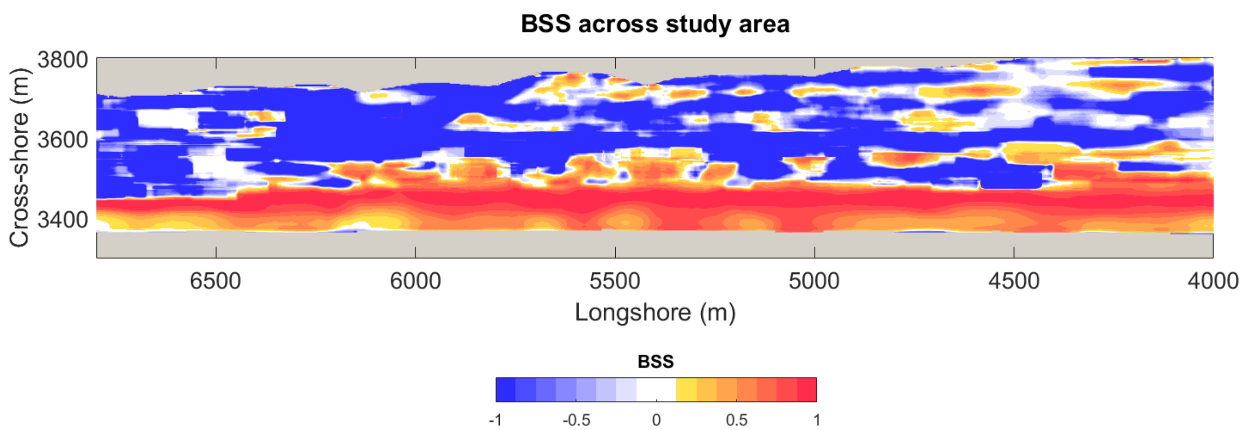

Figure 28. Skill score plotted with a moving window across study area.

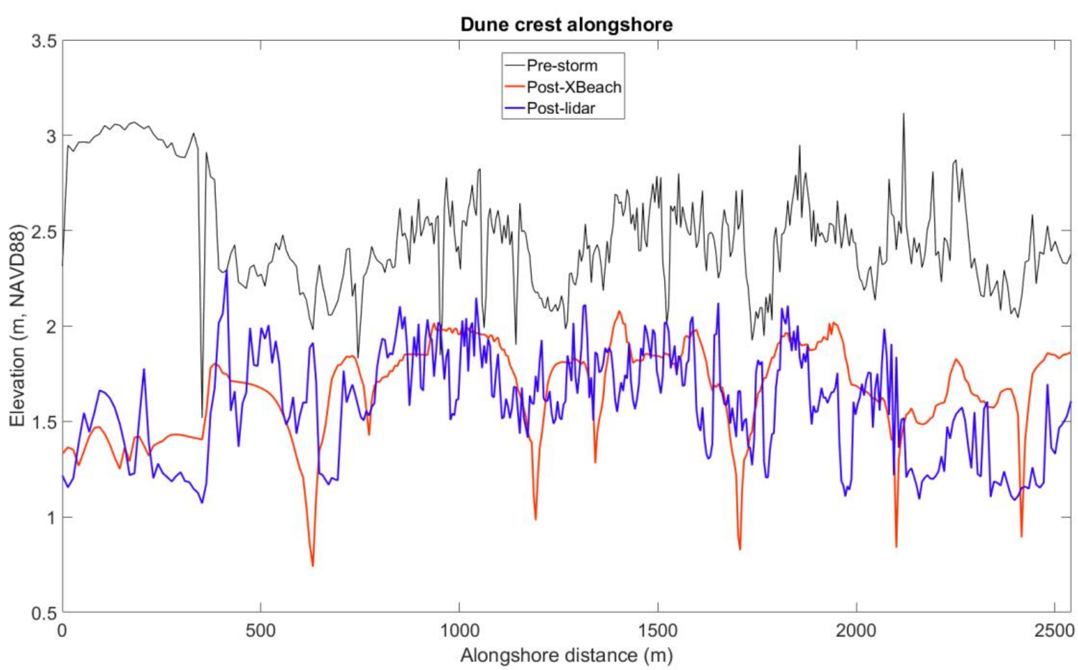

Figure 29. A comparison of the computed and measured dune crest change, plotted alongshore.

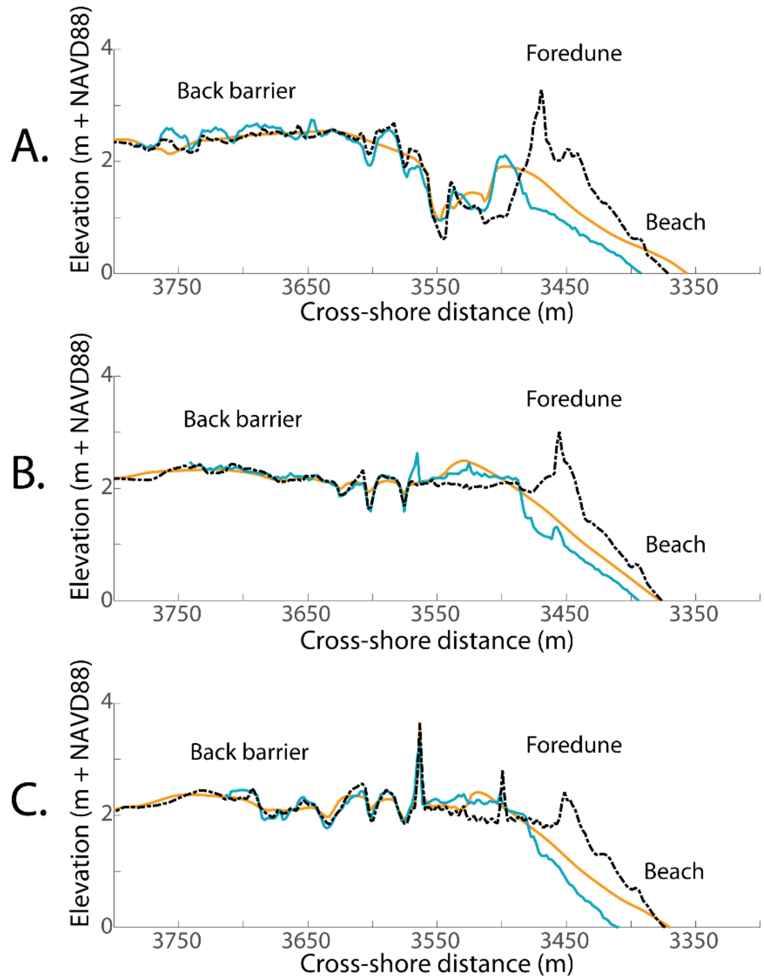

Figure 30. Three cross-shore profiles at (A) x = 4400, (B) x = 5100, and (C) x = 5500. The dashed black line is the pre-storm surface, the orange line is the post-storm computed surface, the blue line is the measured lidar.

Model calibration results: Increasing bed friction

In the previous sections, the model results were based on the results of a calibrated model. Calibration was carried out by varying the roughness on the barrier island. A total of 5 simulations were run to test the influence of a lower Chezy coefficient (C) over the top of the barrier island. The following coefficients were tested: 20, 25, 30, 35, and the default of 55. In table 2, the skill score and bias are calculated for the entire study area (BSS; Bias), for only the cells where erosion occurred (BSS_{ero}; $Bias_{ero}$), and for only the foredune zone (BSS_{fd}; $Bias_{fd}$). The volume of eroded sediment is calculated (V_{ero}), and the maximum dune crest (D_{max}) within the foredune zone is calculated to compare with the post-storm measured lidar. From the table, it is clear the default model performed worse than the calibrated model. The default model simulated a greater volume of erosion, a lower D_{max}, and a much lower skill score with a negative bias. A plot of the dune crest alongshore for the calibrated model and the default model can be seen in figure 31. An interesting observation in this graph is the areas where the breaches occurred in the calibrated model are not present within the default model. The frictionless surface of the island with the default Chezy value increased the velocity of the sheet flow over the island during the inundation regime. This likely moved large concentrations of sediment around the island, and resulted in a more generalized surface as water levels retreated. Figure 32 shows the comparison of the final bed level for C = 20 and C = 55, as well as the storm-averaged maximum velocity for each.

Table 2. Calculated comparisons between the different Chezy values.

	BSS	**BSS_{ero}**	**BSS_{fd}**	**Bias (m)**	**$Bias_{ero}$ (m)**	**$Bias_{fd}$ (m)**	**D_{max} (m)**	**Vol_{ero} (m^3)**
C = 20	0.67	0.80	0.92	0.06	0.12	0.28	2.10	-12,566
C = 25	0.62	0.80	0.90	0.05	0.10	0.26	2.03	-13,813
C = 30	0.58	0.80	0.91	0.03	0.08	0.25	1.97	-15,087
C = 35	0.54	0.79	0.91	0.02	0.07	0.25	1.95	-16,139
C = 55	0.23	0.69	0.92	-0.12	-0.003	0.16	1.83	-23,956
lidar	----	----	----	----	----	------	2.15	-16,845

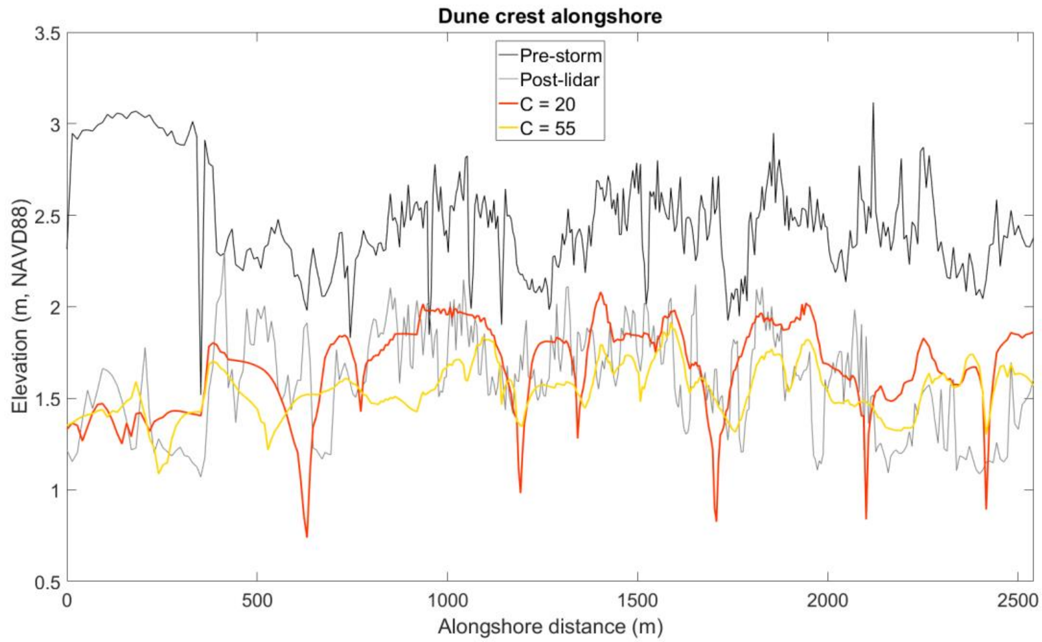

Figure 31. Comparison of pre- and post-storm dune crest change alongshore between the default and calibrated model

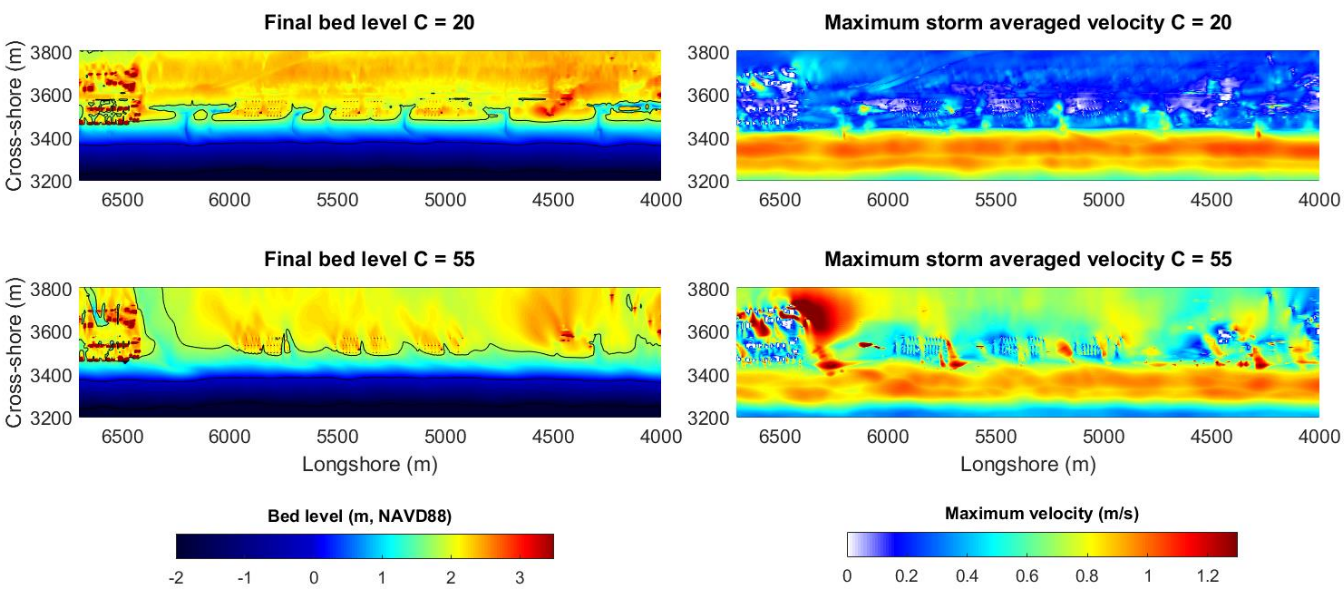

Figure 32. Final bed level compared between the default and calibrated model. Contour lines drawn at -2 m, 0 m, and 1.8 m. Maximum storm averaged velocity compared between the default model and the calibrated model.

Hypothetical soft engineering scenarios

In order to investigate possible protection practices that could have prevented the extensive damage from Hurricane Ike, three dune enhancement designs and three beach nourishment alternatives were tested. The results of the dune enhancement and beach nourishment scenarios are presented in the following figures, tables and graph, followed by a discussion of the results. The values in the table are derived by the following: The beach region is the volume of sediment from a 0 m shoreline to the PVL, and the foredune region is the volume of sediment between the PVL and the landward dune boundary. The foredune region is redefined for the post-storm surface to account for the landward deposition of foredune sediment. The first image in figures 33-38 is the final bed level for the enhanced scenario, the second is the total erosion and deposition for that scenario, and the third is the difference between the final bed level of the enhanced scenario and the final bed level of the non-enhanced surface. The non-enhanced surface is subtracted from the enhanced surface, so the yellow to reds in the third image reveal areas where the post-storm enhanced surface is higher, and the blues represent where the post-storm non-enhanced surface is lower.

Beach Nourishment Only

The simulation results with only the added beach nourishment showed positive results when compared to the results of the non-enhanced surface. Although the added sediment did not help the survival of the foredune, it did aid in dissipating the storm surge energy, resulting in less net change in sediment volume of the beach and foredune zones. The beach only lost 9% of its sediment, in comparison to a 33% loss without the nourishment. The foredune retained 1,381 m^3 more of its sediment than without nourishment. The post-storm surface is higher within the beach and foredune zones, compared to the non-enhanced post-storm surface, and there is less deposition landward of the foredune (figure 33).

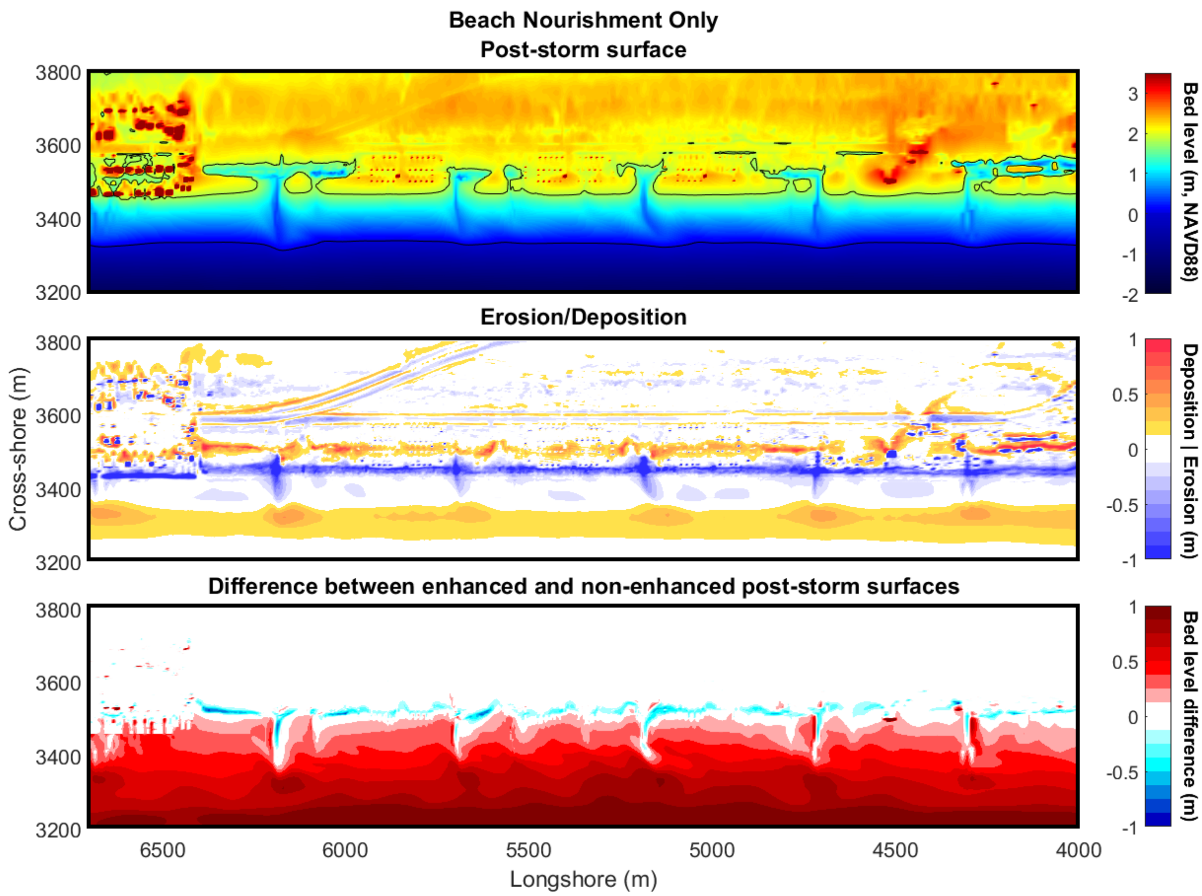

Figure 33. First image shows the final bed level for the enhanced scenario, "Beach Nourishment Only", with contour lines drawn at -2m, 0m, and 1.8m. The second image shows the final erosion and deposition patterns. The third image shows the final bed level difference between the enhanced surface and the non-enhanced surface. Reds in the third image reveal higher bed levels than the non-enhanced surface, and blues reveal lower bed levels than the non-enhanced surface.

Dune A : 4.5 m dune crest; 21 m wide; 4 m crest width

The simulation results of the dune repair scenario where the dune crest height was set at 4.5 m with a 21 m width exhibited similar final bed level results as did the non-enhanced surface. The foredune did not withstand the energy from the storm surge and was washed over during the peak of the surge. The location of the overwash throats are also the same. The volume of sediment left in each the foredune and beach regions of this scenario is only about 1,000 m^3

greater than the volume of sediment left in each of these regions with the non-enhanced surface, even though 6,537 m^3 of sand was added. The enhanced foredune lost 43% of its sediment, whereas the non-enhanced foredune lost only 33% of its sediment. The difference in the volume deposited in the surf zone is only 855 m^3 greater than the non-enhanced surface simulation results. Dune A resulted in the greatest loss of sediment from the beach and foredune areas.

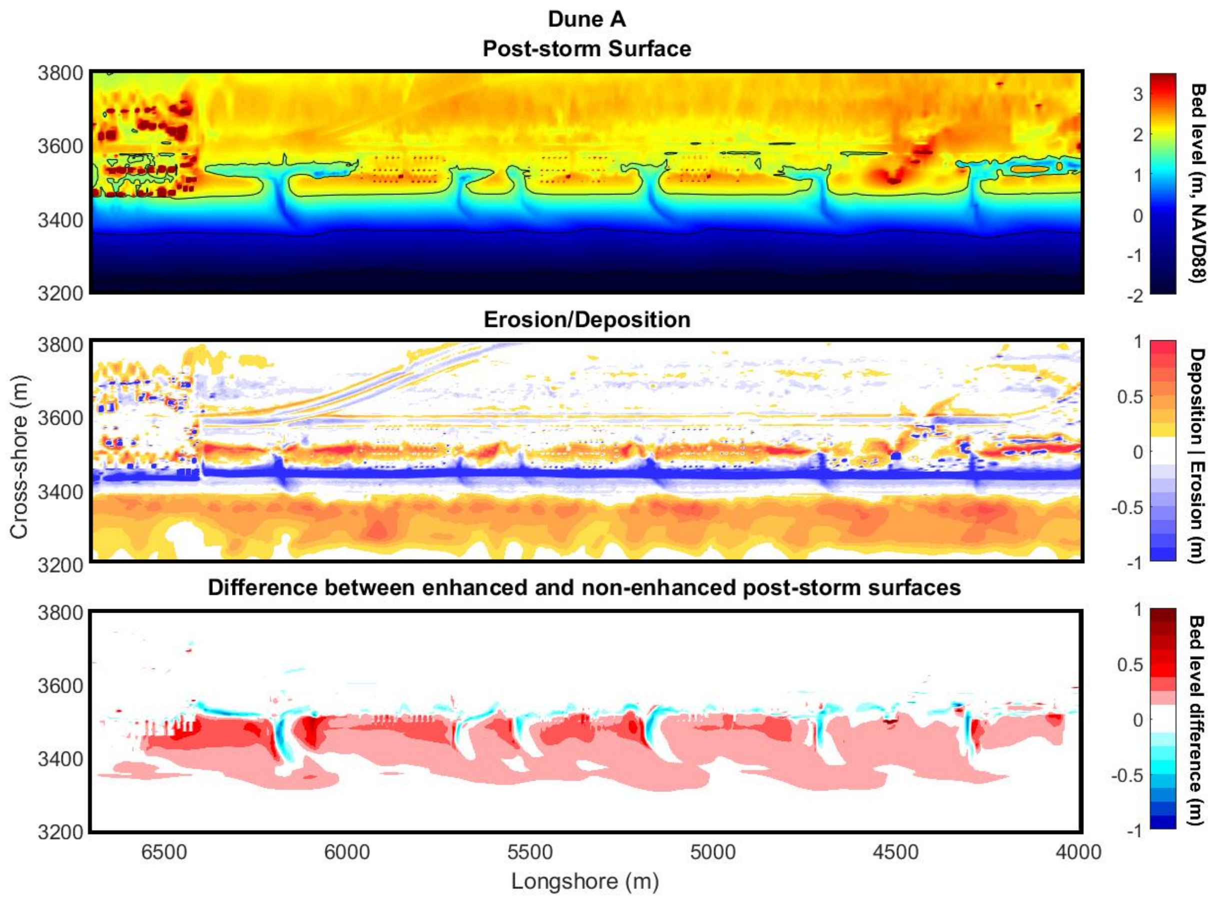

Figure 34. First image shows the final bed level for the enhanced scenario, "Dune A ", with contour lines drawn at -2m, 0m, and 1.8m. The second image shows the final erosion and deposition patterns. The third image shows the final bed level difference between the enhanced surface and the non-enhanced surface. Reds in the third image reveal higher bed levels than the non-enhanced surface, and blues reveal lower bed levels than the non-enhanced surface.

Dune A + Beach Nourishment

The addition of sediment to the system along with the dune A repair scenario resulted in a net sediment gain of 670 m^3 to the beach region after the storm, an increase of almost 8%

compared to the non-enhanced scenario. This scenario, however, did not provide the best protection, as the foredune failed to endure the energy of the surge. The dunes were also breached in the same locations, however, the widths of the throats were slightly narrower in this scenario. Even though the foredune was washed over, a greater volume of sediment is remaining in the foredune zone than what was remaining in the non-enhanced foredune zone after the storm (figure 35).

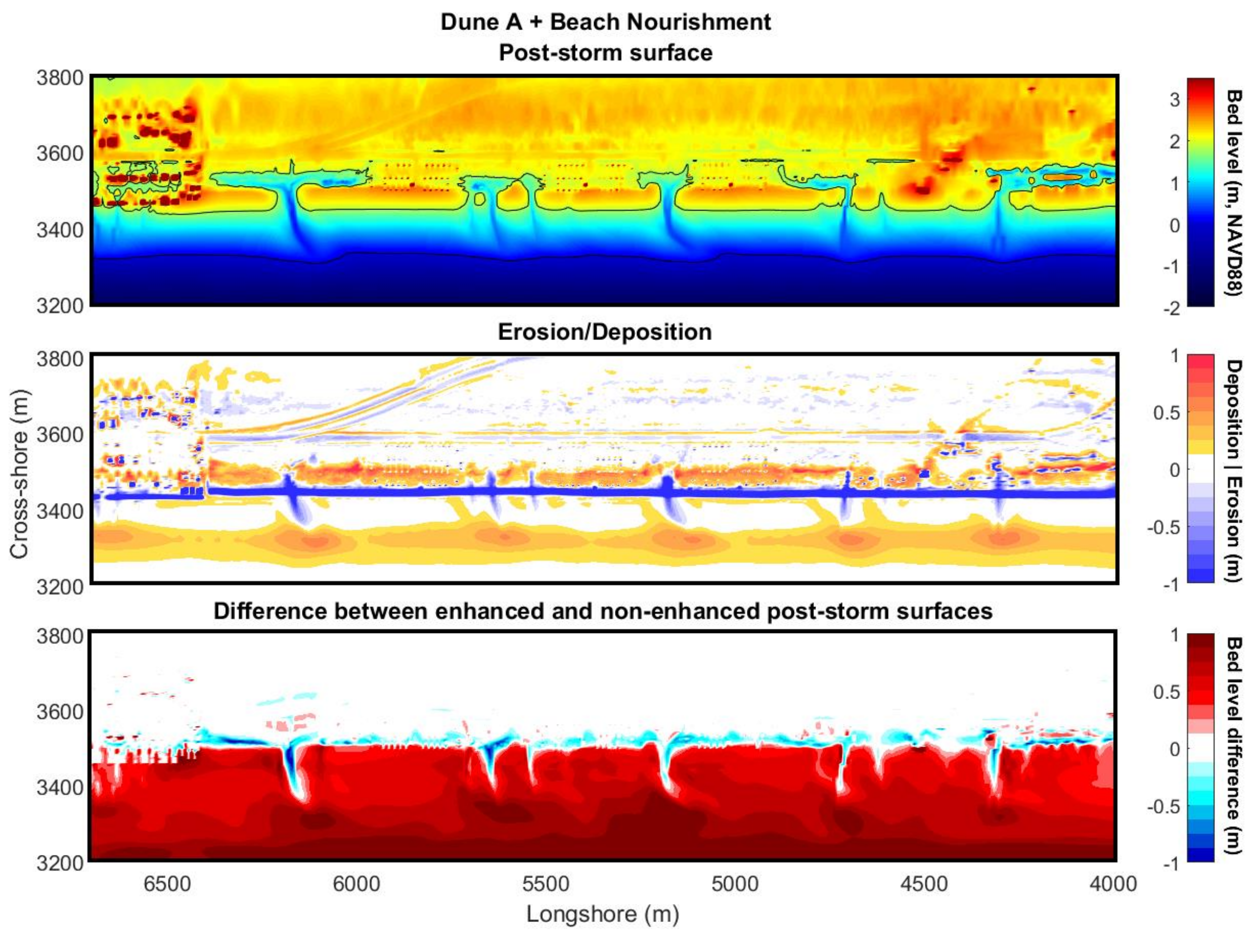

Figure 35. First image shows the final bed level for the enhanced scenario, "Dune A + Beach Nourishment", with contour lines drawn at -2m, 0m, and 1.8m. The second image shows the final erosion and deposition patterns. The third image shows the final bed level difference between the enhanced surface and the non-enhanced surface. Reds in the third image reveal higher bed levels than the non-enhanced surface, and blues reveal lower bed levels than the non-enhanced surface.

Dune B: 4.5 m dune crest; 37 m wide; 10 m crest width

The increase in the crest width, dune width, and slope for the 4.5 m dune provided greater protection than the narrower, steeper dune. Dune B resulted in only a 1% decrease in sediment to the beach, in comparison to Dune A, which lost 14% of sediment from the beach. The difference in volume of sand for each of these dune designs is only 4,193 m^3. The remaining volume of sediment left in the foredune zone was twice as much as was remaining of Dune A.

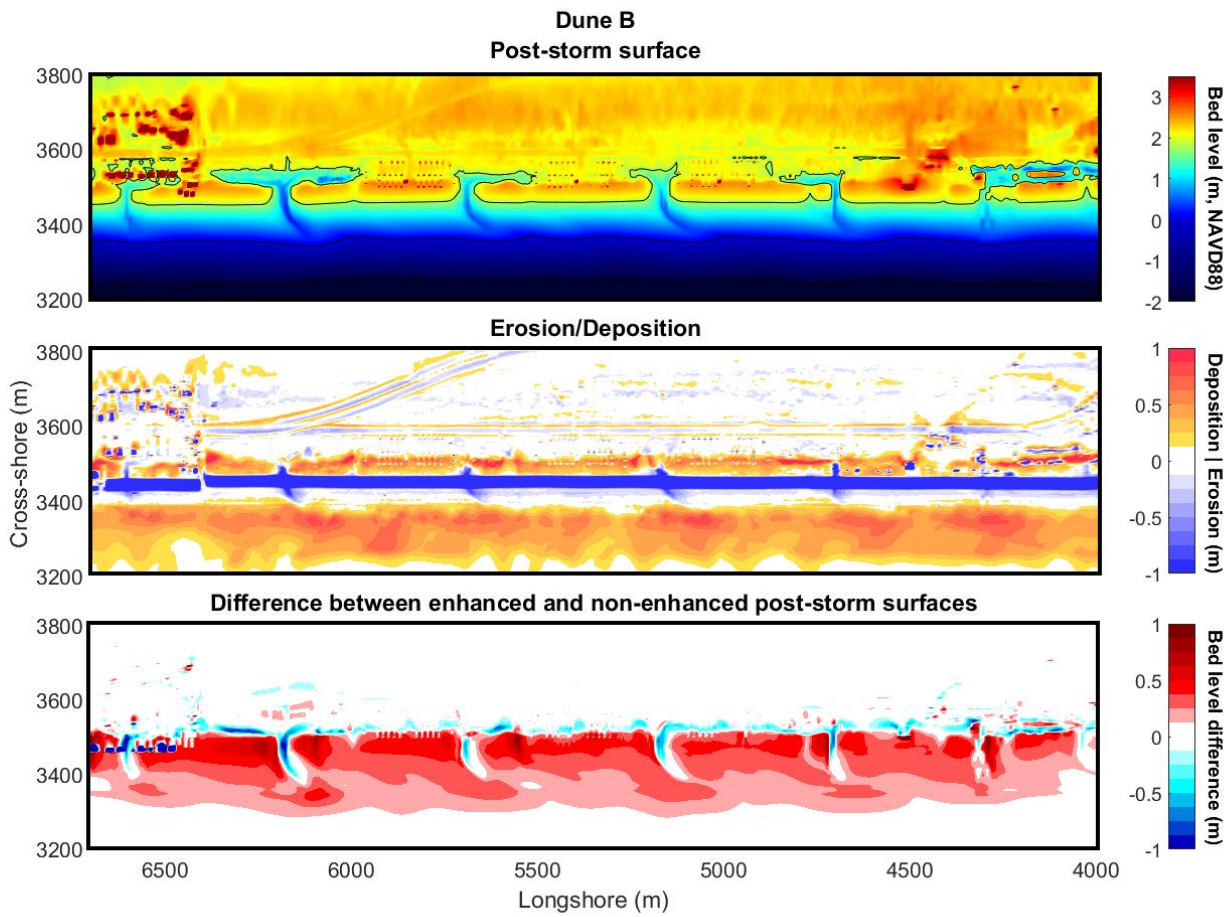

Figure 36. First image shows the final bed level for the enhanced scenario, "Dune B", with contour lines drawn at -2m, 0m, and 1.8m. The second image shows the final erosion and deposition patterns. The third image shows the final bed level difference between the enhanced surface and the non-enhanced surface. Reds in the third image reveal higher bed levels than the non-enhanced surface, and blues reveal lower bed levels than the non-enhanced surface.

Dune B + Beach Nourishment

The addition of beach nourishment to Dune B resulted in the strongest configuration. The dune system breached only during the return flow. The foredune remains intact, with only 28% of sediment lost, in comparison to 45% lost without the nourishment. Net volume increase on the beach for this scenario was 2,042 m^3, an increase of 23%. This scenario had the lowest percentage of net volume lost for both the beach and foredune zones, calculated at only 14%.

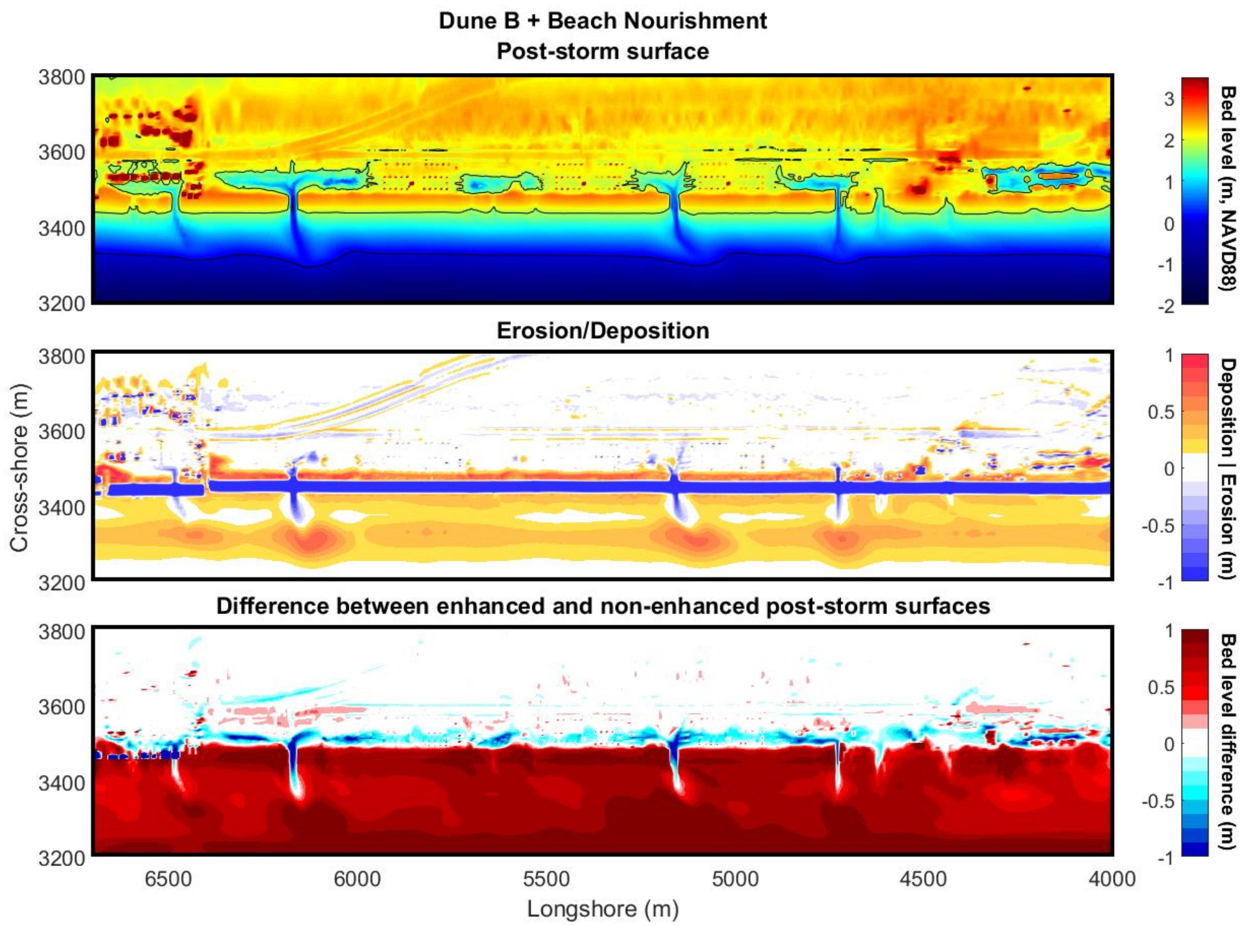

Figure 37. First image shows the final bed level for the enhanced scenario, "Dune B + Beach Nourishment", with contour lines drawn at -2m, 0m, and 1.8m. The second image shows the final erosion and deposition patterns. The third image shows the final bed level difference between the enhanced surface and the non-enhanced surface. Reds in the third image reveal higher bed levels than the non-enhanced surface, and blues reveal lower bed levels than the non-enhanced surface.

Dune C: 6.5 m dune crest; 37 m wide; 10 m crest width

The final scenario was designed to see how high a foredune needed to be to provide protection against another Ike-like storm event, while still abiding by Galveston's dune restoration minimum design codes, and without having to take out any more rows of development. As mentioned previously, a row of development was removed from the pre-storm surface to make room for the 37-meter-wide dune. The mighty 6.5-meter-high dune kept the surge from overtopping. Minor breaches occurred during the return flow. The seaward transport of sediment from the erosion of the dune provided plenty of nourishment to the beach and nearshore, increasing the net volume of the beach by 32%, a sediment gain of 1,801 m^3. This large dune ridge was still severely eroded and lost 39% of its sediment, leaving only 15,590 m^3 of sediment in the foredune zone. In comparison, the post-storm foredune volume of the smaller Dune B + nourishment configuration was greater, calculated at 16,133 m^3. It should also be noted that approximately the same amount of sand was added to the beach and foredune regions for both configurations.

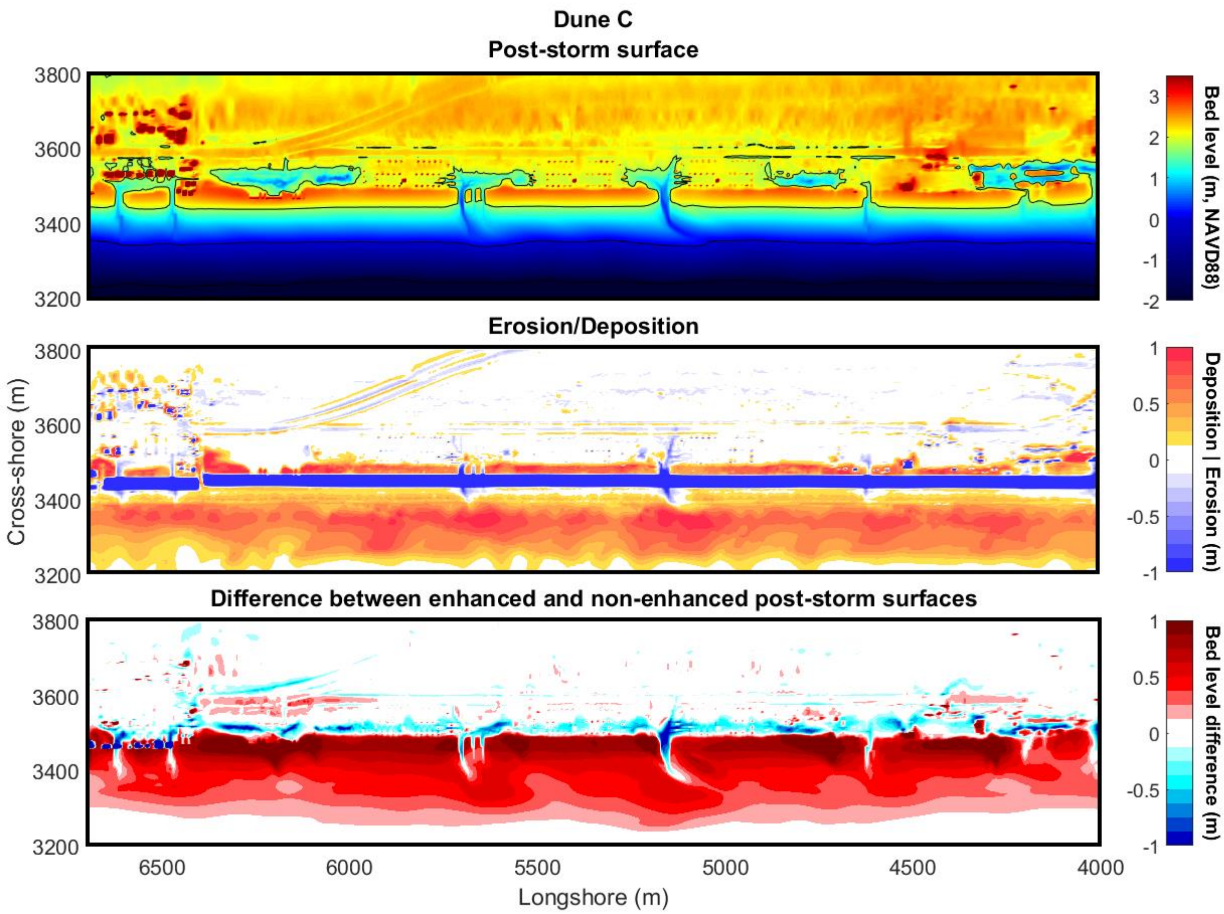

Figure 38. First image shows the final bed level for the enhanced scenario, "Dune C", with contour lines drawn at -2m, 0m, and 1.8m. The second image shows the final erosion and deposition patterns. The third image shows the final bed level difference between the enhanced surface and the non-enhanced surface. Reds in the third image reveal higher bed levels than the non-enhanced surface, and blues reveal lower bed levels than the non-enhanced surface

Table 3. Non-enhanced surface sediment volume changes for the beach and foredune zones. A comparison between the measured and computed results.

		Volume (m^3)		
		Beach	**Dune**	**Total**
Non-enhanced surface	Pre	5,592	11,885	17,477
	Post-XBeach	3,693	5,416	9,109
	Change-XBeach	-1,899	-6,469	-8,368
	Post-lidar	778	3,870	4,648
	Change-lidar	-4,814	-8,015	-12,829

Table 4. Enhanced surface sediment volume changes for the beach and foredune zones

		Volume (m^3)		
		Beach	**Dune**	**Total**
Dune A	Pre	5,586	18,421	24,007
	Post	4,783	6,361	11,144
	Change	-803	-12,060	-12,863
Dune B	Pre	5,587	22,614	28,201
	Post	5,526	12,329	17,855
	Change	-61	-10,285	-10,346
Dune C	Pre	5,585	32,191	37,776
	Post	7,384	15,590	22,974
	Change	1,801	-16,601	-14,800
Nourish Only	Pre	8,744	11,885	20,623
	Post	7,957	6,797	14,754
	Change	-787	-5,088	-5,875
Nourish + Dune A	Pre	8,738	18,421	27,159
	Post	9,408	8,012	17,420
	Change	670	-10,409	-9,739
Nourish + Dune B	Pre	8,739	22,614	31,353
	Post	10,781	16,133	26,914
	Change	2,042	-6,481	-4,439

Figure 39 provides a visual for the best project considering the amount of sand added to enhance the pre-storm beach and foredune regions in comparison to the degree of protection it provided. The additional post-storm beach and foredune zone volume for each scenario is calculated by subtracting the post-storm non-enhanced scenario total foredune and beach volume (table 3) from the post-storm enhanced scenario total volume (table 4). The amount of sand added to the beach and foredune zone is calculated by subtracting the pre-storm non-enhanced surface from the pre-storm enhanced surface. A 1:1 line is drawn to represent an equal ratio of the additional sediment remaining in the beach and foredune zone and the volume of pre-storm sediment added to the zones. Scenarios plotted below the line retained more sand in the beach and foredune zone than what was added to enhance the pre-storm beach and dune, therefore implying a better use of sand resources. Scenarios plotted above and farthest from the line are considered poor project designs because the additional post-storm sediment remaining in the system is less than what was added to enhance the pre-storm surface. For example, Dune A enhancement scenario is the worst use of sand resources because it provided the least amount of protection and required the addition of three times more sand to the pre-storm surface than what was remaining post-storm. In contrast, the beach nourishment only scenario added almost twice as much volume to the post-storm beach and foredune than what was added to the pre-storm beach. Dune B and the beach nourishment + Dune A scenario required similar volumes of sand and provided comparable degrees of protection. Although Dune C was the strongest dune configuration, the amount of sediment added to the pre-storm surface was far greater than the remaining post-storm volume. Finally, the beach nourishment + Dune B enhancement scenario is the most efficient coastal protection project providing the greatest degree of protection from an extreme storm. These results can help coastal managers decide the best use of sand resources for protecting the island from a future hurricane like Ike.

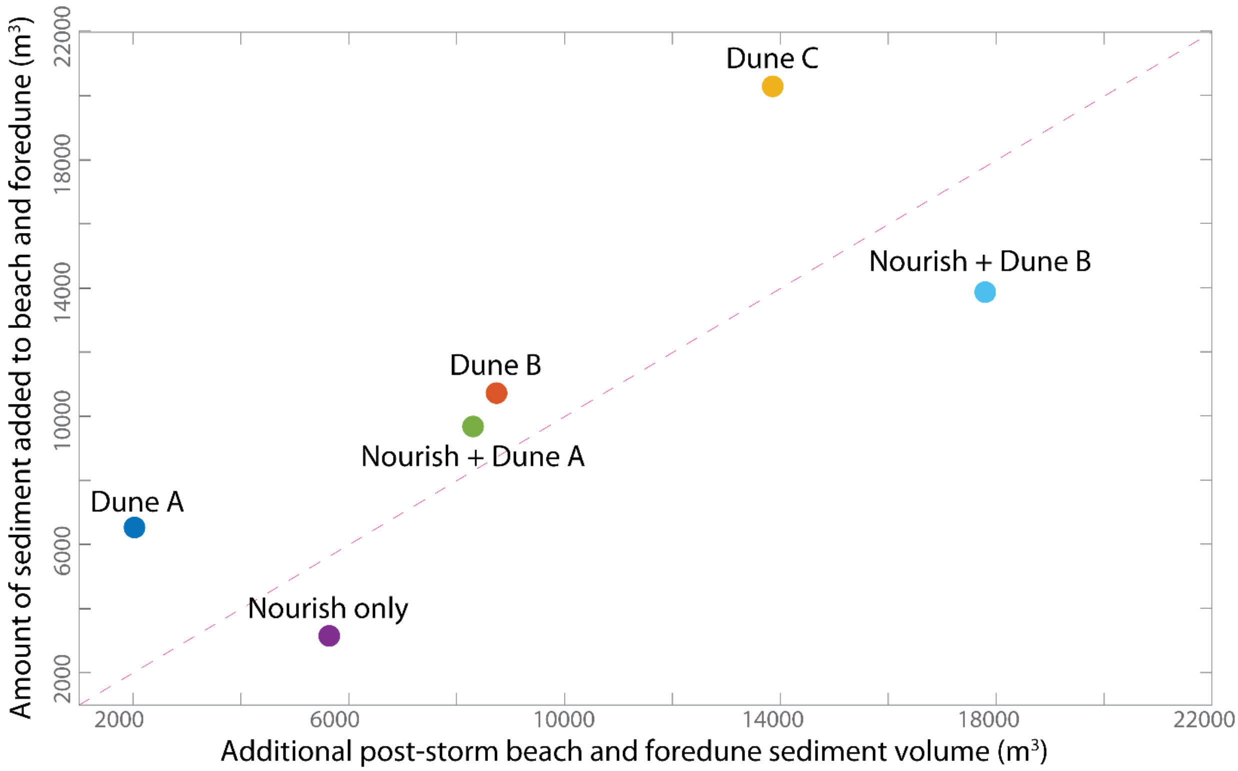

Figure 39. Plot showing the efficacy of each coastal protection project. The additional post-storm beach and foredune zone volume for each scenario is calculated by subtracting the post-storm non-enhanced scenario total foredune and beach volume (table 3) from the post-storm enhanced scenario total volume (table 4). The amount of sand added to the beach and foredune zone is calculated by subtracting the pre-storm non-enhanced surface from the pre-storm enhanced surface. A 1:1 line is drawn to represent an equal ratio of the additional sediment remaining in the beach and foredune zone and the volume of pre-storm sediment added to the zones.

CHAPTER V: DISCUSSIONS AND CONCLUSIONS

In this study, the morphodynamics of a portion of Galveston Island were examined in response to the hydrodynamic forcing conditions generated by Hurricane Ike. Variations of hypothetical topographic conditions were also tested under the same hydrodynamic conditions to identify how dune enhancement and beach nourishment coastal protection practices might help mitigate coastal erosion and the effects of storm surge during such an event.

The objectives of this research were accomplished by the application of XBeach, a process-based model that solves coupled equations for cross-shore and longshore hydrodynamics and morphodynamics in a two-dimensional spatial domain under hurricane conditions. The predicted topographic response was evaluated against topographic data collected three months after Hurricane Ike made landfall. Measured wave and surge data were used to generate parametric boundary conditions for the XBeach model. The simulation of Galveston Island showed that XBeach is capable of simulating inundation overwash over a varying longshore topography, by producing morphological features common to overwash such as foredune erosion and back barrier deposition. The quantitative skill of the model was determined by comparing the subaerial post-storm surface with a zero bed level change estimate. The model Brier skill score had a mean value of 0.67, and upwards of up to 0.92 in the foredune zone alone. The quality of the model performance in the foredune zone is important for the second objective of this research, which was to determine how large a foredune needed to be to protect against Ike's wave and surge energy.

An interesting response the model continued to resolve was the location of dune breaches. The channelization of the surge through the dunes was localized where an area of lower-lying swale topography existed landward of the foredune, in between the higher and flatter paved parking lots. Dune breaching typically occurs in between dune crests where the elevations are lower, and/or areas of less dense vegetation stabilizing the dune. In each hypothetical topographic scenario, the crest of the dune was uniform alongshore, and yet the dune breached in relatively the same locations. Such implications can be useful for developers on barrier islands. Building development in close proximity to these weak spots will result in greater chance of flooding due to dune failure.

The morphological state of the island during the storm was described using the storm regimes defined by Sallenger (2000) as a template. During the swash and collision regimes, the greatest amount of beach erosion occurred. The overwash regime lead to the largest reduction in the foredune, and there were minimal changes in the state of the island during the inundation regime. These results show that the increase in surge elevation during the inundation regime does not necessarily result in greater destruction of the dune elevation, a phenomenon also found by Long *et al.,* 2014.

The second objective of this study was to determine if a larger foredune would have provided greater protection against Hurricane Ike hydrodynamic conditions. The first dune design was based on the minimum criteria set by the Galveston Code of Ordinances (GCO) for man-made dune restoration. The determined height of the dune was 1.5 meters above the maximum surge tide elevation measured at Pleasure Pier. The width of the designed dune was limited by the presence of development and the location of the natural dune toe. This first dune design resulted in the greatest amount of net sediment loss in the system, even when compared to the non-enhanced surface. The second and third dunes were designed based on guidelines established within the Coastal Engineering Manual, which recommend a more gradual seaward slope and a wide dune crest. The second dune design was able to delay the timing of inundation overwash over the island by about five hours, however, the enhanced dune failed to prevent the incoming peak in storm surge and waves from overtopping the foredune. The final dune enhancement design did not fail; however, the height of the dune was unrealistic for Galveston Island. The configuration of the dune was also inefficient, as it required a large volume of sand. The addition of a beach nourishment to Dune B utilized less additional sediment within the pre-storm beach and foredune system than Dune C and resulted in the greatest protection to the system. This dune design, however, required the removal of the first row of development to provide room for a wider dune. The city of Galveston should consider this if they would like to protect the greater extent of development on the island from future extreme storm events. The existing narrow foredune zone provides minimal protection from a storm that generates high surge and waves along Galveston Island's coastline.

In summary, an enhanced foredune alone could not suppress the high surge and wave energy from breaching and overwash. The beach nourishment projects helped to dampen the storm surge energy. Each coastal protection project supplied additional sand to the system, which may perhaps aid and possibly speed up the post-storm recovery process. The additional sediment remaining in the system can serve as protection in case of frequent storm events.

Limitations of the study

There are a few limitations in this study to consider. First of all, it is important to note that although XBeach is a robust model, it is computationally expensive. Without the use of a high-performance computer, it can take days to compute the morphodynamics of a single storm event. Even with a HPC, the domain size is constrained if restricted on time. Additionally, the model simplifies certain processes, and such assumptions in the model should be made aware. An example of this is the depth averaging process. The spatial domain is divided in grid cells, but the vertical dimension is modeled by only one layer of cells. Often, sediment concentrations are larger near the bottom than near the surface, however all information in the vertical structure is put in one single number for each grid cell. Therefore, spiral flow motions and depth varying flow directions are not taken into account. The XBeach model should therefore only be used as a prediction tool, and not as an exact representation of reality.

Additional limitations exist due to the uncertainty in the accuracy of the topographic and bathymetric data to represent exactly what the bed level was both before and after the passage of Hurricane Ike. The most recent pre-storm lidar data were collected in 2006, two years before Ike. Because the foredune system in this region is densely vegetated, there are likely minimal changes in the dune size and shape. The beach system however is a more dynamic system, especially with the passing of storms both tropical and extratropical as well as nuisance flooding. The elevation and width of the beach during the 2006 lidar survey may not accurately reflect the state of the beach just before Ike made landfall. Further discrepancies in the model's output could exist due to the three-month gap between the measured post-Ike lidar data and Ike's landfall. And finally, the dynamic nearshore creates a difficult area to accurately represent, especially without any recent pre- or post-storm data.

Another limitation to consider is the fact that the coastal protection projects tested in this study only covered a small percentage of Galveston Island. When tested, the same elevations for the bay surge were used during the simulation. If a nourishment and dune restoration project was applied to the entire island, as well as Bolivar Peninsula, the height of the bay surge could be lowered, resulting in completely different results. The elevations of the bay surge could be resolved by running an ADCIRC model with the manipulated topography.

Last of all, the XBeach model simulation largely under-predicted the volume of sediment eroded from the beach when compared to the post-storm measured lidar. This type of response is unusual for the XBeach model, which typically over-predicts the volume of storm-induced erosion (Nederhoff, 2014). The under-predicted response could be related to the limitations of the pre- and post-storm lidar data, as discussed previously. Alternative causes could be explained by the presence of geo-textile tubes built into the foredunes on the adjacent beach to the north, Pirate's Beach. Large volumes of sediment are locked inside these tubes, which the model is unaware of. The foredune system on Pirate's Beach was also completely eroded during Ike, and that volume of sediment that would have nourished the beach and nearshore was locked inside the tubes. In addition, longshore currents would have transported that sediment to the southwest. To test this hypothesis, the model domain should be extended further to the northeast and include a hard layer inside the foredune system for Pirate's Beach. This test is limited, however, due to the reflective physics of a rubber sand filled tube compared to a concrete angular configuration that the hard layer represents. Further diagnosis of this limitation should involve an analysis of the sediment concentrations and velocities simulated by the model.

Implications for barrier island management

In order to make this research a plausible resource for providing recommendations to the management and sustainability of Galveston Island, further questions need to be answered, such as how much sand is available for such projects, and how much would it cost to implement? Offshore deposits are the most common source of sediment for large beach nourishment projects in other coastal states, however, offshore sediments along the Texas coastline are largely silts and clays which are unsuitable for recreational beaches. Sediment reserves exist farther offshore in the relic barrier islands, Heald and Sabine Bank. Morton and Gibeaut (1995) estimated that

585 million m^3 of sand is contained in Heald Bank, and Sabine bank holds 1.2 billion m^3 of beach quality sand. These reserves are not utilized due to transportation costs. A more conceivable source of sand would come from dredging the Galveston Entrance Channel, which is already dredged on a regular basis. Dredging records indicate that on average, 1.1 million yd^3 of beach quality sediment is dredged from the Galveston Entrance Channel, the Anchorage area, and inner and outer bar channels every year (Frey *et al.*, 2016). The recent beach nourishment project (CEPRA Project No. 1566) borrowed sand from the South Jetty and the Anchorage Basin. Bathymetric surveys performed in 2015 showed these areas contained a total of 7.1 million yd^3 of beach quality sediment (HDR, 2015). The project only utilized up to 1 million yd^3 of the material to nourish a length of approximately 3.6 miles along the historic seawall, with costs up to $19.5 million dollars. If the same construction template were used to nourish the entire length of the coastline, southwest of the seawall (~30 km), it would take roughly 8 million yd^3 of sand and would cost about $156 million dollars. The design added 60 ft of beach width and is proposed to have a project life of 10 to 15 years, depending on storm activity (HDR, 2015). The project life can be extended with proper maintenance, such as smaller-scale nourishments every 5 years. If the nourishment design incorporated a dune restoration project like the one recommended in this study, Dune B, it would require an additional ~222,000 yd^3 of sand to restore the island’s dune system. This would increase the cost of the project by about $4.3 million dollars, a minimal price in comparison to the amount of protection it will provide for the island. Currently, the largest nourishment project in the U.S. was constructed from 1994-2001 in New Jersey where 21 miles of beach were nourished at a cost of $195 million (USACE 2015).

To compare this type of project to the proposed Ike Dike, the cost of the soft-engineering approach would be considerably lower, and might benefit the island in the end. The coastal spine portion of the Ike Dike design alone is expected to cost upwards of $1.3 billion dollars (Jonkman *et al.*, 2015). When a large storm like Ike strikes the island in the future, the coastal spine might inhibit overtopping and flooding, but the beaches will still erode. If the hard structure becomes exposed, it will likely hinder the recovery process, as it neglects the important beach and dune feedback processes that are necessary for a coastline to recover naturally. Additionally, the exposed hard structure will affect the wave refraction, instigating a negative feedback loop as the refracted waves erode the nearshore bars. Consequently, the beach will need to be completely re-constructed, accruing even more costs to the project. Considering all that has been discussed in this research regarding a barrier island's morphodynamic response to an extreme storm, the final recommendations of the author are the following: (1) The City of Galveston should consider a building set back to make room for a wider dune system; (2) to devise and execute an ongoing sand management plan to provide nourishment to the nearshore; and (3) to proceed with soft-engineering coastal protection projects that encourage the barrier island to preserve its natural state, whether it rolls over with the rising seas, or accretes seaward with a successful sand management plan.

Future research

This project can continue to grow in various ways. First, in order to prove this model can be used as a reliable predictive tool for all storms, it should be validated and calibrated with a storm of smaller magnitude that only caused processes which occur during the collision regime, such as dune scarping. A future research project can then test a whole suite of dune and beach nourishment designs as well as storm intensities to find the optimal configuration and its degree of protection.

REFERENCES

Anderson, J. B., Rodriguez, A., Abdulah, K., Banfield, L. A., Bart, P., Fillon, R., McKeown, H., Wellner, J., 2004. Late Quaternary stratigraphic evolution of the northern Gulf of Mexico: a synthesis. *In:* Anderson, J. B., and Fillon, R. H. (eds.), *Late Quaternary Stratigraphic Evolution of the northern Gulf of Mexico Margin.* Society of Sedimentary Research Special Publication 79, 00. 1-24.

Bascom, W. N., 1951. The relationship between sand size and beach-face slope. *American Geophysical Union*, 32 (6), 866-874.

Berg, R. 2009. Tropical Cyclone Report, Hurricane Ike; 1 – 14 September 2008. National Hurricane Center.

Bernard, H. A., Major, C. F. Jr., Parrott, B. S., LeBlanc, R. J. Sr., 1970. Recent sediments of southeast Texas: A field guide to the Brazos alluvial and deltaic plains and the Galveston barrier island complex. University of Texas, Bureau of Economic Geology, Guidebook 11, Austin, 132 pp.

Bilskie, M. V., S. C. Hagan, K. Alizad, S. C. Medeiros, D. L. Passeri, H. F. Needham, and A. Cox, 2016. Dynamic simulation and numerical analysis of hurricane storm surge under sea level rise with geomorphologic changes along the northern Gulf of Mexico. *Earth's Future*, 4, 177-193.

Bowen, A.J., Inman, D.L., Simmons, V.P., 1968. Wave 'set-down' and 'set-up'. *Journal of Geophysical Research* 73 (8), 2569–2577.

Bruun, P., 1954. Coast Erosion and the Development of Beach Profiles. *Technical Memorandum No. 44*. Beach Erosion Board.

Bruun, P., 1962. Sea-level rise as a cause of shore erosion. J. Waterways Harbors Div., A.S.C.E., 88, 117-130.

Clifton, H. E., R. E. Hunter, R. L. Phillips, 1971. Depositional structures and processes in the non-barred high-energy nearshore. *Journal of Sedimentary Petrology*, 4 (3), 651-670.

Church, J. A., and White, N. J., 2011. Sea-level rise from the late 19th to the early 21st century. Surv. Geophys., 32:585-602. doi 10.1007/s10712-011-9119-1

Daly, C., 2009. Low Frequency Waves in the Shoaling and Nearshore Zone A Validation of XBeach. MSc thesis, Delft University of Technology, Delft.

Davis, Jr., Richard A. *Geology of Holocene Barrier Island Systems*. New York: Springer-Verlag, 1994. Print.

Dean, R. G., 1991. Equilibrium beach profiles: characteristics and applications. *Journal of Coastal Research*, 7(1), 53-84.

De Vet, P. L. M., McCall, R., den Bieman, J. P., Stive, M. J. F., van Ormondt, M., 2015. Modelling dune erosion, overwash and breaching at Fire Island (NY) during Hurricane Sandy. *Coastal Sediments*, 1-10.

Donnelly, C.; Kraus, N., Larson, M. 2006. State of knowledge on measurement and modeling of coastal overwash. *Journal of Coastal Research*, 22(4), 965-991.

Doran, S., Plant, N. G., Stockdon, H. F., Sallenger, A. H., Serafin, K. A., 2009. Hurricane Ike: Observations of Coastal Change: U.S. Geological Survey Open-File Report 2009-1061.

East, J.W., Turco, M.J., and Mason, R.R., Jr., 2008, Monitoring inland storm surge and flooding from Hurricane Ike in Texas and Louisiana, September 2008: U.S. Geological Survey Open-File Report 2008–1365 [https://pubs.usgs.gov/of/2008/1365/].

Federal Emergency Management Agency (FEMA), 2008. *Hurricane Ike Impact Report*. Retrieved from: https://www.fema.gov/pdf/hazard/hurricane/2008/ike/impact_report.pdf

Frey, A. E., Morang, A., and King, D. B., 2016. Galveston Island, Texas, Sand Management Strategies. U.S. Army Engineer Research and Development Center, Coastal and Hydraulics Laboratory, Vicksburg, Mississippi: U.S. Army Corps of Engineers, 200 p.

Galveston, Texas – Code of Ordinances, July 21, 2017 (current). Chapter 29 – Planning – Beach access dune protection and beach front construction. https://library.municode.com/tx/galveston/codes/code_of_ordinances?nodeId=PTIICOCI_CH29PLEAACDUPRBEFRCO_ARTIIBEACDUPRBEFRCORE

Gibeaut, J.C., Gutierrez, R., and Hepner, T.L. 2002. Threshold Conditions for Episodic Beach Erosion along the Southeast Texas Coast. Gulf Coast Association of Geological Societies Transactions. Vol 52.

Gibeaut, J. C., Waldinger, W. A., Hepner, T. L., White, R., 2003. Changes in bay shoreline position, West Bay system, Texas. Bureau of Economic Geology, The University of Texas at Austin, Austin, Texas.

Guza, R. T., and Bowen, A. J., 1977. Resonant interactions from waves breaking on a beach. Proc. 15th Int. Conf. Coastal Eng., Honolulu, pp 560-579.

Guza, R. T., and Inman, D. L., 1975. Edge waves and beach cusps. *Journal of Geophysical Research,* 80: 2997-3012.

Guza, R. T., and Thornton, E. B., 1982. Swash oscillations on a natural beach. *Journal of Geophysical Research,* 87, 483-491.

Harte Research Institute (HRI), 2009. Analysis of shoreline change caused by Hurricane Ike on the Upper Texas Coast. GLO Contract No. 06-801-007.

Harte Research Institute (HRI), 2012. Post-Ike volume change report. GLO Contract No. 10-103-005.

Harter, C., and Figlus, J., 2017. Numerical modeling of the morphodynamic response of a low-lying barrier island beach and foredune system inundated during Hurricane Ike using XBeach and CSHORE. *Coastal Engineering*, 120: 64-74.

Hayes, M. O., 1979. Barrier island morphology as a function of tidal and wave regime, *in* S. P. Leatherman, ed., Barrier Islands from the Gulf of St. Lawrence of the Gulf of Mexico: Academic Press, New York, p. 1-28.

Hesp, P., 2002. Foredunes and blowouts: initiation, geomorphology and dynamics. *Geomorphology*, 48, 245-268.

HDR, 2014. Beach and Shoreline Changes along the Upper Texas Coast: Recovery from Hurricane Ike. Final report prepared for the Texas General Land Office.

HDR, 2015. Beach Nourishment along Galveston Seawall. Final report prepared for the Texas General Land Office. HDR Project No. 260554.

Hine, A. C., 1979. Mechanisms of berm development and resulting beach growth along a barrier spit complex. *Sedimentology*, 26, 333-351.

Holman, R. A., Huntley, D. A., Bowen, A. J., 1978. Infragravity waves in storm conditions, in *Proceedings of the 16th Conference on Coastal Engineering*, pp. 268-284, American Society of Civil Engineers, New York, 1978.

Holman, R. A., and Sallenger Jr., A.H., 1985. Setup and swash on a natural beach. *Journal of Geophysical Research* 90 (C1), 945–953.

Holman, R. A., 1986. Extreme value statistics for wave run-up on a natural beach. *Coastal Engineering* 9, 527–544.

Houser, C., Hapke, C., Hamilton, S., 2008. Controls on coastal dune morphology, shoreline erosion and barrier island response to extreme storms. *Geomorphology*, 100, 223-240.

Houser, C., P. Wernette, E. Rentschlar, H. Jones, B. Hammond, S. Trimble, 2015. Post-storm beach and dune recovery: Implications for barrier island resilience. *Geomorphology*. 234, 54-63.

Hubertz, J. M., and Brooks, R. M., 1989. Gulf of Mexico hindcast wave information. Wave Information Studies of U.S. Coastlines, WIS Report 18: Department of the Army, Corps of Engineers, Waterways Experiment Station, Vicksburg, Mississippi.

Hunt, I.A., 1959. Design of seawalls and breakwaters. *Journal of Waterways and Harbors Division*, ASCE 85 (WW3), 123–152.

Irish, J., Frey, A., Mousavi, M.E., Olivera, F., Edge, B., Kaihatu, J., Song, Y., Dunkin, L.M., and S. Finn. 2010. Potential implications of global warming and barrier island degradation on future hurricane inundation, property damages, and population impacted, *Ocean & Coastal Management*, 53, 645-657

Israel, A. M., Ethridge, F. G., Estes, E. L., 1987. A sedimentologic description of a micro-tidal, flood-tidal delta, San Luis Pass, Texas. *Journal of Sedimentary Petrology*, 47(2), 288-300.

Jonkman, S. N., K. T. Lendering, E. C. van Berchum, A. Nillesen, L. Mooyaart, P. de Vries, M. van Ledden, A. Willems, R. Nooij, 2015. Coastal spine system – interim design report. Version 0.6 (final report). Retrieved from online: http://www.tamug.edu/ikedike/images_and_documents/20150620_Coastal_spine_system-interim_design_report_v06.pdf

Kennedy, A. B., Gravois, U., Zachry, B. C., Westerink, J. J., Hope, M. E., Dietrich, J. C., Powell, M. D., Cox, A. T., Luettich Jr., R. A., Dean, R. G., 2011. Origin of the Hurricane Ike forerunner surge. *Geophysical Research Letters,* 28, LO8608, doi:10.1029/2011GL047090.

King, D., 2007. Wave and beach processes modeling: Sabine Pass to Galveston Bay, Texas, shoreline erosion feasibility study. Technical report ERDC/CHL TR-07-6. Vicksburg, MS: U.S. Army Engineer Research and Development Center.

Kriebel, D. and Dean, R. G., 1985. Numerical simulation of time-dependent beach and dune erosion. *Coastal Engineering,* 9, 221-245.

Kurum, M. O, and Overton, M. F., 2013. Scenario testing on the impact of topography, land cover and sea-level rise on barrier island breaching. *Coastal Dynamics*, 1025-1036

Larson, M., and Kraus, N. C., 1989. *SBEACH: Numerical model for simulating storm-induced beach change*. *Report 1-Emperical Foundation and Model Development.* Coastal Engineering Research Center, *Technical report CERC-89-9*. Vicksburg, Mississippi: U.S. Army Corps of Engineers, 256 p.

Leatherman, S.P., 1976. Barrier island dynamics: overwash processes and eolian transport. *Coastal Engineering*, Proceedings of the 15th International Conference, Honolulu, Hawaii. American Society of Civil Engineers, pp. 1958–1974.

Leatherman, S.P., 1979. Barrier dune systems: a reassessment. Sedimentary Geology 24, 1–16.

Lisle, J. T., and Comer, N. N., 2011. Characterization of sediments from the Gulf of Mexico and Atlantic shorelines, Texas to Florida: U.S. Geological Survey Open File Report 2011-1199, xxp.

Lindemer, C. A., N. G. Plant, J. A. Puelo, D. M. Thompson, T. V. Wamsley, 2010. Numerical simulation of low-lying barrier island's morphological response to Hurricane Katrina. *Coastal Engineering,* 57, 985-995.

Longuet-Higgins, M. and Stewart, R., 1964. Radiation stress in water waves: a physical discussion with applications. *Deep-Sea Research*, II: 529–562.

McBride, R. A., Byrnes, M. R., Hiland, M. W., 2015. Geomorphic response-type model for barrier coastlines: a regional perspective, *Marine Geology*, 126, 143-159.

McCall, R., van Thiel de Vries, J. S. M., Plant, N., Van Dongeren, A., Roelvink, J., Thompson, D., and Reniers, A. (2010b). Two-dimensional time dependent hurricane overwash and erosion modeling at Santa Rosa Island. *Coastal Engineering*, 57(7):668–683.

McGowen, J. H., Garner, L. E., Wilkinson, B. H., 1977. The gulf shoreline of Texas: process characteristics, and factors in use, The University of Texas at Austin Bureau of Economic Geology, geological circular, 77-3.

McLean, R. and Shen, J-S., 2006. From foreshore to foredune: foredune development over the last 30 years at Moruya Beach, New South Wales, Australia. *Journal of Coastal Research*, 22(1), 28-36.

Mehvar, S., Dastgheib, A., Roelvink, D., 2015. Validation of XBeach model for wave run-up. E-Proceedings of the 36th IAHR World Congress.

Morang, A., 2006. *North Texas Sediment Budget.* Galveston, Texas: U.S. Army Corps of Engineers, Engineer Research and Development Center, 55 pp.

Morton, R. A., 1976. Effects of Hurricane Eloise on beach and coastal structures, Florida Panhandle. *Geology*, 4, 277-280.

Morton, R. A., Paine, J. G., 1985. Beach and vegetation line changes at Galveston Island, Texas: Erosion, deposition, and recovery from Hurricane Alicia. University of Texas, Bureau of Economic Geology, Geological Circular 75-2, Austin, 47 pp.

Morton, R. A., 1988. Interactions of storm, seawalls, and beaches of the Texas coast. In: Kraus, N.C., Pilkey, O.H. (eds) Effects of seawalls on the beach. Journal of Coastal Research Special Volume 4, 113-134.

Morton, R. A., 1994. Texas Barriers. *In:* Davis, R. A. (ed.), *Geology of Holocene Barrier Island Systems.* New York: Springer-Verlag, pp. 75-111. Print.

Morton, R.A., Paine, J.G., Gibeaut, J.C., 1994. Stages and durations of post-storm beach recovery, southeastern Texas coast, USA *Journal of Coastal Research*, 884–908.

Morton, R. A., Gibeaut, J. C., Paine, J. G., 1995. Meso-scale transfer of sand during and after storms: implications for prediction of shoreline movement, *Marine Geology*, 126, 161-179.

Morton, R.A., 2002. Factors controlling storm impacts on coastal barriers and beaches — a preliminary basis for near real-time forecasting. *Journal of Coastal Research*. 18, 486–501.

Munk, W. H., 1949. The solitary wave theory and its application to surf problems. New York Acad. Science Annuals, 51, 376, 1949.

Nederhoff, K., 2014. Modeling the effects of hard structures on dune erosion and overwash; Hindcasting the impact of Hurricane Sandy on New Jersey with XBeach. PhD thesis, Delft University of Technology, Delft.

Neumann J. E., K. Emanual, S. Ravela, L. Ludwig, P. Kirshen, K. Bosma, J. Martinich, 2015. Joint effects of storm surge and sea-level rise on US Coasts: new economic estimates of impacts, adaptation, and benefits of mitigation policy. *Climate Change,* 129, 337-349.

Niedoroda, A. W. and Swift, D. J. P., 1981. Maintenance of the shoreface by wave orbital currents and mean flow: observations from the Long Island coast. *Geophysical Research Letters,* 8: 337-340.

Niedoroda, A. W., D. J.P. Swift, T. S. Hopkins, C. Ma, 1984. Shoreface morphodynamics on wave-dominated coasts. *Marine Geology,* 60, 331-354.

Paine, J. G., Caudle, T., Andrews, J., 2012. Shoreline movement along the Texas Gulf Coast, 1930's to 2012. The University of Texas at Austin Bureau of Economic Geology, final report prepared for the Texas General Land Office.

Paine, J. G., Caudle, T., Andrews, J., 2013. Shoreline, beach, and dune morphodynamics, Texas Gulf coast. The University of Texas at Austin Bureau of Economic Geology, final report prepared for the Texas General Land Office.

Plant, N. G., and Stockdon, H. F., 2012. Probabilistic prediction of barrier-island response to hurricanes. *Journal of Geophysical Research,* 117, F03015, doi:10.1029/2011JF002326.

Psuty, N. P., 1988. Sediment budget and beach/dune interaction. In: Psuty, N. P. (Ed.), *Journal of Coastal Research Special Issue,* vol. 3. C.E.R.F., Florida, pp. 1-4.

Ravens, T. M., and Sitanggang, K. I., 2007. Numerical modeling and analysis of shoreline change on Galveston Island. *Journal of Coastal Research,* 23(3), 699-710.

Rebuild by Design, The Blue Dunes Report. Retrieved from online: http://www.rebuildbydesign.org/data/files/669.pdf

Rodriguez, A. B., Hamilton, M. D., Anderson, J. B., 2001. Variations in shoreface progradation and ravinement along the Texas coast., Gulf of Mexico. *Sedimentology,* 48, 837-853.

Roelvink, D. A., van Dongeren, A., McCall R., Hoonhout, B., van Rooijen, A., van Geer, P., de Vet, L., Neederhof, K., Quataert, E., 2015. XBeach Technical Reference: Kingsday Release. Deltares.

Roelvink, D., A. Reniers, A. Van Dogeren, J.S.M. Van Thiel de Vries, R. McCall and J. Lescinski. 2009. Modeling storm impacts on beaches, dunes and barrier islands. *Coastal Engineering*, 56, 1133–1152.

Rogers, A. L., and Ravens, T. M., 2008. Measurement of longshore transport rates in the surf zone on Galveston Island. *Journal of Coastal Research,* 24(2B), 62-73.

Roth, D., 2013. Texas hurricane history: National Weather Service, Camp Springs, Maryland, 80 p. https://www.weather.gov/media/lch/events/txhurricanehistory.pdf

Ruggiero, P., P. D. Komar, W. G. McDougal, J. J. Marra, R. A. Beach, 2001. Wave runup, extreme water levels and the erosion of properties backing beaches. *Journal of Coastal Research,* 17 (2), 407-419.

Sallenger, A.H., 2000. Storm impact scale for barrier islands, *Journal of Coastal Research*, 16(3), 890-895.

Stockdon, H. F., Holman, R. A., Howd, P. A., Sallenger, A. H., 2006. Empirical parameterization of setup, swash, and runup. *Coastal Engineering*, 53, 573-588.

Stockdon, H. F., Sallenger, A. H., Holman, R. A., Howd, P. A., 2007. A simple model for the spatially-variable coastal response to hurricanes. *Marine Geology,* 238, 1-20.

Stone, G.W., Liu, B., Pepper, D.A., Wang, P., 2004. The importance of extratropical and tropical cyclones on the short-term evolution of barrier islands along the northern Gulf of Mexico. *Marine Geology*. 210, 63–78.

Sutherland, J., Peet, A.H., and Soulsby, R. L., 2004. Evaluating the performance of morphological models. *Coastal Engineering,* 51, 917-939.

Thornton, E.B., MacMahan, J.H., Sallenger Jr., A.H., 2007. Rip currents, mega cusps and eroding dunes. *Marine Geology,* 240, 151–167.

U.S. Army Corps of Engineers, (USACE), 2015. Coastal Texas protection and restoration study. Final Reconnaissance 905(b) Report. Galveston District, Southwestern Division. 79 pp. http://www.swg.usace.army.mil/Portals/26/docs/PAO/TC/Coastal%20Texas%20Section%20905_b_%20-2015%20May%2018.pdf

U.S. Army Corps of Engineers, (USACE), 2008. “Beach Fill Design”, *Coastal Engineering Manual (CEM), 1110-2-1100,* U.S. Army Corps of Engineers, Washington, D.C.

Van Thiel de Vries, J. S. M., 2009. Dune erosion during storm surges. PhD thesis, Delft University of Technology, Delft.

Vousdoukas, M. L., O. Ferreira, L. P. Almeida, A. Pacheco, 2012. Toward reliable storm-hazard forecasts: XBeach calibration and its potential application in an operational early-warning system. *Ocean Dynamics,* 62, 1001-1015.

Wallace, D. J., Anderson, J. B., Fernandez, R. A., 2010. Transgressive ravinement versus depth of closure. *Journal of Coastal Research,* 26(6), 1057-1067.

Wright, L.D., and Short, A.D., 1984. Morphodynamic variability of surf zones and beaches: A synthesis. *Marine Geology,* 56, 93:118.

APPENDIX

XBeach model input files

Params.txt

```
%%%%%%%%%%%%%%%%%%%%%%%%%%%%%%%%%%%%%%%%%%%%%%%%%%%%%%%%%%%%%%%%%%%%%%%%%%%%%%%
%%% XBeach parameter settings input file                                    %%%
%%%                                                                    %%%
%%% date:  23-Mar-2017 16:22:27                                          %%%
%%% function: xb_write_params                                            %%%
%%%%%%%%%%%%%%%%%%%%%%%%%%%%%%%%%%%%%%%%%%%%%%%%%%%%%%%%%%%%%%%%%%%%%%%%%%%%%%%

%%% Bed composition parameters %%%%%%%%%%%%%%%%%%%%%%%%%%%%%%%%%%%%%%%%%%%%%%%

D50   = 0.000132
D90   = 0.000187

%%% Flow parameters %%%%%%%%%%%%%%%%%%%%%%%%%%%%%%%%%%%%%%%%%%%%%%%%%%%%%%%%%%

bedfriction = chezy
bedfricfile = bedfricfile.txt

%%% Grid parameters %%%%%%%%%%%%%%%%%%%%%%%%%%%%%%%%%%%%%%%%%%%%%%%%%%%%%%%%%%

depfile  = bed.dep
posdwn  = 0
nx   = 1348
ny   = 620
alfa   = 0
vardx  = 1
xfile  = x.grd
yfile  = y.grd
xori   = 0
yori   = 0
thetamin  = 45
thetamax  = 245
dtheta  = 20
thetanaut = 1

%%% MPI parameters %%%%%%%%%%%%%%%%%%%%%%%%%%%%%%%%%%%%%%%%%%%%%%%%%%%%%%%%%%%

mpiboundary = x

%%% Model time %%%%%%%%%%%%%%%%%%%%%%%%%%%%%%%%%%%%%%%%%%%%%%%%%%%%%%%%%%%%%%%

tstop  = 345600

%%% Morphology parameters %%%%%%%%%%%%%%%%%%%%%%%%%%%%%%%%%%%%%%%%%%%%%%%%%%%%

morfac  = 10
struct  = 1
```

```
ne_layer  = nebed.dep

%%% Tide boundary conditions %%%%%%%%%%%%%%%%%%%%%%%%%%%%%%%%%%%%%%%%%%%%%%%%

zs0file  = tide.txt

%%% Wave boundary condition parameters %%%%%%%%%%%%%%%%%%%%%%%%%%%%%%%%%%%%%%

instat  = jons_table

%%% Wave-spectrum boundary condition parameters %%%%%%%%%%%%%%%%%%%%%%%%%%%%%

bcfile  = jonswap3.txt

%%% Output variables %%%%%%%%%%%%%%%%%%%%%%%%%%%%%%%%%%%%%%%%%%%%%%%%%%%%%%%%

outputformat = netcdf
tintg  = 3600
tstart  = 0

nglobalvar = 6
zb
zs
H
ue
ve
sedero
```

Table 5. Description of recorded input parameters. All other required XBeach parameters use default values.

Parameter	Description	Value	Units
depfile	Name of input bathymetry file	Bed.dep	<file>
nx	Number of grid cells in x-direction	1348	
ny	Number of grid cells in y-direction	620	
vardx	Switch for variable grid spacing	1	
xfile	Name of file containing x-coordinates	x.grd	<file>
yfile	Name of file containing y-coordinates	y.grd	<file>
thetamin	Lower wave directional limit	45	Nautical degrees
thetamax	Higher wave directional limit	245	Nautical degrees
dtheta	Directional resolution	20	degrees
tstop	Stop time of simulation	345600	seconds
instat	Wave boundary condition type	Jons_table	
bcfile	Name of spectrum file	Jonswap.txt	<file>
zs0file	Name of tide boundary condition series	Tide.txt	<file>
bedfriction	Bed friction formulation	Chezy	
bedfricfile	Bed friction file	Bedfricfile.txt	<file>
D50	D50 grain size per grain type	0.000132	m
D90	D90 grain size per grain size type	0.000187	m
morfac	Morphological acceleration factor	10	
struct	Switch for enabling hard structures	1	
ne_layer	Name of file containing depth of hard structure	Nebed.dep	<file>

mpiboundary	Fix mpi boundaries along y-lines, x-lines, use manual defined domains or find shortest boundary automatically	x	

Tide.txt

```
0.0000000e+00 1.3800000e-01 1.2557760e+00
3.6000000e+03 1.3800000e-01 1.2557760e+00
7.2000000e+03 1.9800000e-01 1.2557760e+00
1.0800000e+04 2.5400000e-01 1.2557760e+00
1.4400000e+04 3.7800000e-01 1.2527280e+00
1.8000000e+04 4.8200000e-01 1.2557760e+00
2.1600000e+04 6.0100000e-01 1.2557760e+00
2.5200000e+04 6.7800000e-01 1.2557760e+00
2.8800000e+04 8.0200000e-01 1.2588240e+00
3.2400000e+04 8.1300000e-01 1.2588240e+00
3.6000000e+04 8.1700000e-01 1.2557760e+00
3.9600000e+04 7.9000000e-01 1.2527280e+00
4.3200000e+04 7.7400000e-01 1.2527280e+00
4.6800000e+04 7.6300000e-01 1.2557760e+00
5.0400000e+04 7.1800000e-01 1.2527280e+00
5.4000000e+04 7.9000000e-01 1.2557760e+00
5.7600000e+04 8.2100000e-01 1.2557760e+00
6.1200000e+04 7.8200000e-01 1.2557760e+00
6.4800000e+04 8.5800000e-01 1.2557760e+00
6.8400000e+04 7.5500000e-01 1.2527280e+00
7.2000000e+04 7.3300000e-01 1.2557760e+00
7.5600000e+04 7.1800000e-01 1.2588240e+00
7.9200000e+04 7.5600000e-01 1.2618720e+00
8.2800000e+04 6.0700000e-01 1.2588240e+00
8.6400000e+04 5.4400000e-01 1.2618720e+00
9.0000000e+04 4.7900000e-01 1.2618720e+00
9.3600000e+04 5.5600000e-01 1.2618720e+00
9.7200000e+04 6.3800000e-01 1.2618720e+00
1.0080000e+05 7.3200000e-01 1.2618720e+00
1.0440000e+05 8.2400000e-01 1.2649200e+00
1.0800000e+05 1.0060000e+00 1.2679680e+00
1.1160000e+05 1.2490000e+00 1.2618720e+00
1.1520000e+05 1.1310000e+00 1.2801600e+00
1.1880000e+05 1.3690000e+00 1.3594080e+00
1.2240000e+05 1.4150000e+00 1.4264640e+00
1.2600000e+05 1.4560000e+00 1.5179040e+00
1.2960000e+05 1.7320000e+00 1.6245840e+00
1.3320000e+05 1.7430000e+00 1.7129760e+00
1.3680000e+05 1.8300000e+00 1.8196560e+00
1.4040000e+05 1.9000000e+00 1.9171920e+00
1.4400000e+05 2.0450000e+00 2.0269200e+00
1.4760000e+05 2.0560000e+00 2.1336000e+00
1.5120000e+05 2.1860000e+00 2.2037040e+00
1.5480000e+05 2.3330000e+00 2.2860000e+00
1.5840000e+05 2.3260000e+00 2.2707600e+00
1.6200000e+05 2.2590000e+00 2.2951440e+00
1.6560000e+05 2.0880000e+00 2.2890480e+00
```

```
 1.6920000e+05 2.0150000e+00 2.3713440e+00
 1.7280000e+05 1.8580000e+00 2.4444960e+00
 1.7640000e+05 2.0040000e+00 2.4871680e+00
 1.8000000e+05 1.9150000e+00 2.7066240e+00
 1.8360000e+05 2.2170000e+00 2.7523440e+00
 1.8720000e+05 2.5040000e+00 3.1485840e+00
 1.9080000e+05 2.7000000e+00 3.0662880e+00
 1.9440000e+05 3.0930000e+00 3.0449520e+00
 1.9800000e+05 3.2190000e+00 2.8651200e+00
 2.0160000e+05 3.2200000e+00 2.5847040e+00
 2.0520000e+05 3.1850000e+00 2.2738080e+00
 2.0880000e+05 2.4680000e+00 2.1976080e+00
 2.1240000e+05 2.2720000e+00 2.0695920e+00
 2.1600000e+05 1.4860000e+00 1.9293840e+00
 2.1960000e+05 1.2810000e+00 1.8013680e+00
 2.2320000e+05 1.1240000e+00 1.7830800e+00
 2.2680000e+05 7.8900000e-01 1.6794480e+00
 2.3040000e+05 5.6100000e-01 1.6184880e+00
 2.3400000e+05 4.9600000e-01 1.5849600e+00
 2.3760000e+05 5.5900000e-01 1.5666720e+00
 2.4120000e+05 8.3400000e-01 1.4904720e+00
 2.4480000e+05 1.0330000e+00 1.4417040e+00
 2.4840000e+05 1.1610000e+00 1.3929360e+00
 2.5200000e+05 1.0630000e+00 1.3167360e+00
 2.5560000e+05 1.0330000e+00 1.2527280e+00
 2.5920000e+05 8.9100000e-01 1.2466320e+00
 2.6280000e+05 7.2400000e-01 1.2588240e+00
 2.6640000e+05 6.0100000e-01 1.2679680e+00
 2.7000000e+05 7.1800000e-01 1.3045440e+00
 2.7360000e+05 9.0200000e-01 1.3502640e+00
 2.7720000e+05 1.0440000e+00 1.4081760e+00
 2.8080000e+05 1.1820000e+00 1.4142720e+00
 2.8440000e+05 1.2710000e+00 1.3776960e+00
 2.8800000e+05 1.3940000e+00 1.3289280e+00
 2.9160000e+05 1.3840000e+00 1.2618720e+00
 2.9520000e+05 1.3290000e+00 1.2771120e+00
 2.9880000e+05 1.1660000e+00 1.2588240e+00
 3.0240000e+05 1.0360000e+00 1.2557760e+00
 3.0600000e+05 8.2500000e-01 1.2527280e+00
 3.0960000e+05 6.6900000e-01 1.2527280e+00
 3.1320000e+05 5.2600000e-01 1.2496800e+00
 3.1680000e+05 4.6600000e-01 1.2466320e+00
 3.2040000e+05 5.0400000e-01 1.2466320e+00
 3.2400000e+05 5.2300000e-01 1.2466320e+00
 3.2760000e+05 5.6200000e-01 1.2466320e+00
 3.3120000e+05 6.2000000e-01 1.2527280e+00
 3.3480000e+05 6.0600000e-01 1.2527280e+00
 3.3840000e+05 5.2200000e-01 1.2527280e+00
 3.4200000e+05 4.4800000e-01 1.2527280e+00
 3.4560000e+05 3.3600000e-01 1.2527280e+00
```

Jonswap.txt

```
0.8738 14.2222 153.0000 3.3000 10.0000 3600.0000 1.0000
0.9239 14.2222 150.0000 3.3000 10.0000 3600.0000 1.0000
0.9590 14.2222 157.0000 3.3000 10.0000 3600.0000 1.0000
```

1.0282	12.8000	153.0000	3.3000	10.0000	3600.0000	1.0000
1.0654	12.9293	155.0000	3.3000	10.0000	3600.0000	1.0000
1.1036	12.8000	135.0000	3.3000	10.0000	3600.0000	1.0000
1.1563	11.7333	147.0000	3.3000	10.0000	3600.0000	1.0000
1.1009	12.4444	152.0000	3.3000	10.0000	3600.0000	1.0000
1.2204	11.7333	148.0000	3.3000	10.0000	3600.0000	1.0000
1.2490	12.8000	145.0000	3.3000	10.0000	3600.0000	1.0000
1.3416	13.5111	123.0000	3.3000	10.0000	3600.0000	1.0000
1.4324	14.2222	132.0000	3.3000	10.0000	3600.0000	1.0000
1.4880	11.7333	149.0000	3.3000	10.0000	3600.0000	1.0000
1.4693	12.9293	146.0000	3.3000	10.0000	3600.0000	1.0000
1.5737	13.5111	128.0000	3.3000	10.0000	3600.0000	1.0000
1.7809	14.4000	128.0000	3.3000	10.0000	3600.0000	1.0000
1.7651	14.4000	124.0000	3.3000	10.0000	3600.0000	1.0000
1.8254	15.1111	103.0000	3.3000	10.0000	3600.0000	1.0000
2.0792	15.1111	112.0000	3.3000	10.0000	3600.0000	1.0000
2.0703	16.0000	115.0000	3.3000	10.0000	3600.0000	1.0000
2.1397	16.0000	102.0000	3.3000	10.0000	3600.0000	1.0000
2.2103	16.0000	109.0000	3.3000	10.0000	3600.0000	1.0000
2.2840	15.1111	107.0000	3.3000	10.0000	3600.0000	1.0000
2.2371	16.0000	110.0000	3.3000	10.0000	3600.0000	1.0000
2.3080	14.4000	117.0000	3.3000	10.0000	3600.0000	1.0000
2.3475	13.5111	116.0000	3.3000	10.0000	3600.0000	1.0000
2.6328	14.2222	110.0000	3.3000	10.0000	3600.0000	1.0000
2.5896	14.2222	107.0000	3.3000	10.0000	3600.0000	1.0000
2.7434	15.1111	96.0000	3.3000	10.0000	3600.0000	1.0000
2.9603	13.5111	108.0000	3.3000	10.0000	3600.0000	1.0000
3.1813	14.2222	110.0000	3.3000	10.0000	3600.0000	1.0000
3.1126	16.0000	109.5000	3.3000	10.0000	3600.0000	1.0000
3.1966	16.0000	109.0000	3.3000	10.0000	3600.0000	1.0000
3.5415	16.0000	110.0000	3.3000	10.0000	3600.0000	1.0000
3.4692	16.0000	100.0000	3.3000	10.0000	3600.0000	1.0000
3.9011	15.1111	117.0000	3.3000	10.0000	3600.0000	1.0000
4.1395	15.1111	119.0000	3.3000	10.0000	3600.0000	1.0000
4.2487	16.0000	118.0000	3.3000	10.0000	3600.0000	1.0000
4.2484	14.2222	117.0000	3.3000	10.0000	3600.0000	1.0000
4.5365	16.0000	113.0000	3.3000	10.0000	3600.0000	1.0000
4.6218	14.2222	116.0000	3.3000	10.0000	3600.0000	1.0000
4.8372	14.2222	128.0000	3.3000	10.0000	3600.0000	1.0000
4.5997	15.1111	139.0000	3.3000	10.0000	3600.0000	1.0000
4.9466	14.2222	149.0000	3.3000	10.0000	3600.0000	1.0000
4.4532	14.2222	152.0000	3.3000	10.0000	3600.0000	1.0000
4.2035	14.2222	125.0000	3.3000	10.0000	3600.0000	1.0000
3.5927	12.8000	157.0000	3.3000	10.0000	3600.0000	1.0000
3.8169	12.8000	149.6000	3.3000	10.0000	3600.0000	1.0000
3.9778	12.8000	149.6000	3.3000	10.0000	3600.0000	1.0000
4.0322	8.7704	142.2000	3.3000	10.0000	3600.0000	1.0000
4.5604	4.7473	134.8000	3.3000	10.0000	3600.0000	1.0000
4.5219	4.6561	127.4000	3.3000	10.0000	3600.0000	1.0000
4.6946	4.7407	120.0000	3.3000	10.0000	3600.0000	1.0000
4.5153	4.8319	99.0000	3.3000	10.0000	3600.0000	1.0000
3.7352	5.7388	103.0000	3.3000	10.0000	3600.0000	1.0000
2.6616	7.1331	59.0000	3.3000	10.0000	3600.0000	1.0000
2.9078	8.4786	51.0000	3.3000	10.0000	3600.0000	1.0000
3.5397	9.8462	77.6667	3.3000	10.0000	3600.0000	1.0000
3.7766	9.1429	104.3333	3.3000	10.0000	3600.0000	1.0000
3.4480	8.8381	131.0000	3.3000	10.0000	3600.0000	1.0000

3.5729	8.5714	188.0000	3.3000	10.0000	3600.0000	1.0000
3.5457	9.1429	151.0000	3.3000	10.0000	3600.0000	1.0000
3.2243	9.1429	188.0000	3.3000	10.0000	3600.0000	1.0000
2.6299	8.5333	200.0000	3.3000	10.0000	3600.0000	1.0000
2.4005	7.7647	201.0000	3.3000	10.0000	3600.0000	1.0000
2.5504	8.8381	182.0000	3.3000	10.0000	3600.0000	1.0000
2.5367	9.1429	193.0000	3.3000	10.0000	3600.0000	1.0000
2.3222	9.1429	194.0000	3.3000	10.0000	3600.0000	1.0000
2.0674	9.1429	174.0000	3.3000	10.0000	3600.0000	1.0000
1.6439	8.8381	174.0000	3.3000	10.0000	3600.0000	1.0000
1.5474	8.8381	158.0000	3.3000	10.0000	3600.0000	1.0000
1.3851	7.0493	143.0000	3.3000	10.0000	3600.0000	1.0000
1.2913	8.2667	148.0000	3.3000	10.0000	3600.0000	1.0000
1.0634	7.0476	159.0000	3.3000	10.0000	3600.0000	1.0000
1.0507	8.2667	184.0000	3.3000	10.0000	3600.0000	1.0000
0.9563	5.1530	153.0000	3.3000	10.0000	3600.0000	1.0000
0.9025	5.2267	167.0000	3.3000	10.0000	3600.0000	1.0000
0.8791	5.3426	169.0000	3.3000	10.0000	3600.0000	1.0000
0.8132	5.1282	154.0000	3.3000	10.0000	3600.0000	1.0000
0.7433	5.3426	183.0000	3.3000	10.0000	3600.0000	1.0000
0.7287	5.0215	180.0000	3.3000	10.0000	3600.0000	1.0000
0.7056	5.2267	187.0000	3.3000	10.0000	3600.0000	1.0000
0.6914	4.9304	179.0000	3.3000	10.0000	3600.0000	1.0000
0.6008	4.6561	191.0000	3.3000	10.0000	3600.0000	1.0000
0.5891	4.8457	183.0000	3.3000	10.0000	3600.0000	1.0000
0.5703	4.8736	186.0000	3.3000	10.0000	3600.0000	1.0000
0.4229	5.3426	186.0000	3.3000	10.0000	3600.0000	1.0000
0.3998	4.8736	218.0000	3.3000	10.0000	3600.0000	1.0000
0.3834	5.0370	288.0000	3.3000	10.0000	3600.0000	1.0000
0.3699	5.3333	174.0000	3.3000	10.0000	3600.0000	1.0000
0.3832	5.3333	188.0000	3.3000	10.0000	3600.0000	1.0000
0.3505	5.2267	135.0000	3.3000	10.0000	3600.0000	1.0000
0.3329	4.4926	161.0000	3.3000	10.0000	3600.0000	1.0000
0.3362	5.3333	146.0000	3.3000	10.0000	3600.0000	1.0000
0.3102	5.3333	144.0000	3.3000	10.0000	3600.0000	1.0000
0.3016	8.0000	156.0000	3.3000	10.0000	3600.0000	1.0000